Schweizerische Eidgenossenschaft
Confédération suisse
Confederazione Svizzera
Confederaziun svizra

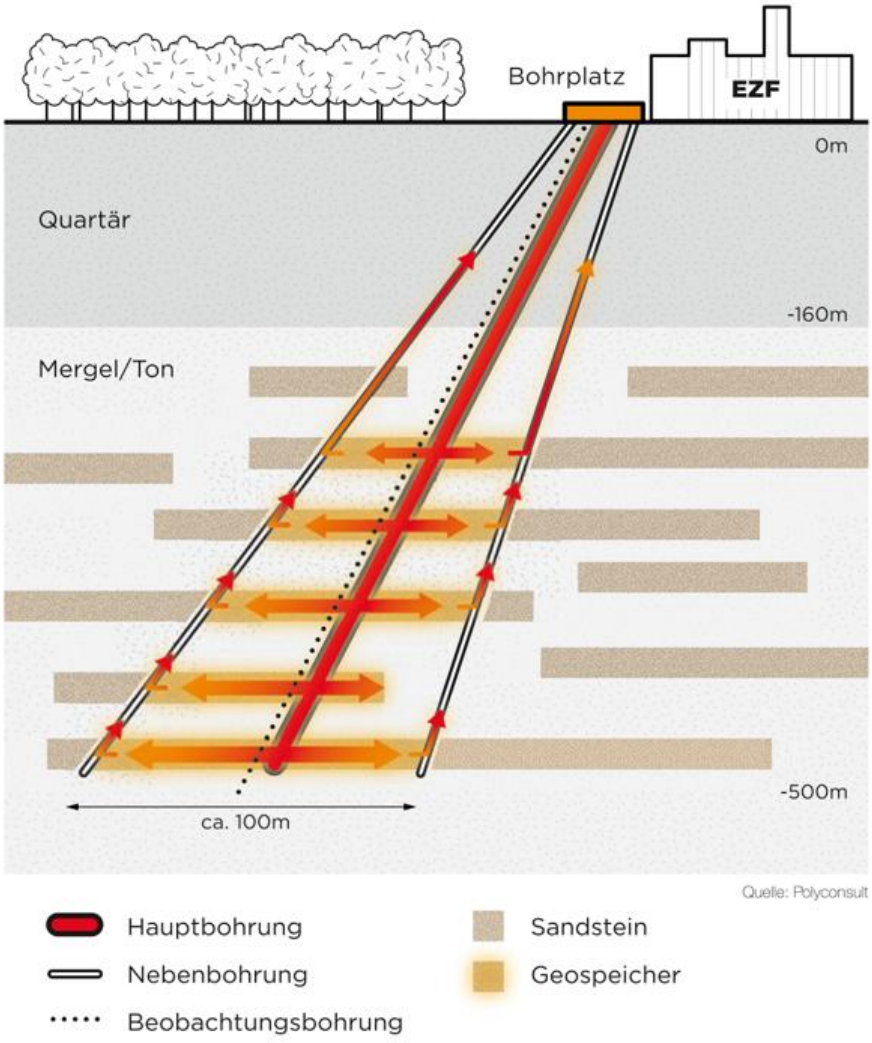
Federal Department of the Environment,
Transport, Energy and Communications DETEC

Swiss Federal Office of Energy
Energy Research and Cleantech

Final report from 19 August 2026

VESTA-CH

Very High Temperature Heat Aquifer Storage



Source: Geo-Energie Suisse AG, 2022.



Publisher:
Swiss Federal Office of Energy SFOE
Energy Research and Cleantech
CH-3003 Berne
www.energy-research.ch

Subsidy recipients:
Geo-Energie Suisse AG
Reitergasse 11, CH-8004 Zürich
https://www.geo-energie.ch

Authors:
Andrés Alcolea, Geo-Energie Suisse AG, a.alcolea@geo-energie.ch
Peter Meier, Geo-Energie Suisse AG, p.meier@geo-energie.ch

SFOE project coordinators:
Stefano Benato, stefano.benato@bfe.admin.ch
Florence Begue, florence.begue@bfe.admin.ch
SFOE contract number: SI/502362-01

The authors bear the entire responsibility for the content of this report and for the conclusions drawn therefrom.

10.5281/zenodo.22081310

Summary

High Temperature Storage systems (HTS) aim at balancing the mismatch between energy production and demand by injecting surplus or residual heat from industrial processes, waste-to-energy plants, or renewable energy sources into deep geological reservoirs for seasonal storage and subsequent recovery when required. As such, they constitute a key enabling technology for increasing the flexibility of renewable energy systems, improving energy security, and reducing greenhouse gas emissions. The VESTA-CH project addresses one of the main challenges limiting the large-scale deployment of High-Temperature Thermal Energy Storage (HTS) systems: the long-term preservation of storage performance under repeated high-temperature operation. Over successive injection and production cycles, coupled thermo-hydro-chemical (THC) processes may alter reservoir properties through permeability changes, mineral dissolution and precipitation, progressively reducing injectivity, productivity, thermal recovery efficiency, and ultimately operational safety. The project therefore aims to develop scientific and engineering methodologies that enable the definition of safe operating envelopes and support the design of more efficient, reliable, and durable HTS systems.

To achieve this objective, VESTA-CH combines advanced numerical modelling with laboratory experiments and field observations to investigate the evolution of HTS under different operating conditions. The project develops fully coupled THC simulations to quantify the interaction between fluid flow, heat transport, and geochemical reactions over repeated storage cycles. Particular emphasis is placed on identifying the physical and chemical mechanisms responsible for performance degradation, evaluating the sensitivity of system behaviour to key geological and design and operational parameters, and assessing innovative engineering concepts, including distributed fibre-optic monitoring, horizontal multilateral wells, and advanced well architectures designed to improve heat exchange. Rather than defining site-specific operating limits, which inherently depend on local hydrogeological and thermal conditions, the modelling framework is used to establish generic relationships between reservoir performance and the governing geological, design, and operational parameters. This approach enables the identification of the factors primarily controlling thermal efficiency and provides transferable design principles that can be readily adapted to future HTS projects by incorporating site-specific geology, well architecture, and completion design.

VESTA-CH benefits from datasets acquired in the context of the Forsthaus Geospeicher High-Temperature Aquifer Thermal Energy Storage (HT-ATES) project. This project aimed to store excess heat generated by the local utility company Energie Wasser Bern (ewb) within sandstone layers in the Lower Freshwater Molasse (Untere Süsswassermolasse; USM) located at depths ranging from 240 to 500 meters. Following extensive field-testing and stimulation campaigns, it became evident that the permeability of the sandstone formations was too low to allow significant thermal energy storage. As a result, only partial datasets, mainly related to the characterization of the hydrogeological system, were obtained. This limited the achievement of several of the original objectives of the VESTA-CH project, including: (1) the optimization of the injection scheme (pressure and temperature) for the Bern Forsthaus pilot site, (2) the design and validation of the monitoring system, and (3) the assessment of geochemical processes.

In the absence of key datasets, this report provides generic recommendations based on the available data and numerical analyses. In particular, the outcomes of VESTA-CH are (1) an advanced, fully coupled numerical framework for simulating TH(M)C processes in both wellbores and reservoirs; (2) generic engineering recommendations for the design of future HTS systems; (3) an integrated monitoring and surveillance concept combining surface instrumentation, downhole sensors, and distributed fibre-optic technologies; (4) generic guidelines for defining safe operational envelopes, including injection and production rates and pressure limits; and (5) a comprehensive assessment of the geochemical risks affecting long-term HTS performance and reliability.

By extending the operational lifetime and reliability of HTS installations, VESTA-CH will contribute to reducing the levelised cost of stored thermal energy and facilitate the broader deployment of seasonal heat storage technologies. The project therefore supports the objectives of the Swiss Energy Strategy by providing the scientific and engineering basis required for safe, efficient, and economically viable

underground thermal energy storage systems capable of integrating increasing shares of renewable energy into the future energy system.

Zusammenfassung

Hochtemperatur-Wärmespeichersysteme (HTS) dienen dazu, das Ungleichgewicht zwischen Energieerzeugung und Energienachfrage auszugleichen, indem überschüssige oder industrielle Abwärme aus Produktionsprozessen, Kehrichtverwertungsanlagen oder erneuerbaren Energiequellen in tiefe geologische Reservoirs eingebracht, dort saisonal gespeichert und bei Bedarf wiedergewonnen wird. Damit stellen sie eine Schlüsseltechnologie zur Erhöhung der Flexibilität erneuerbarer Energiesysteme, zur Verbesserung der Versorgungssicherheit sowie zur Verringerung der Treibhausgasemissionen dar. Das Projekt VESTA-CH befasst sich mit einer der wesentlichen Herausforderungen, welche den großflächigen Einsatz von Hochtemperatur-Wärmespeichersystemen (HTS) begrenzen: der langfristigen Erhaltung der Speicherleistung unter wiederholtem Hochtemperaturbetrieb. Während aufeinanderfolgender Injektions- und Förderzyklen können gekoppelte thermo-hydro-chemische (THC-)Prozesse die Eigenschaften des Reservoirs durch Änderungen der Permeabilität sowie durch Mineralauflösung und -ausfällung verändern. Dadurch werden die Injektivität, die Produktivität, die thermische Rückgewinnungseffizienz und letztlich die Betriebssicherheit schrittweise beeinträchtigt. Ziel des Projekts ist daher die Entwicklung wissenschaftlicher und ingenieurtechnischer Methoden zur Definition sicherer Betriebsbereiche („safe operating envelopes“) sowie zur Unterstützung der Auslegung effizienterer, zuverlässigerer und langlebigerer HTS-Systeme.

Zur Erreichung dieses Ziels kombiniert VESTA-CH fortschrittliche numerische Modellierung mit Laborexperimenten und Felddaten, um die Entwicklung von HTS-Systemen unter unterschiedlichen Betriebsbedingungen zu untersuchen. Hierzu werden vollständig gekoppelte THC-Simulationen entwickelt, welche die Wechselwirkungen zwischen Fluidströmung, Wärmetransport und geochemischen Reaktionen während wiederholter Speicherzyklen quantifizieren. Ein besonderer Schwerpunkt liegt auf der Identifizierung der physikalischen und chemischen Mechanismen, die für die Leistungsdegradation verantwortlich sind, auf der Bewertung der Sensitivität des Systemverhaltens gegenüber wesentlichen geologischen, auslegungs- und betriebsrelevanten Parametern sowie auf der Untersuchung innovativer ingenieurtechnischer Konzepte. Hierzu zählen insbesondere verteilte faseroptische Überwachungssysteme, horizontale multilaterale Bohrungen sowie fortschrittliche Bohrlocharchitekturen zur Verbesserung des Wärmeaustauschs. Anstatt standortspezifische Betriebsgrenzen festzulegen, die naturgemäß von den lokalen hydrogeologischen und thermischen Bedingungen abhängen, wird der Modellierungsrahmen genutzt, um allgemeingültige Zusammenhänge zwischen der Reservoirleistung und den maßgebenden geologischen, konstruktiven und betrieblichen Parametern abzuleiten. Dieser Ansatz ermöglicht die Identifizierung der wichtigsten Einflussgrößen auf die thermische Effizienz und liefert übertragbare Auslegungsprinzipien, die sich durch Berücksichtigung der standortspezifischen Geologie, der Bohrlocharchitektur und des Bohrlochausbaus („Completion Design“) auf zukünftige HTS-Projekte anwenden lassen.

VESTA-CH profitiert von Datensätzen, die im Rahmen des Projekts Forsthaus Geospeicher High-Temperature Aquifer Thermal Energy Storage (HT-ATES) erhoben wurden. Ziel dieses Projekts war es, überschüssige Wärme des lokalen Energieversorgers Energie Wasser Bern (ewb) in Sandsteinschichten der Unteren Süsswassermolasse (USM) in Tiefen zwischen 240 und 500 Metern zu speichern. Nach umfangreichen Feldversuchen und Stimulationskampagnen zeigte sich jedoch, dass die Permeabilität der Sandsteinformationen zu gering war, um eine wirtschaftlich relevante thermische Energiespeicherung zu ermöglichen. Infolgedessen konnten lediglich unvollständige Datensätze gewonnen werden, die sich hauptsächlich auf die Charakterisierung des hydrogeologischen Systems beschränkten. Dadurch konnten mehrere der ursprünglichen Ziele des VESTA-CH-Projekts nur teilweise erreicht werden. Dazu zählen: (1) die Optimierung des Injektionskonzepts (Druck und Temperatur) für den Pilotstandort Bern

Forsthaus, (2) die Entwicklung und Validierung des Überwachungs- und Monitoringsystems sowie (3) die Bewertung geochemischer Prozesse.

Mangels entscheidender Datensätze enthält dieser Bericht allgemeingültige Empfehlungen, die auf den verfügbaren Daten und numerischen Analysen basieren. Die Ergebnisse von VESTA-CH umfassen (1) ein fortschrittliches, vollständig gekoppeltes numerisches Simulationswerkzeug für TH(M)C-Prozesse in Bohrungen und Reservoiren, (2) allgemeingültige ingenieurtechnische Empfehlungen für die Auslegung zukünftiger HTS-Systeme, (3) ein integriertes Monitoring- und Überwachungskonzept, das Oberflächenmessungen, Bohrlochinstrumentierung und verteilte faseroptische Messtechnologien kombiniert, (4) allgemeingültige Leitlinien zur Definition sicherer Betriebsbereiche einschließlich Injektions- und Förderraten sowie zulässiger Druckgrenzen und (5) eine umfassende Bewertung geochemischer Risiken, welche die langfristige Leistungsfähigkeit und Zuverlässigkeit von HTS-Systemen beeinflussen.

Durch die Verlängerung der Betriebsdauer und die Erhöhung der Zuverlässigkeit von HTS-Anlagen wird VESTA-CH dazu beitragen, die spezifischen Kosten gespeicherter Wärmeenergie zu senken und den breiteren Einsatz saisonaler Wärmespeichertechnologien zu fördern. Das Projekt unterstützt damit die Ziele der Schweizer Energiestrategie, indem es die wissenschaftlichen und ingenieurtechnischen Grundlagen für sichere, effiziente und wirtschaftlich tragfähige unterirdische Hochtemperatur-Wärmespeichersysteme bereitstellt, die einen wachsenden Anteil erneuerbarer Energien in das zukünftige Energiesystem integrieren können.

Résumé

Les systèmes de stockage thermique à haute température (HTS) visent à équilibrer le décalage entre la production et la demande d'énergie en injectant la chaleur excédentaire ou résiduelle provenant de procédés industriels, d'installations de valorisation énergétique des déchets ou de sources d'énergie renouvelables dans des réservoirs géologiques profonds, afin d'assurer un stockage saisonnier et une récupération ultérieure lorsque cela est nécessaire. À ce titre, ils constituent une technologie clé permettant d'accroître la flexibilité des systèmes énergétiques fondés sur les énergies renouvelables, d'améliorer la sécurité énergétique et de réduire les émissions de gaz à effet de serre. Le projet VESTA-CH s'attaque à l'un des principaux défis limitant le déploiement à grande échelle des systèmes de stockage thermique à haute température (HTS) : la préservation à long terme des performances de stockage lors d'un fonctionnement répété à haute température. Au cours des cycles successifs d'injection et de production, les processus thermo-hydro-chimiques (THC) couplés peuvent modifier les propriétés du réservoir par des variations de perméabilité ainsi que par la dissolution et la précipitation des minéraux, réduisant progressivement l'injectivité, la productivité, l'efficacité de récupération thermique et, en définitive, la sécurité d'exploitation. Le projet vise donc à développer des méthodologies scientifiques et d'ingénierie permettant de définir des domaines de fonctionnement sûrs (« safe operating envelopes ») et de soutenir la conception de systèmes HTS plus efficaces, plus fiables et plus durables.

Pour atteindre cet objectif, VESTA-CH combine une modélisation numérique avancée avec des expériences en laboratoire et des observations de terrain afin d'étudier l'évolution des systèmes HTS dans différentes conditions d'exploitation. Le projet développe des simulations THC entièrement couplées afin de quantifier les interactions entre l'écoulement des fluides, le transport de chaleur et les réactions géochimiques au cours de cycles répétés de stockage. Une attention particulière est portée à l'identification des mécanismes physiques et chimiques responsables de la dégradation des performances, à l'évaluation de la sensibilité du comportement du système aux principaux paramètres géologiques, de conception et d'exploitation, ainsi qu'à l'évaluation de concepts d'ingénierie innovants, notamment la surveillance distribuée par fibre optique, des puits horizontaux multilatéraux et des architectures de puits avancées destinées à améliorer les échanges thermiques. Plutôt que de définir des limites d'exploitation spécifiques à un site, qui dépendent intrinsèquement des conditions hydrogéologiques et thermiques locales, le cadre de modélisation est utilisé pour établir des relations génériques entre les performances du réservoir et les principaux paramètres géologiques, de conception et d'exploitation. Cette approche permet d'identifier les facteurs qui contrôlent principalement l'efficacité thermique et fournit des principes

de conception transférables pouvant être facilement adaptés à de futurs projets HTS en intégrant la géologie propre au site, l'architecture des puits et leur conception de complétion.

VESTA-CH s'appuie sur les jeux de données acquis dans le cadre du projet Forsthaus Geospeicher High-Temperature Aquifer Thermal Energy Storage (HT-ATES). Ce projet avait pour objectif de stocker l'excédent de chaleur produit par le fournisseur local d'énergie Energie Wasser Bern (ewb) dans des couches de grès de la Molasse d'eau douce inférieure (USM), situées à des profondeurs comprises entre 240 et 500 mètres. À la suite de vastes campagnes d'essais sur le terrain et de stimulation, il s'est avéré que la perméabilité des formations gréseuses était trop faible pour permettre un stockage significatif d'énergie thermique. En conséquence, seuls des jeux de données partiels, principalement consacrés à la caractérisation du système hydrogéologique, ont pu être obtenus. Cette situation a limité la réalisation de plusieurs des objectifs initiaux du projet VESTA-CH, notamment : (1) l'optimisation du schéma d'injection (pression et température) pour le site pilote de Bern Forsthaus ; (2) la conception et la validation du système de surveillance et de suivi ; et (3) l'évaluation des processus géochimiques.

En l'absence de certaines données essentielles, le présent rapport fournit des recommandations génériques fondées sur les données disponibles et les analyses numériques. Plus précisément, les principaux résultats de VESTA-CH sont: (1) un cadre numérique avancé et entièrement couplé pour la simulation des processus TH(M)C dans les puits et les réservoirs ; (2) des recommandations génériques d'ingénierie pour la conception des futurs systèmes HTS ; (3) un concept intégré de surveillance et de suivi combinant instrumentation de surface, capteurs de fond de puits et technologies distribuées par fibre optique ; (4) des lignes directrices génériques pour la définition des domaines de fonctionnement sûrs, incluant les débits d'injection et de production ainsi que les limites de pression ; et (5) une évaluation complète des risques géochimiques affectant les performances et la fiabilité des systèmes HTS à long terme.

En prolongeant la durée de vie opérationnelle et la fiabilité des installations HTS, VESTA-CH contribuera à réduire le coût actualisé de l'énergie thermique stockée et à favoriser le déploiement à plus grande échelle des technologies de stockage saisonnier de chaleur. Le projet soutient ainsi les objectifs de la Stratégie énergétique suisse en fournissant les bases scientifiques et d'ingénierie nécessaires au développement de systèmes souterrains de stockage thermique sûrs, efficaces et économiquement viables, capables d'intégrer une part croissante d'énergies renouvelables dans le futur système énergétique.

Main findings («Take-Home Messages»)

- The modelling workflow developed within the VESTA-CH project illustrates conceptual pathways to optimize thermal recovery and mitigate long-term performance decline. Translating this modelling workflow into transferable design recommendations ultimately depends on validation data from upcoming operational high-temperature storage (HTS) pilot projects.
- HTS performance is primarily controlled by the number of wells, well spacing, well architecture and reservoir connectivity. Modeling results suggest that configurations like radial jet drilling (RJD) and horizontal multilateral wells may offer conceptual pathways to enhance thermal performance.
- A generic monitoring and surveillance concept combining surface measurements, downhole instrumentation and distributed fibre-optic sensing has been developed for the early detection of HTS degradation and can be readily transferred to future projects.
- Rather than defining site-specific operating limits, VESTA-CH established a methodology for deriving safe operating envelopes and assessing long-term degradation risks, providing a preliminary numerical framework that can guide future exploratory and feasibility workflows for high-temperature storage projects in Switzerland.

Contents

Summary ... **3**
Zusammenfassung ... **4**
Résumé ... **5**
Main findings («Take-Home Messages») ... **6**
Contents ... **7**
List of figures ... **8**
List of tables ... **11**
List of abbreviations ... **12**
1 Introduction ... **13**
1.1 Context and motivation ... 13
1.2 Project objectives ... 15
1.3 Structure of the report ... 17
2 Approach, method, results and discussion ... **17**
2.1 Brief description of the MOSKITO-MOOSE framework ... 17
2.2 The Bern-Forstaus HTS project. Brief description of the data set ... 23
2.3 Objective 1. Wellbore simulation and optimization of HTS design and performance. Conceptual developments ... 29
2.4 Objective 2. Development of monitoring concepts and operational surveillance strategies ... 60
2.5 Objective 3. Definition of safe operating envelopes for HTS systems. ... 61
2.6 Objective 4. Assessment of geochemical risks and mitigation strategies. ... 66
2.7 Objective 5 Design implications ... 69
3 Conclusions and outlook ... **69**
4 National and international cooperation ... **70**
5 Publications and other communications ... **71**
6 References ... **72**

List of figures

Figure 1. (a) Illustration of the full coupling between the 1D wellbore simulator and the 3D reservoir simulator based on the finite element method; (b) numerical algorithm of the fully coupled simulator at each time interval. From Yang et al. (2025) 19

Figure 2. Simulated wellbore outlet fluid temperature during the first 5 days, compared with the analytical solution of Ramey Jr (1962). From Yang et al. (2025). 20

Figure 3. Workflow of the gene expression programming (GEP) approach. Pressure, enthalpy, and two-phase fluid composition are used as inputs. The coefficient of determination (R^2) for temperature and equilibrium constants is used as the fitness function. The final output consists of explicit analytical expressions valid over a wide range of thermodynamic conditions (pressure, enthalpy, and composition). 21

Figure 4. Calculation and validation of thermal conductivity of (a) a single gas (b) pure water and binary H2O-CaCl2 brine. From Esmailpour et al., 2024. 21

Figure 5. Workflow of the reactive-transport simulation to assess the geochemical risks. T represents temperature and V_m is the change rates of fluid-component mass. 23

Figure 6. Well paths in vertical section and map view for wells GES-F1-2/2A-3/3A. 24

Figure 7. Correlation of main reservoir units RG (channel belt sandstones) in the explored USM, based on the GR/grainsize profiles. Measured porosity/permeability data in wells F2A and F3 compares with porosity/hydraulic conductivity logs (NMR) in well F3A. Red arrows indicate the geographic orientation and distance between the wells of comparable depth points. 25

Figure 8. 3D model of the so-called “optimistic” and “pessimistic” scenarios (left and right, respectively) showing different reservoir lateral extension. Only the base of each reservoir is shown for clarity. 26

Figure 9. Summary of measured petrophysical properties. 27

Figure 10. Overview of operations conducted in wells F2A and F3A, including the micro-side-drill campaigns, the initial characterization phase, a stimulation phase, two CO_2 injection phases and a production phase. Arrows and corresponding insets indicate the timing of key events and hydrotests performed during each campaign. 27

Figure 11. Summary of the calibrated parameters of both skins and formation. Temporal gaps where no hydrotests were conducted are indicated by zig-zag lines. The formation transmissivity and storage coefficient consistently show values of $2 \cdot 10^{-7}$ m²/s and $2 \cdot 10^{-5}$, respectively, across all hydrotests. The stimulation campaigns indicate the elimination of the positive skin zone (characterized by lower transmissivity) around both F3A and F2A (highlighted by blue and magenta arrows), with values improving from $5.0 \cdot 10^{-8}$ m²/s to near formation baseline transmissivity. The CO_2 injection campaigns show a general enhancement in transmissivity in F2A (magenta arrow) and F3A. These results were confirmed by final hydrotests in December 2024 and January 2025, which show a 2-fold increase in transmissivity over a 2.5 m skin-zone around F3A (blue arrow). 28

Figure 12. Sketch of the wells at Bern Forsthaus. 30

Figure 13. Temporal evolution of fluid temperature at the bottom of the well (measured depth, MD = 600 m) for different injection rates, accounting for conductive heat exchange between the wellbore and the surrounding formation according to the analytical solution of Ramey (1962). The initial formation temperature at MD = 600 m is approximately 28°C. Following the onset of injection at 90°C, downhole temperatures increase rapidly and approach thermal equilibrium, largely irrespective of the injection rate. This demonstrates that, under high flow rate circulation, conductive heat exchange along the cased section of the well has only a minor influence on the long-term thermal behaviour of the system under typical HTS operating conditions. 31

Figure 14: Impact of injection temperature on fluid temperature at the bottom of the wellbore. The injection temperatures of 50°C and 90°C represent typical unload-cycle reinjection and load-cycle injection conditions, respectively. A constant injection rate of 25 L/s was imposed in both simulations. 32

Figure 15: Temperature profiles along the wellbore for injection temperatures of 50°C (left) and 90°C (right). 32

Figure 16. Impact of injection rate on bottomhole temperature. 33

Figure 17. Temperature profiles along the wellbore for different injection rates after one year (left) and thirty years (right) of continuous injection. 34

Figure 18 . Influence of injection pressure on bottomhole temperature. 35

Figure 19. Pressure change relative to initial hydrostatic conditions for injection temperatures of 50°C (left) and 90°C (right). 36

Figure 20. Impact of an additional conductive layer located at 403 m depth on the temperature profile after an eight-month load cycle with an injection temperature of 90°C. 36

Figure 21 Temperature dependence of fluid density and dynamic viscosity over the expected operating range of the HTS system. 39

Figure 22. Hydraulic conductivity enhancement factor relative to initial reservoir conditions as a function of fluid temperature. 39

Figure 23 **.** Evolution of temperature and pressure at a monitoring point located 5 m from the injection well during a load cycle. Comparison between simulations assuming constant fluid properties and temperature-dependent density and viscosity. 40

Figure 24. 2D mesh for the modelling of the impact of heterogeneity: (left) global mesh; (right) finely discretized mesh near the boreholes. 41

Figure 25. Results for a homogeneous siltstone: (a and b) Location of boreholes; (c and d) pressure and temperature distributions after a load cycle; (e and f) pressure and temperature distributions after the unload cycle. 42

Figure 26. Results for a homogeneous sandstone. See caption of Figure 25. 43

Figure 27. Results for one heterogeneous facies field (sandstone in red; siltstone in blue) assuming parallel flow (i.e., fast flow between boreholes along the channel connecting them). See caption of Figure 25. 43

Figure 28. Results for one heterogeneous case (sandstone in red; siltstone in blue) assuming orthogonal flow (i.e., perpendicular flow along various channels. See caption of Figure 25. 44

Figure 29. Temporal evolution of hydraulic head at the injection borehole under (a) parallel flow conditions (fast flow between boreholes along the channel connecting them), and (b) perpendicular flow (perpendicular flow along various channels). 44

Figure 30. Temporal evolution of temperature at the injection and production boreholes assuming both homogeneous and heterogeneous conditions. Panels a and b: parallel flow case. Panels c and d: perpendicular flow case. 45

Figure 31. Temporal evolution of heated area (above 85ºC) under parallel (panel a) and perpendicular flow conditions (panel b). 45

Figure 32. Three-dimensional model setup used to evaluate the influence of the number of auxiliary boreholes and Radial Jet Drilling (RJD) on HTS performance. 46

Figure 33. Two-well and four-well configurations representing, respectively, the current layout and the initial target design of the Bern-Forsthaus pilot project. 46

Figure 34. 3D finite-element mesh used to assess the influence of RJD and the number of auxiliary wells on HTS performance: (a) global 3D view; (b) zoom into the sandstone layer and surrounding claystone formations; (c) plan view; (d) horizontal section through the centre of the sandstone layer; (e) detailed view of the central portion of panel (d); and (f) detailed representation of a radial-jet “crown”. Although the rapid rendering mode displays boreholes and jets as planar features, both are explicitly discretized as cylindrical elements in the numerical mesh. 47

Figure 35. Distribution of temperature (left panels) and absolute pressure (right panels) along a vertical profile intersecting the main well (upper panels) and the observation point (lower panels). Results are shown for the four-well configuration with radial jets (solid lines) and without radial jets (dashed lines). Colours indicate different times during the loading phase. 49

Figure 36. Spatial distribution of temperature (°C) at the end of the first loading cycle (top row) and first unloading cycle (bottom row) for simulations with and without radial jets (left and right columns, respectively) using the four-well configuration. Results are shown on a horizontal plane through the centre of the sandstone layer. 50

Figure 37. Spatial distribution of absolute pressure (MPa) at the end of the first loading cycle (top row) and first unloading cycle (bottom row) for simulations with and without radial jets (left and right columns, respectively) using the four-well configuration. Results are shown on a horizontal plane through the centre of the sandstone layer. 51

Figure 38. Temporal evolution of temperature (left) and pressure (right) at the main well for the four-well configuration and different radial-jet lengths. The case L = 0 m corresponds to the configuration without radial jets. 51

Figure 39. Influence of the number of boreholes on HTS thermal performance. Temporal evolution of temperature at the main and auxiliary wells for the two-well and four-well configurations under the unforced operating regime. 53

Figure 40. Influence of the number of boreholes on HTS hydraulic performance. Temporal evolution of absolute pressure at the main and auxiliary wells for the two-well and four-well configurations under the unforced operating regime. 53

Figure 41. Influence of the number of boreholes on HTS thermal performance. Temporal evolution of temperature at the main and auxiliary wells for the two-well and four-well configurations under the forced operating regime. 54

Figure 42. Influence of the number of boreholes on HTS hydraulic performance. Temporal evolution of absolute pressure at the main and auxiliary wells for the two-well and four-well configurations under the forced operating regime. 54

Figure 43. Comparison of temperature evolution at the main well for the four-well configuration under the forced and unforced operating regimes. 55

Figure 44. Spatial distribution of temperature (°C) at the end of the first and tenth loading and unloading cycles for the forced and unforced operating regimes (top and bottom rows, respectively). Simulations correspond to the four-well configuration with radial jets. Results are shown on a horizontal plane through the centre of the sandstone layer. 55

Figure 45. Configurations of the multilateral wells considered in the synthetic numerical study. (a) Well layouts comprising (1) vertical wells SV and MV only (i.e., without laterals), (2) one horizontal lateral per well (the vertical wells SV, MV, and lateral wells SL1, ML1), (3) two horizontal laterals per well (the vertical wells SV, MV and lateral wells SL1, SL2, ML1, ML2) and (4) three horizontal laterals per well (all). Panels (b-d) illustrate the temperature distribution for the configuration with three horizontal laterals after (b) the first loading period (t = 0.75 years), (c) the second unloading period (t = 2 years), and (d) the twenty-fifth unloading period (t = 25 years). 56

Figure 46. Temporal evolution of production temperature at borehole SV for a circulation rate of 25 L/s. Orange symbols indicate the annual thermal recovery efficiency (RE) for the configuration with three horizontal laterals. ‘RE’ means recovery efficiency (%). 57

Figure 47. Influence of circulation rate on production temperature for the configuration with three horizontal laterals. Results are shown for flow rates of 15, 25 and 35 L/s. Orange symbols indicate the annual thermal recovery efficiency (RE) for the case with Q = 35 L/s. 58

Figure 48. Temporal evolution of DTS profiles along well F1, showing the thermal perturbation relative to the thermostatic temperature profile before, during, and after the flushing operation. The black arrows indicate significant events, particularly the two 24-hour cold water circulation periods. During the recovery phase, the sections above 220 meters (corresponding to the cased Quaternary clay section) return rapidly to formation temperature, whereas the screened open-hole section below 220 meters exhibits a more prolonged recovery. The thick black line indicates the top of the originally clogged section of F1. Results are expressed as differential temperature, defined as the difference between the temperature at any given time and the thermostatic temperature (mean temperature profile from 10/03/2024 to 20/03/2024). 62

Figure 49. Vertical cross-section showing simulated (a) temperature and (b) pressure distributions at the end of the 1st and 10th load and unload cycles. 63

Figure 50. Vertical cross-section showing simulated (a) volumetric strain and (b) vertical displacement at the end of the 1st and 10th load and unload cycles. 64

Figure 51. Calculated corrosion rates for a) pH=4.5 b) pH=5.5 c) pH=6.5. 68

List of tables

Table 1: Calculations carried out under Objective 1, corresponding tasks and responsibilities. 16

Table 2: Input parameters used for the synthetic sensitivity analysis of the response of primary variables to operational boundary conditions. To isolate the influence of the selected operational parameters, conductive heat exchange between the wellbore and the surrounding formation was neglected in these initial simulations. 30

Table 3. Solid and fluid parameters for the modelling of the impact of heterogeneity. Note that the mechanical effect is not considered. A= $2.1 \cdot 10^{-12}$ MPa·s and B=1808.5 K for the calculation of water viscosity. 41

Table 4. Summary of internal boundary conditions applied in the 3D model used to evaluate the impact of RJD and the number of auxiliary wells. Positive flow rates (Q) denote injection, whereas negative values denote pumping. The parameter n_{aux} represents the number of auxiliary wells (1 or 3 in the present study). 48

Table 5. Main findings from the synthetic wellbore and reservoir simulations performed for HTS design optimization. 58

Table 6. Summary of the principal parameters controlling the safe operating envelope of HTS systems identified in VESTA-CH. 66

List of abbreviations

ATES	Aquifer Thermal Energy Storage
ewb	Energie Wasser Bern
EOS	Equation of state
GEP	Gene Expression Programming
GES	Geo-Energie Suisse AG
HTS	High Temperature Storage
KIT	Karlsruhe Institute of Technology
OMM	Upper Marine Molasse
MOOSE	An open-source, parallel finite element framework
MOSKITO	Fully transient geothermal Wellbore Simulator based on the MOOSE framework
MST	Micro-side-track drilling
RJD	Radial Jet Drilling
SFOE	Swiss Federal Office of Energy
SWM	Stadtwerke München
THC	Thermo-Hydro-Chemical
TIGER	High-Performance simulator for nonlinear coupled THMC processes based on the MOOSE framework
USM	Untere Süsswassermolasse (Lower Freshwater Molasse)
VESTA	Very High Temperature Heat Aquifer Storage

1 Introduction

1.1 Context and motivation

Seasonal variations in heat demand create a significant mismatch between energy production and consumption. Bridging this temporal gap is essential for improving energy efficiency, increasing renewable energy utilization, and supporting the transition toward a CO_2-neutral supply. To address this challenge, seasonal Aquifer Thermal Energy Storage (ATES) systems are being developed to store excess thermal energy during periods of low demand and recover it during periods of high demand (Nordbeck et al., 2023; Heldt et al., 2024; Dobson et al., 2025). Beyond conventional ATES, many industrial processes generate waste heat at temperatures exceeding 100°C. The ability to store and recover such thermal energy would significantly improve the economic viability of underground High Temperature Storage (HTS) systems and expand their commercial potential. The Very High Temperature Heat Aquifer Storage (VESTA) project, was initiated to address the scientific and technical challenges associated with thermal energy storage at temperatures exceeding 100°C. Specifically, the objectives of VESTA are:

- Demonstration of HTS at selected pilot sites, with recommendations and conclusions for future projects.
- Assessment of technical and non-technical barriers, building on the experience gained to date.
- Support for the development and implementation of commercial projects by providing process understanding, modelling and monitoring techniques, and optimized component design.
- Support for public authorities through scientific and technical findings as a basis for the further development of regulatory provisions.

VESTA was organized in three work packages:

- **WP1 "R&D Roadmap"** developed a roadmap with corresponding impulses for the research phase in WP2 and 3. To this end, the current state of research was evaluated and "lessons learned" from previous experience with underground thermal storage were compiled.
- **WP2 "Generic HTS Development"** focused on generic design and operational investigations for the planning of HTS projects. It included data collection, development of process understanding, formulation of numerical models and benchmarking, technical and economic system analyses, and regulatory framework conditions. The aim was to define specific methods for optimized monitoring and prediction of system performance.
- **WP3 "Pilot Projects"** comprised pilot projects for HTS demonstrators at different stages of development, ranging from conceptual and feasibility studies to construction. In the pilot projects, the methods and approaches developed in WP2 were validated and demonstrated. The activities focus on experimental validation in the demonstrators and detailed modelling of the performance of the HTS systems, demand-side management, and other flexibility options within an integrated district heating network, in order to determine optimal design and operational strategies for the HTS systems. Conceptual studies of HTS were analysed in München (SWM; https://www.swm.de/unternehmen/waermewende) and HEATSTORE in Bochum (IEG; https://www.ieg.fraunhofer.de/en/references/heatstore.html). Demonstrator projects considered were DeepStor in Karlsruhe (https://www.geoenergiecampus.kit.edu/english/59.php), and, initially, the Bern Forsthaus project.

In parallel, the VESTA-CH project, fully founded by the BFE, was initiated in 2022 to reinforce the link with the overarching VESTA project and its application to the Bern Forsthaus HTS pilot project.

Despite its considerable potential, the widespread implementation of HTS technology faces numerous technical, regulatory, environmental, legal, and economic challenges. From a technical perspective, a better understanding is required of the coupled thermal, hydraulic, and chemical processes occurring

during the operation of HTS systems. These include fluid and heat transport under elevated temperature conditions, pressure and temperature interactions between wells, chemical reactions such as corrosion, dissolution, scaling, and sand production, as well as their impact on well integrity and long-term system performance. Under dynamic operating conditions, geothermal wells are characterized by strongly coupled thermo-hydro-chemical (THC) processes that exhibit highly nonlinear behaviour. Key parameters such as temperature, pressure, density, viscosity, enthalpy, specific heat capacity, flow regime, heat transfer, steam quality, degassing behaviour, fluid chemistry, pH, and salinity interact continuously throughout operation. Furthermore, seasonal heat storage systems are particularly demanding because they are subjected to repeated temperature and pressure fluctuations during so-called loading (injection) and unloading (production) cycles. These fluctuations affect well integrity, casing performance, completion design, and fluid chemistry, while also influencing reservoir behaviour and surface facility operation. Optimizing injection and production strategies therefore requires both a thorough understanding of the governing processes and reliable numerical simulation tools capable of representing them.

Over the past decades, numerous simulation tools have been developed to support geothermal well and reservoir engineering. Most existing wellbore simulators focus on steady-state conditions. Examples include HEX-82 (Mégel et al., 2007), which solves single-phase water flow in boreholes, and FloWell (Gudmundsdottir et al., 2013), which additionally considers two-phase flow and supercritical conditions. Other simulators, such as SwelFlo (McGuinness, 2015) and GWELL (Aunzo, 1990), address systems containing significant concentrations of non-condensable gases, while WellSim (Gunn and Freeston, 1991), GWNACL (Aunzo et al., 1991), and SIMU2000 (Sanchez-Upton, 2000) incorporate the effects of dissolved salts on fluid properties. Most of these models represent reservoir behaviour using simplified boundary conditions, such as productivity indices, inflow performance relationships, or prescribed feed-zone inflows. More advanced approaches have coupled wellbore and reservoir simulators, for example by linking dedicated wellbore models with the reservoir simulator TOUGH2 (Pruess, 2004), thereby enabling more realistic representations of the interaction between wells and reservoirs. However, the chemical interactions between formation fluids, reservoir rocks, and engineered components (e.g., casing materials, completion elements, or pumps) remain largely unexplored, particularly under the cyclic thermal and hydraulic conditions characteristic of HTS operations.

Within the framework of VESTA, the Karlsruhe Institute of Technology (KIT) has developed the software MOSKITO (Korzani et al., 2019; Wang et al. 2019), a dedicated transient wellbore simulator specifically designed for HTS applications. MOSKITO supports multiphase and multicomponent flow and is capable of simulating the transient operating conditions characteristic of seasonal heat storage systems. MOSKITO is built within the solver environment MOOSE (Gaston et al., 2009; Permann et al., 2020), thus providing a multi-physics, object-oriented and easy to enrich simulation environment. The simulation of two-phase flow (i.e., gas and water) uses a drift-flux approach to quantify the properties of the liquid and gas mixture and the resulting flow patterns. An important feature of MOSKITO is its ability to explicitly couple with other MOOSE-based simulators, including reservoir flow and reactive transport models. Such coupling, referred to as two-way coupling, accounts for the impact of pressure and temperature variations in the reservoir on the borehole and vice versa. MOSKITO overcomes the usually applied "reservoir-mimicking" boundaries (e.g., inflow performance relationships, productivity index, inflows, etc., which provide a one-way coupling only, from the reservoir to the borehole but not the other way around) by coupling to the reservoir simulator PorousFlow (Wilkins et al., 2020 and 2021a). Within VESTA, KIT has also included the coupling to a geochemical reactive-transport module (Guo et al., 2013), which is particularly important for HTS simulations.

The importance of seasonal heat storage is widely recognized as a key component of Switzerland's future sustainable energy infrastructure. To investigate the feasibility of HTS in Switzerland, a pilot project was developed in Bern to store waste heat from the nearby power station Bern-Forsthaus. The power generation site is operated by the local utility company Energie Wasser Bern (ewb) and includes a combined-cycle plant, a waste-to-energy plant and a wood-fired power station for electricity and heat production. The project aimed at constructing a fully functional HTS system capable of storing approximately 7-10 MWth of otherwise unused thermal energy at a maximum storage temperature of 100°C. Geo-Energie Suisse AG (GES) planned and conducted a hydrogeological survey to characterize the Lower Freshwater Molasse (Untere Süsswassermolasse, or USM) to assess its adequacy for seasonal

heat storage. The characterization program of the Forsthaus project included 3 wells, out of six initially envisaged, to characterize the reservoir up to a depth of approximately 520m. Laboratory measurements and field tests revealed the initially very low permeability of the sandstone layers of the USM at the tested depth range. Several attempts were made to improve reservoir performance, including the drilling of micro-side-tracks (analogue to radial jet drilling) to enhance connectivity between the borehole and reservoir and the chemical enhancement of formation permeability through acid stimulation using diluted CO_2. The final results demonstrated a measurable improvement in reservoir transmissivity. However, the achieved productivity remained below the threshold required for economically viable HTS operation.

Nevertheless, the extensive dataset collected during the characterization program provided a unique opportunity for numerical model development and software validation. These data were used to establish two three-dimensional models of the system: (1) a model developed by KIT serving as a testbed for the development of the MOOSE-MOSKITO framework, and (2) a model developed by GES to support reservoir characterization and evaluate potential permeability-enhancement strategies. Since MOSKITO has not yet been applied to a real HTS system, this research project is of particular scientific and practical relevance, contributing to the development of in-house expertise within GES, facilitating access to advanced simulation capabilities, and providing valuable insights into the coupled thermo-hydro-chemical processes governing future HTS projects.

1.2 Project objectives

The overarching objective of VESTA is to improve the understanding of the coupled THC processes governing the operation of HTS systems and to provide practical recommendations for the design, monitoring, and operation of future HTS installations. Building upon the datasets acquired during the Bern-Forsthaus characterization and development program and the capabilities of the MOSKITO simulator and its coupled reservoir and geochemical modules, the project aims to address several of the key technical challenges identified in Section 1.1.

A particular focus has been placed on quantifying the interactions between wellbore hydraulics, heat transport, and, in a synthetic manner, geochemical processes under the cyclic loading and unloading conditions characteristic of seasonal heat storage systems. Through a combination of numerical simulations, sensitivity analyses, and interpretation of field observations, the VESTA project will contribute to reducing technical uncertainties associated with the deployment of future HTS facilities.

More specifically, the project pursues the following objectives:

- **Objective 1. Wellbore simulation and optimization of HTS design and performance.** Advanced simulations have been performed using the coupled MOSKITO-PorousFlow framework to evaluate the impact of elevated temperatures and pressures on well performance, completion design, and operational efficiency. Particular attention has been given to identifying critical parameters controlling heat recovery, pressure losses, thermal breakthrough, and the long-term integrity of technical installations.
- **Objective 2. Development of monitoring concepts and operational surveillance strategies.** The project has evaluated monitoring approaches suitable for HTS systems, with particular emphasis on distributed fiber-optic sensing technologies. Experience gained during the Bern-Forsthaus project demonstrated the potential of fiber-optic measurements for the continuous monitoring of temperature evolution and operational conditions within boreholes.
- **Objective 3. Definition of safe operating envelopes for HTS systems.** Numerical simulations have been used to investigate the influence of injection and production temperatures, flow rates, and well configurations on HTS thermal efficiency.
- **Objective 4. Assessment of geochemical risks and mitigation strategies.** The coupled reactive transport capabilities incorporated within the MOSKITO-MOOSE framework have been

utilized to evaluate, in a generic manner, potential geochemical alterations induced by HTS operation.

- **Objective 5. Development of engineering guidelines for future HTS projects.** The results obtained during the project have been consolidated into a set of recommendations and best-practice guidelines addressing well design, completion concepts, monitoring requirements, operational procedures, and risk mitigation measures. These guidelines provide a technical basis for the planning and implementation of future HTS installations in Switzerland and elsewhere.

To achieve the aforementioned objectives, two main tasks were defined in the proposal of VESTA-CH (SI/502362-01):

- Task 1.1: Numerical characterization of borehole processes, which primarily consists of synthetic simulations (although partly based on, or inspired by, data from the Bern Forsthaus project) aimed at identifying the critical parameters controlling HTS performance, and
- Task 1.2: Update of the reservoir model, which involves refining and validating the aforementioned numerical models using data from the Bern Forsthaus pilot project. The delays in the Bern Forsthaus pilot project precluded model updates.

Table 1 summarizes the calculations carried out, assigns them to the corresponding tasks in the original proposal, and defines the respective responsibilities.

Table 1: Calculations carried out under Objective 1, corresponding tasks and responsibilities.

Objective	Parameter	Task	Section	Data set	Conceptual model	Simulation	Analysis
1	Injection temperature	1.1	2.3.1	Bern Forsthaus borehole design (GES)	GES-KIT	KIT	GES-KIT
1	Injection flow rate	1.1	2.3.2	Bern Forsthaus borehole design (GES)	GES-KIT	KIT	GES-KIT
1	Injection pressure	1.1	2.3.3	Bern Forsthaus borehole design (GES)	GES-KIT	KIT	GES-KIT
1	Additional conductive layers	1.1	2.3.4	Bern Forsthaus borehole design (GES)	GES-KIT	KIT	GES-KIT
1	Reservoir temperature	1.1	2.3.5	Synthetic	GES	GES	GES
1	Reservoir heterogeneity	1.1	2.3.6	Synthetic	GES	GES	GES
1, 2	Radial Jet Drilling (RJD)	1.1 & 1.2	2.3.7	Bern Forsthaus (GES)	GES	GES	GES
1, 2	Number of boreholes and injection scheme	1.1 & 1.2	2.3.7	Bern Forsthaus (GES)	GES	GES	GES
1, 2	Horizontal Multilateral Wells	1.1	2.3.8	Synthetic	KIT	KIT	KIT
2	Monitoring concept and surveillance strategies	N.A.	2.4	Bern Forsthaus (GES)	GES	N.A.	GES

3	Safe operating envelopes for HTS systems	N.A.	2.5	Generic	GES	N.A.	GES
4	Geochemical risks	N.A.	2.6	Synthetic	KIT	KIT	KIT
5	Design implications	N.A.	2.7	Generic	GES	N.A.	GES

1.3 Structure of the report

Following a general description of the modelling workflow developed within the VESTA-CH project (section 2.1) and the datasets from the Bern Forsthaus project used in some calculations presented here (section 2.2), the individual objectives are described in sections 2.3 to 2.7. It concludes with a synthesis of findings in Section 3 and a catalog of publications and collaborations in Sections 4 and 5.

2 Approach, method, results and discussion

2.1 Brief description of the MOSKITO-MOOSE framework

The numerical assessment of HTS systems requires the simultaneous simulation of multiple strongly coupled physical and chemical processes occurring in both the wellbore and the surrounding reservoir. These include fluid flow, heat transport, fluid-rock interactions, phase behaviour, mechanical response, and geochemical reactions, all of which evolve under transient operating conditions and may significantly affect system performance and long-term reliability. Accurately capturing these interactions while maintaining computational efficiency remains one of the major challenges in the numerical modelling of geothermal and subsurface energy storage systems.

To address these challenges, VESTA-CH employs the MOSKITO-MOOSE framework, a state-of-the-art numerical platform specifically developed for the simulation of coupled thermo-hydraulic-mechanical-chemical (THMC) processes in wellbore-reservoir systems. Unlike conventional workflows, which often treat the wellbore and the reservoir separately or rely on loosely coupled simulations, MOSKITO performs a fully coupled solution of the governing equations, allowing the mutual interactions between both domains to be resolved consistently throughout the simulation. This enables realistic modelling of transient injection and production operations, including the prediction of pressure evolution, heat exchange, fluid circulation, and reactive transport within a unified computational framework.

Compared to other existing software packages, a distinctive feature of MOSKITO is its advanced thermodynamic formulation. Conventional geothermal simulators generally rely on computationally intensive iterative Equation-of-State (EOS) calculations, which typically require temperature as an input variable. In contrast, MOSKITO incorporates a machine-learning thermodynamic module based on Gene Expression Programming (GEP) that directly predicts the required thermophysical properties from the primary variables solved by the numerical model, namely pressure, enthalpy, and phase composition. By replacing repeated iterative EOS calculations with explicit analytical expressions, this approach substantially reduces computational costs while maintaining the level of accuracy required for engineering-scale simulations involving millions of thermodynamic evaluations.

The modular architecture of the MOSKITO-MOOSE framework further enables the integration of additional physical processes relevant to underground thermal energy storage. Besides fully coupled thermo-hydraulic simulations, MOSKITO incorporates reactive-transport capabilities for evaluating mineral dissolution, precipitation, scaling, and other geochemical processes that may compromise long-term system performance.

These capabilities make MOSKITO a cutting-edge engineering tool to reproduce the complex multiphysics behaviour of HTS systems, while enabling the computationally efficient evaluation of alternative operational strategies, well designs, and long-term system performance. The following sections summarize the principal components of the framework, including the coupled wellbore-reservoir formulation, the machine-learning-based thermodynamic module, and the reactive-transport capabilities employed throughout the VESTA-CH project.

2.1.1 Equations and coupling methods

The coupled MOSKITO-PorousFlow framework simultaneously solves the governing equations for fluid flow and heat transport in both the wellbore and the surrounding reservoir (Pan and Oldenburg, 2014; Korzani et al., 2019; Wilkins et al., 2021a). A detailed mathematical description of the implemented equations and coupling strategy is provided by Yang et al. (2025).

The reservoir is represented as a porous medium in which fluid flow is governed by Darcy's law, while heat transport accounts for conductive and advective processes. Owing to the low flow velocities typically encountered in porous formations, inertial effects, kinetic energy, and gravitational potential energy contributions are neglected in the reservoir energy balance. In contrast, fluid flow within the wellbore is described by a one-dimensional Navier-Stokes formulation that explicitly accounts for inertial forces. The corresponding energy equation includes conductive and convective heat transport, as well as kinetic and gravitational energy terms, which may significantly influence fluid temperature evolution under dynamic operating conditions.

The exchange of mass and heat between the reservoir and the wellbore is treated differently depending on the completion type:

- In open-hole intervals, hydraulic communication exists between the well and the formation, allowing both mass and energy transfer. Fluid exchange is calculated using a Peaceman-type well model (Peaceman, 1983), in which the flow rate across the well-reservoir interface is driven by the local pressure difference between the formation and the wellbore. Associated energy transfer includes both advective heat transport carried by the exchanged fluid and conductive heat transfer driven by temperature gradients across the interface.
- In cased or non-open-hole sections, hydraulic communication between the wellbore and the formation is prevented and therefore no mass exchange occurs. Heat transfer, however, remains active and is represented through radial conductive heat exchange between the wellbore and the surrounding geological formation. The overall thermal resistance between the flowing fluid and the formation is calculated by considering the thermal resistances of all well components, including tubing, annular fluid, casing, and cement. Detailed formulations can be found in Willhite (1967) and Xiong et al. (2016).

The fully coupled implementation combines a one-dimensional wellbore model with a three-dimensional finite-element reservoir model (Figure 1a). During each simulation time step, the wellbore and reservoir domains are solved iteratively using Newton-Raphson nonlinear solvers. Information is exchanged between both simulators until convergence of the coupled system is achieved. In addition to the convergence of the individual wellbore and reservoir solutions, convergence of the coupling procedure itself must be satisfied at every time step.

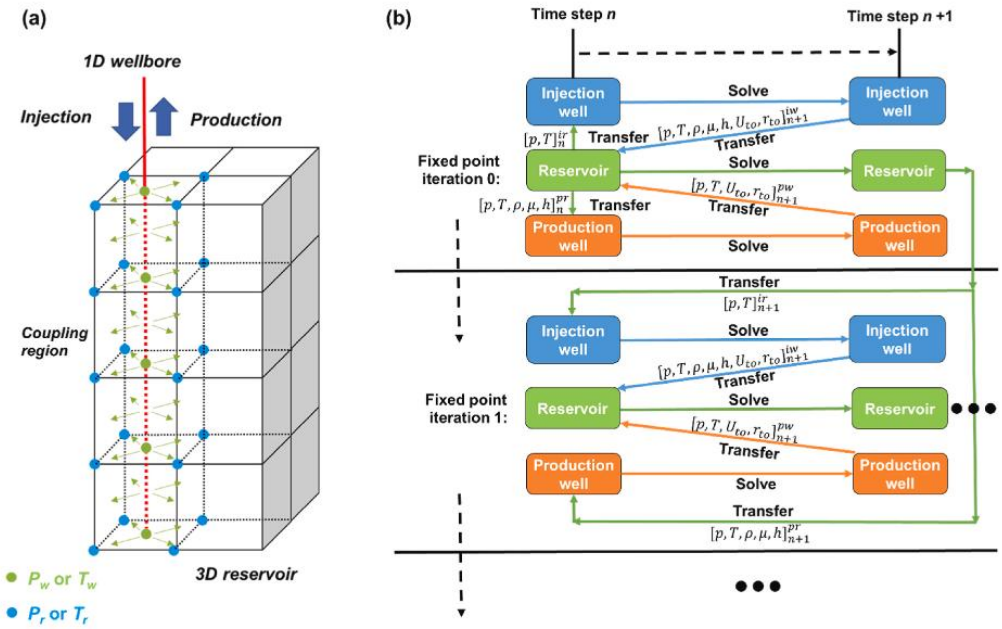


Figure 1. (a) Illustration of the full coupling between the 1D wellbore simulator and the 3D reservoir simulator based on the finite element method; (b) numerical algorithm of the fully coupled simulator at each time interval. From Yang et al. (2025)

The coupling is implemented through a Picard iteration scheme within the MOOSE framework. During each iteration, pressures, temperatures, and flow-related quantities are exchanged across the wellbore-reservoir interface. For cased intervals, temperatures of the surrounding formation are transferred to the wellbore model, while dynamically updated thermal resistances are communicated back to the reservoir model. This two-way exchange ensures a consistent representation of the mutual thermal and hydraulic interactions between both domains (Figure 1b).

The integrated modelling framework enables the simulation of a wide range of operational scenarios relevant to geothermal and thermal energy storage applications, including prescribed injection or production rates, wellhead pressure constraints, and transient operating conditions. The implementation has been verified against the analytical solution of Ramey (1962) for transient wellbore heat transfer. Figure 2 compares the simulated evolution of the outlet fluid temperature with the corresponding analytical solution, demonstrating excellent agreement and providing confidence in the accuracy of the thermal coupling approach implemented in MOSKITO.

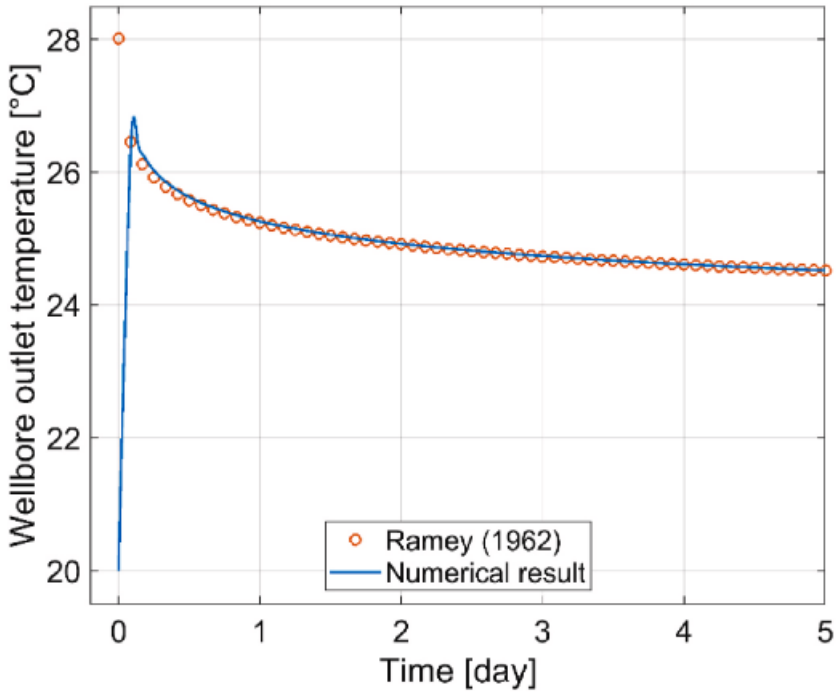


Figure 2. Simulated wellbore outlet fluid temperature during the first 5 days, compared with the analytical solution of Ramey Jr (1962). From Yang et al. (2025).

2.1.2 Accurate equation of state based on gene expression programming

The conservation equations described in the previous section are solved to obtain the primary variables governing fluid flow and heat transport, including pressure, enthalpy, phase velocities, and fluid composition. However, the evaluation of these governing equations also requires a large set of thermophysical properties, such as density, viscosity, temperature, phase equilibrium constants, and other fluid-specific parameters. These properties are not solved directly but are obtained through appropriate equations of state (EOS). The accurate representation of thermodynamic properties is particularly important in geothermal applications because fluid behaviour may change significantly over the wide pressure and temperature ranges encountered in the subsurface. In multiphase and multicomponent systems, EOS calculations often become one of the most computationally demanding components of the numerical simulation.

Most thermodynamic formulations available in the literature (e.g., Ziabakhsh-Ganji and Kooi, 2012; Pruess and Battistelli, 2002; Pruess, 2005 to cite a few; see also the comprehensive review in Esmaeilpour et al., 2024) require temperature as a primary input variable. This introduces a fundamental numerical challenge because MOSKITO solves for pressure, enthalpy, and fluid composition rather than temperature. As a result, conventional EOS implementations would require an additional iterative procedure to estimate temperature from calculated variables before fluid properties can be calculated. In large-scale three-dimensional simulations involving millions of EOS evaluations, these repeated iterations can significantly increase computational costs and simulation times. Guessing temperature as an unknown input imposes more iterations on the already demanding iterative algorithm of the EOS and increases the computational cost, especially in highly accurate 3D models.

To overcome this limitation, MOSKITO has been enhanced by KIT in the context of VESTA through the integration of a machine-learning-based thermodynamic module based on Gene Expression Programming (GEP; Esmaeilpour, 2023). The objective of this approach is to replace computationally expensive iterative EOS calculations with explicit analytical expressions that directly map the primary simulation variables to the required thermophysical properties. The GEP module was trained by KIT to reproduce

the behaviour of conventional thermodynamic EOS models over the range of conditions relevant to geothermal systems.

Instead of requiring temperature as an input, the developed implementation directly uses pressure, enthalpy, and phase composition as predictor variables (Figure 3). The resulting regression expressions provide direct estimates of temperature, equilibrium constants, and other thermodynamic properties without requiring additional nonlinear iterations.

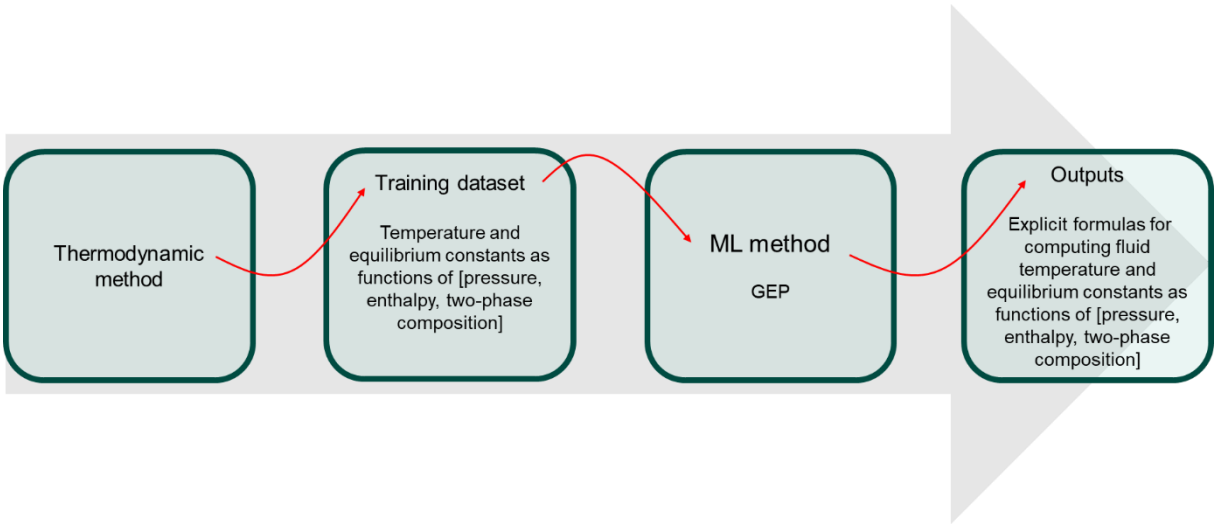


Figure 3. Workflow of the gene expression programming (GEP) approach. Pressure, enthalpy, and two-phase fluid composition are used as inputs. The coefficient of determination (R^2) for temperature and equilibrium constants is used as the fitness function. The final output consists of explicit analytical expressions valid over a wide range of thermodynamic conditions (pressure, enthalpy, and composition).

The GEP-based thermodynamic module implemented in MOSKITO has been validated by KIT through comparisons with analytical solutions and published reference datasets (Figure 4). The benchmarking results show excellent agreement with conventional thermodynamic formulations while achieving a substantial reduction in computational cost.

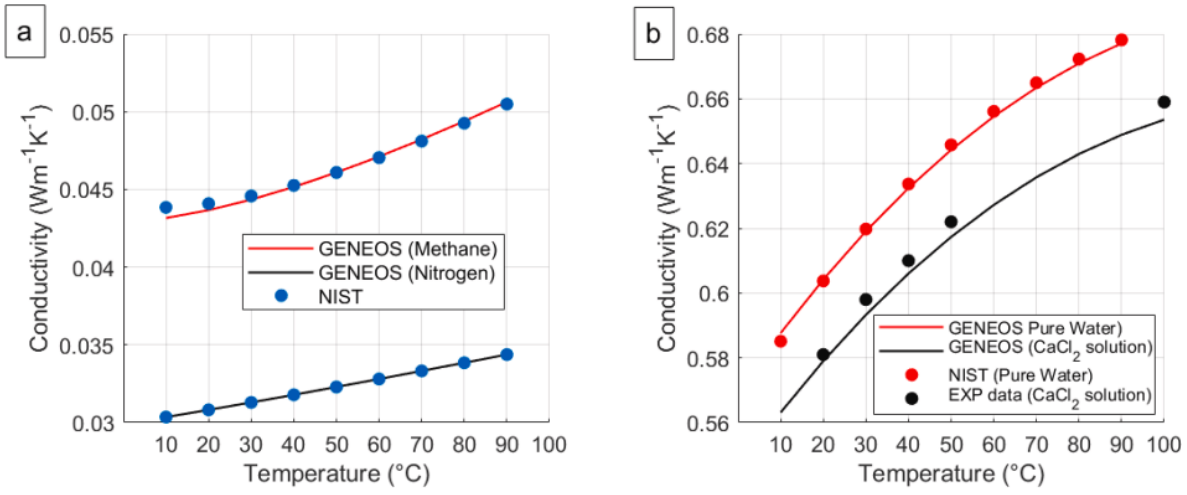


Figure 4. Calculation and validation of thermal conductivity of (a) a single gas (b) pure water and binary H2O-CaCl2 brine. From Esmailpour et al., 2024.

2.1.3 Reactive-Transport Modelling Framework

Reactive-transport simulations of the coupled wellbore-reservoir system are generally performed to assess potential geochemical risks associated with HTS operation. In the context of VESTA-CH, KIT has given particular attention to the formation of calcite and quartz scaling, although the modelling framework is readily extensible to additional mineral reactions and geochemical processes, as explained below.

Fluid flow and heat transport are simulated using the fully coupled MOSKITO-PorousFlow framework described previously, whereas chemical equilibrium and kinetic reactions are handled by the Geochemistry module implemented within the MOOSE framework (Wilkins et al., 2021b). Within this framework, MOSKITO-PorousFlow acts as the primary application and computes pressure, temperature, fluid flow, and heat transport throughout the wellbore-reservoir system, as described in section 2.1.1 (with the required EOS described in section 2.1.2). These results are subsequently transferred to the Geochemistry module, which evaluates the corresponding aqueous and mineral reactions under the prevailing hydraulic and thermal conditions. The updated fluid composition and mineralogical state are then transferred back to the flow and heat transfer simulator and used as input for the next time step. This iterative exchange continues until convergence is achieved for both the individual applications and the coupled solution. The overall workflow of the reactive-transport framework is illustrated in Figure 5.

The simulations require a detailed characterization of:

- the initial chemical and mineralogical conditions. To this end, the composition of the injection fluid is determined through laboratory analyses, including the concentrations of the major dissolved species (e.g., Cl^-, SO_4^{2-}, HCO_3^-, Ca^{2+}, H^+, and SiO2(aq)),
- the mineralogical composition of the reservoir rock, currently represented by calcite and quartz for simplicity, must be characterized or estimated, and
- the chemical composition of the formation fluids under in-situ conditions is obtained from fluid samples whenever available or, alternatively, estimated from laboratory measurements, logging information, and geochemical equilibrium calculations when direct sampling is not feasible.

During the simulation, temperature, pressure, and fluid-component transport calculated by MOSKITO-PorousFlow determine the thermodynamic conditions controlling mineral dissolution and precipitation reactions. In turn, the Geochemistry module updates fluid composition and mineral abundances, thereby capturing the mutual interaction between fluid flow, heat transport, and geochemical processes, the latter including fluid-fluid and solid-fluid interactions.

The resulting simulations allow the temporal and spatial evolution of fluid chemistry and mineralogy to be quantified throughout the operational lifetime of the storage system. By comparing simulated conditions with the initial state, the potential for e.g. mineral precipitation, scaling, dissolution, corrosion and associated operational risks can be evaluated. In addition, dedicated post-processing tools are available to assess the likelihood of scaling and corrosion, thereby supporting the definition of safe operating conditions and mitigation strategies for future HTS projects.

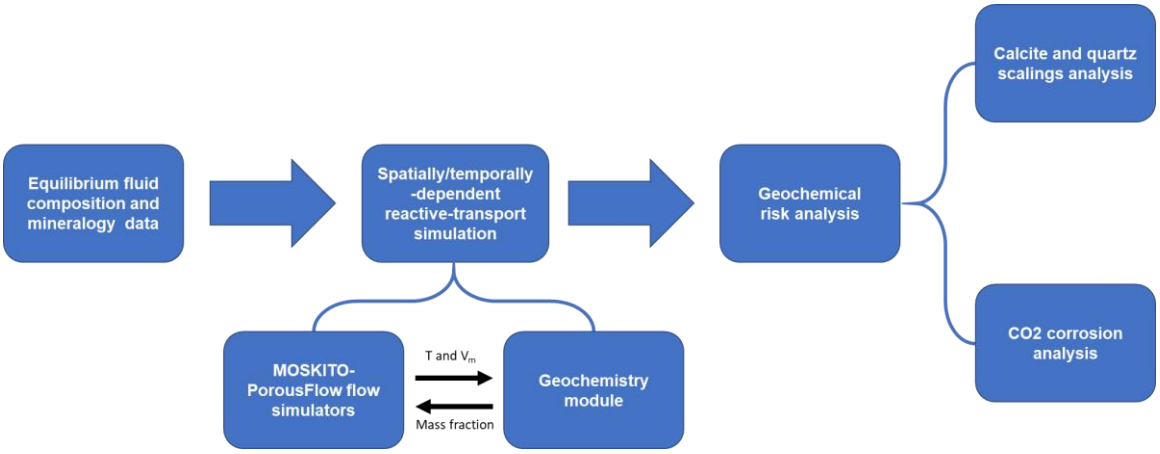


Figure 5. Workflow of the reactive-transport simulation to assess the geochemical risks. T represents temperature and V_m is the change rates of fluid-component mass.

2.2 The Bern-Forstaus HTS project. Brief description of the data set

The Forsthaus Geospeicher High-Temperature Aquifer Thermal Energy Storage (HT-ATES) project aimed to store excess heat generated by the local utility company Energie Wasser Bern (ewb) within sandstone layers in the lower freshwater molasse (Untere Süsswassermolasse = USM) located at depths ranging from 240 to 500 meters. The primary objective of this initiative was to recover the stored thermal energy during periods of peak demand for the local district heating network.

The subsurface geology at the Forsthaus site comprises 240 meters of Quaternary sediments, underlain by a 10-meter-thick moraine gravel layer. The Quaternary sediments are discontinuous with the USM. The USM is characterized by a continental facies, featuring sequences of channel sandstones, overbank mudstones, and lacustrine and pedogenetic carbonates.

Three wells have been drilled at the Forsthaus site (Figure 6): (1) F1: A 226-meter-deep well that reaches the top of the USM. The well is cased but not cemented, and the casing is screened at a depth range of 200 to 226 meters depth. F1 deviates 13° from vertical; (2) F2A: A 526-meter-deep side-track of well F2 that intersects the USM between 240 and 526meters depth. This well is both cased and cemented, featuring a vertical section for the first 200 meters, followed by a 13° deviation; (3) F3A: A 530-meter-deep side-track of well F3 that intersects the USM from 240 to 530 meters depth. Like F2A, it is cased and cemented, with a vertical segment for the initial 200 meters and a subsequent 13° deviation.

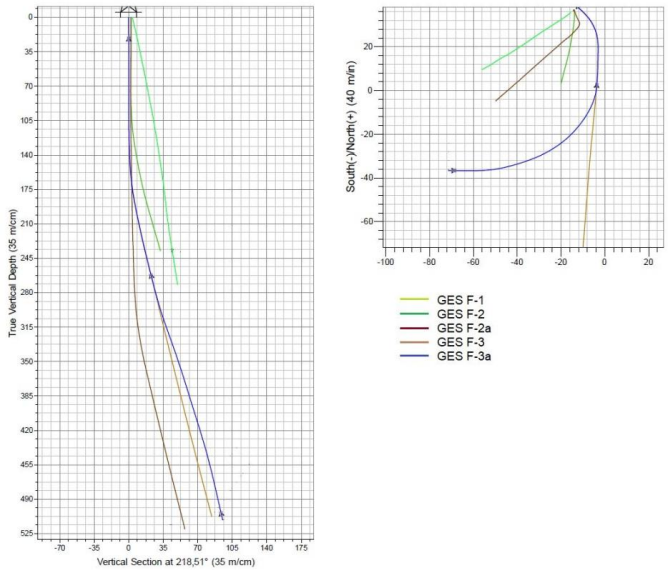


Figure 6. Well paths in vertical section and map view for wells GES-F1-2/2A-3/3A.

A total of seven main medium- to coarse-grained sandstone intervals (RG1-7) can be differentiated (Figure 7). The mineralogical composition is dominated by quartz (ca. 50 wt. %) followed by feldspar, mica, and calcite in similar amounts (10-20 wt.%). The clay content of these sandstone samples is between 4 and 13 wt.%. Detrital clasts are bound by two modes of authigenic calcite cement. The structural analysis of the cross-bed sets allows the determination of the approximate orientations of the channel belt sandstone, which have been used to construct a 3D geometric model of the explored USM interval (Figure 8).

Measured porosities range from 0.018 to 0.217, with a mean value of 0.13 and standard deviation of 0.043. Permeability values range between 1.5 µD and 587 mD ($1.4 \cdot 10^{-18}$ - $5.8 \cdot 10^{-13}$ m^2). For sand-rich reservoir units, permeability is usually in the range of 20-50 mD. Porosity and permeability measured in the lab correlate linearly with a high correlation coefficient. Sediment grain size is typically the main control on porosity and permeability. To a lesser extent, increasing calcite cementation reduces permeability. The measurement of the thermal conductivity of sandstone samples yields very similar wet thermal conductivity values between and 3.48 and 3.65 W/mK. For the mudstone samples, the thermal conductivity is between 1.88 and 2.42 W/mK. Calibrated thermal fluxes retrieved from the fiber-optic data are in the range 0.06 to 0.08 W. Calibrated thermal conductivity of the Quaternary sediments shows a stable value of 2 W/mK and the USM sandstone layers are in the range of 1.74 to 2.30 W/mK. Claystone thermal conductivities are in the range of 1.88 to 2.93 W/mK. Calculated geothermal gradients are in the range 31.4 to 35.2 °C/km. A summary of measured petrophysical properties is displayed in Figure 9.

Initial hydraulic tests conducted during drilling operations indicated low transmissivity of the sandstone layers, which hinders the storage and recovery of excess heat. Both F2A and F3A underwent micro-side-track drilling through the casing, intersecting a sandstone horizon (horizon 6c) at depths of 495- and 502-meters depth, respectively. Overall, 19 micro-side-tracks were drilled, with depths of penetration (highly uncertain) ranging from 1-2 cm to more than one meter. Subsequent hydraulic tests revealed no improvement in transmissivity. Following the micro-side-track drilling, high-pressure water was injected to achieve pressures above jacking that stimulated the sandstone. The results of the stimulation were tested with a heat injection campaign. To further enhance transmissivity, diluted CO_2 was injected into interval 6c of F3A in July and September 2024. The final assessment of the results achieved in well F3A was performed in December 2024 after an extended production period. The evolution of hydraulic parameters is described in detail below.

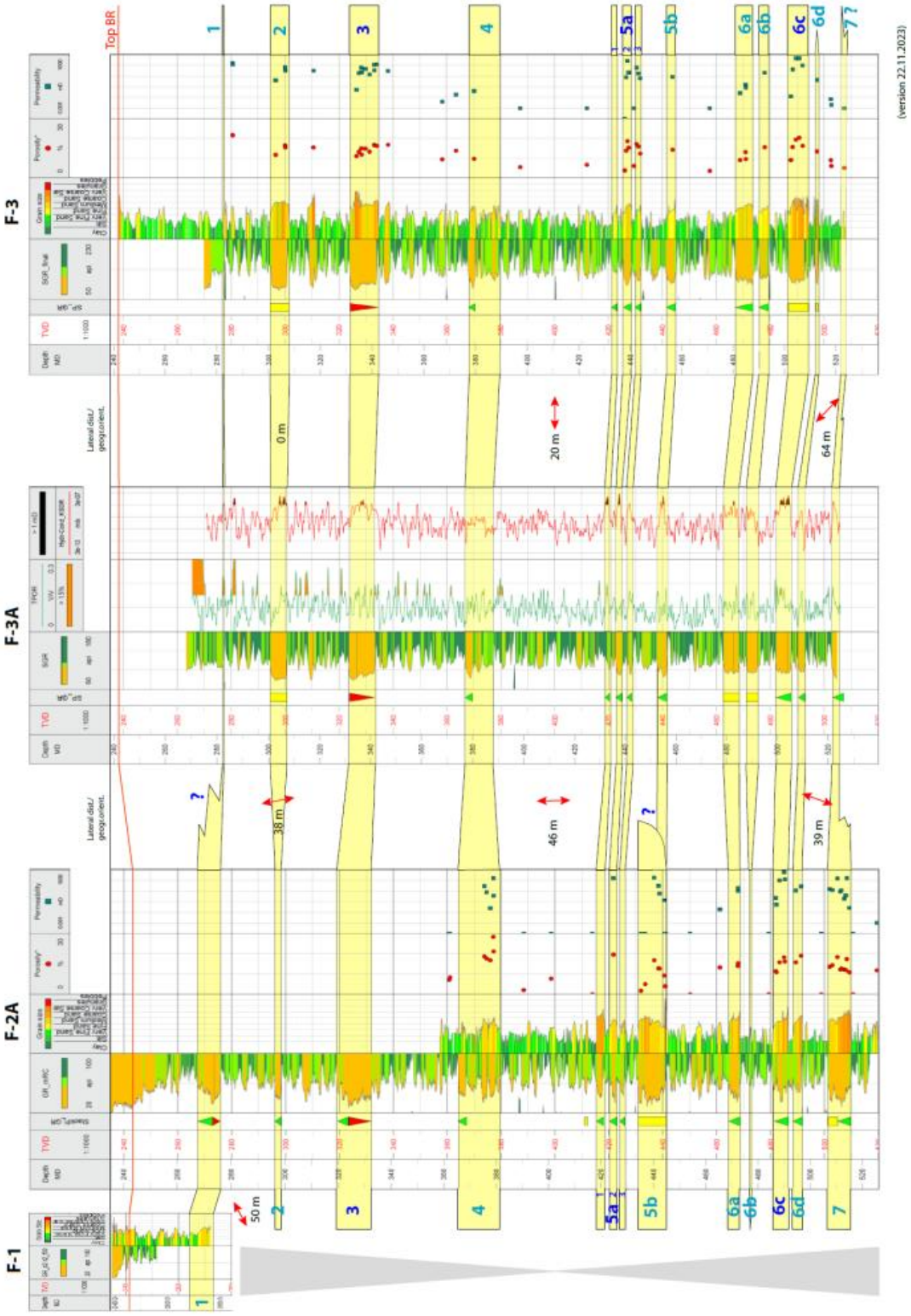


Figure 7. Correlation of main reservoir units RG (channel belt sandstones) in the explored USM, based on the GR/grainsize profiles. Measured porosity/permeability data in wells F2A and F3 compares with porosity/hydraulic conductivity logs (NMR) in well F3A. Red arrows indicate the geographic orientation and distance between the wells of comparable depth points.

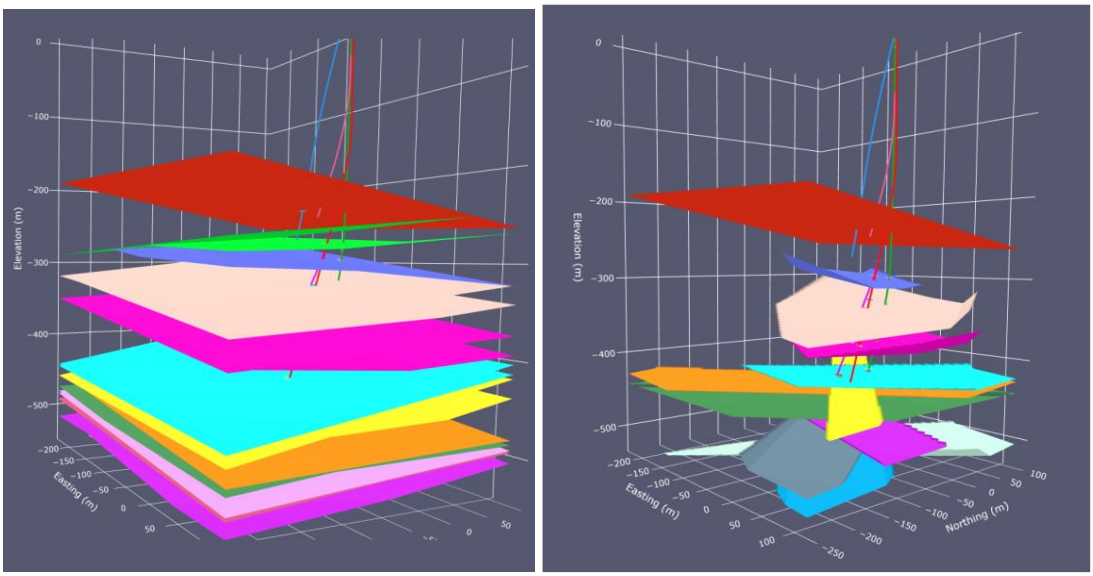


Figure 8. 3D model of the so-called “optimistic” and “pessimistic” scenarios (left and right, respectively) showing different reservoir lateral extension. Only the base of each reservoir is shown for clarity.

Figure 10 and Figure 11 display the timing of operations and the history of estimated parameters, respectively. The initial characterization campaign involved 18 slug tests and concluded that formation transmissivity of horizon 6c had a uniform value of $2 \cdot 10^{-7}$ m²/s, and an average storage coefficient of $2 \cdot 10^{-5}$. These values are considered baseline figures for evaluating the effectiveness of the implemented measures aimed at enhancing formation transmissivity and connectivity between boreholes.

The first stimulation cycle in interval 6c of well F3a detected a low-transmissive skin zone, with an estimated radius of 3m and a transmissivity of 5·10⁻8 m²/s. Subsequent injection cycles involving pressures above the jacking pressure cleared this skin-zone and interval 6c around F3A came back to the uniform baseline value of $2 \cdot 10^{-7}$ m²/s. Similarly, a positive skin zone with radius 2.1 meters and a low transmissivity $2.5 \cdot 10^{-8}$ m²/s. After two high-pressure injection cycles, the transmissivity of the skin zone around F2A increased to $6.5 \cdot 10^{-8}$ m²/s, still below the baseline value of $2 \cdot 10^{-7}$ m²/s. After producing from well F2A transmissivity further increased to the baseline formation value of $2 \cdot 10^{-7}$ m²/s. The presence of positive skin zones with limited extent is attributed to the invasion of mud (or fine particles) into the formation during early stages of hydraulic testing. High-pressure injections or production with high flow rate were sufficient for removing the fine particles around the borehole, but did not enhance the transmissivity of the formation.

The injection of heat into interval 6c of well F3A was hindered by insufficient injection flow rate, unable to compensate heat losses along the tubing. As a result, the experiment was unsuccessful in transporting heat from the surface to interval 6c at a depth of 500 meters. The flushing (injection of cold water) of well F1 yielded excellent results, revealing the gravel shallow aquifer as a potential heat storage reservoir.

The results during and after CO_2 injection revealed the presence of a highly transmissive skin zone around well F3A, with an estimated radius of 2.5 meters, a transmissivity of $5.1 \cdot 10^{-7}$ m²/s, and a storage coefficient of $1.6 \cdot 10^{-5}$. These findings indicate a moderate and local enhancement of transmissivity due to CO_2 injection over a small area around F3A. In contrast, the transmissivity of the formation remained unchanged from pre-injection values, maintaining at $2.2 \cdot 10^{-7}$ m²/s, the storage coefficient averaging $1.6 \cdot 10^{-5}$.

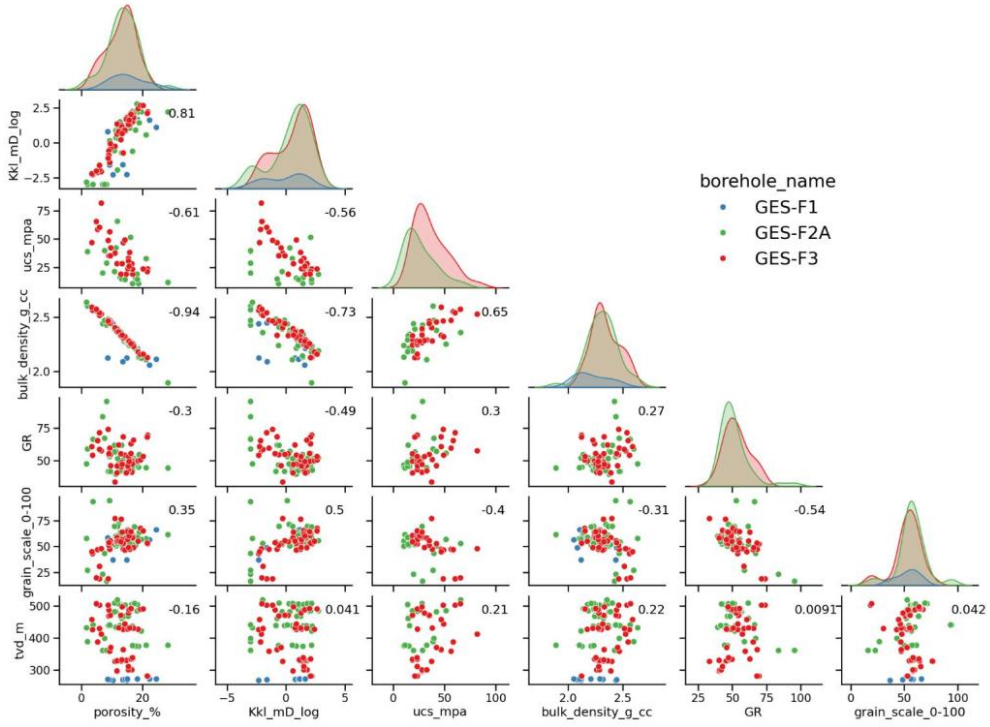


Figure 9. Summary of measured petrophysical properties.

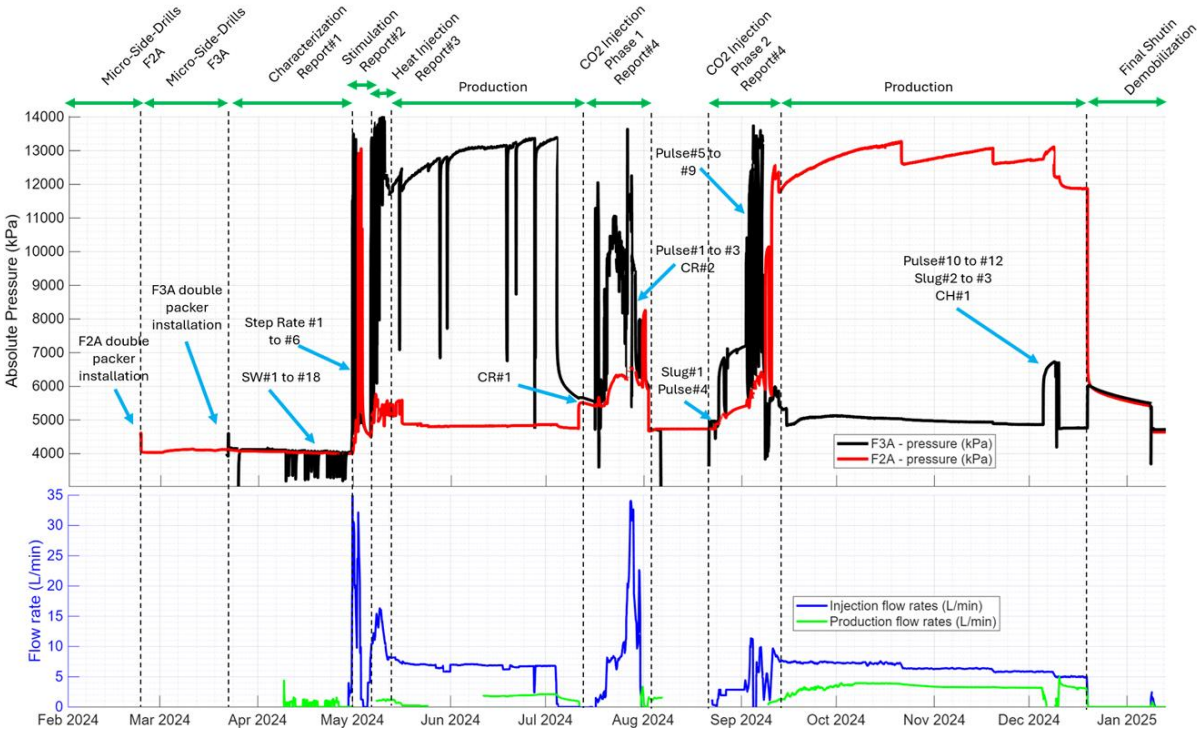


Figure 10. Overview of operations conducted in wells F2A and F3A, including the micro-side-drill campaigns, the initial characterization phase, a stimulation phase, two CO_2 injection phases and a production phase. Arrows and corresponding insets indicate the timing of key events and hydrotests performed during each campaign.

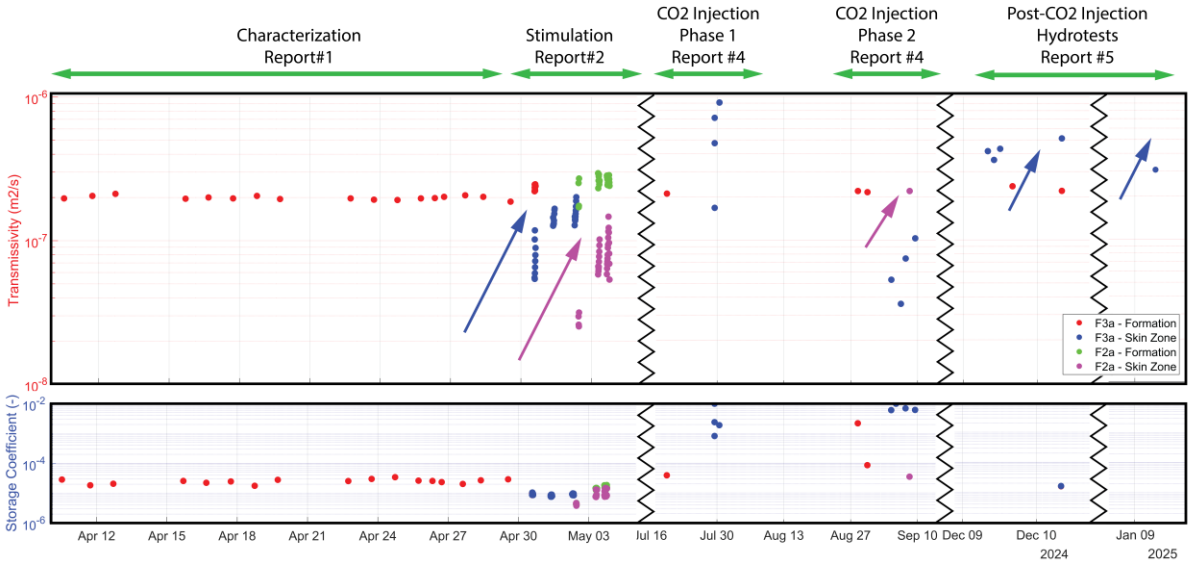


Figure 11. Summary of the calibrated parameters of both skins and formation. Temporal gaps where no hydrotests were conducted are indicated by zig-zag lines. The formation transmissivity and storage coefficient consistently show values of $2 \cdot 10^{-7}$ m²/s and $2 \cdot 10^{-5}$, respectively, across all hydrotests. The stimulation campaigns indicate the elimination of the positive skin zone (characterized by lower transmissivity) around both F3A and F2A (highlighted by blue and magenta arrows), with values improving from $5.0 \cdot 10^{-8}$ m²/s to near formation baseline transmissivity. The CO_2 injection campaigns show a general enhancement in transmissivity in F2A (magenta arrow) and F3A. These results were confirmed by final hydrotests in December 2024 and January 2025, which show a 2-fold increase in transmissivity over a 2.5 m skin-zone around F3A (blue arrow).

Following the stimulation of interval 6c in borehole F3A, a long circulation test was conducted. During the test, dilute surface water was injected in the aforementioned interval, while F2A was used as monitoring well. After approximately 50 days of injection at a rate of 8 L/min, resulting in a total injected volume of 622 m³, breakthrough of dilute water was detected in F2A through a decrease in the EC (electrical conductivity). This test provided constraints on the composition of the pristine saline groundwater originally occupying the pore space of the sandstone formation and progressively displaced by the injected water. The chemical composition of this native groundwater was characterized by the Rock-Water Interaction Group at the University of Bern as an independent activity outside the scope and funding of the VESTA-CH project. Therefore, the corresponding analytical results are not presented in this report (see project HEATSTORE - https://www.aramis.admin.ch/Texte/?ProjectID=41461 - for further details). However, they have been incorporated into several of the numerical simulations presented in the following sections.

To prepare for the subsequent and final hydraulic testing, F3A was shut for five days while the injection in F2A continued, allowing the pressure to stabilize and reach steady state conditions. After this shut-in period, five hydraulic tests were performed on December 9, 2024 (Pulses #10 to #12, Slug #2, and Constant Head #1) in well F3A to ascertain the spatial distribution of transmissivity around horizon 6c of well F3A. This was followed by a three-weeks shut-in period in both wells, after which a final test (Slug #3) was performed on January 9, 2025. The results reveal the presence of a high-transmissivity skin zone around well F3A, with an estimated radius of 2.5 meters, a transmissivity of $5.1 \cdot 10^{-7}$ m²/s, and a storage coefficient of $1.6 \cdot 10^{-5}$. These findings suggest that CO2 injection induced a moderate enhancement in transmissivity in the closest vicinity of the borehole (factor two increase). In contrast, the transmissivity of the surrounding formation remained consistent with pre-injection values at $2.2 \cdot 10^{-7}$ m²/s, the average storage coefficient being $1.6 \cdot 10^{-5}$ ($4.0 \cdot 10^{-5}$ before).

It can be concluded that the different stimulation techniques, both hydraulic and chemical, had only a limited effect. This is attributed to the very low initial transmissivity of the expectedly conductive layers. For future HTS projects, it is therefore recommended to consider the use of proppants in such ultra-low-permeability sedimentary formations.

2.3 Objective 1. Wellbore simulation and optimization of HTS design and performance. Conceptual developments

Before running the more complex fully coupled reservoir-wellbore simulations, a series of simplified synthetic wellbore simulations was performed by KIT and GES to investigate the sensitivity of wellbore behaviour to key operational boundary conditions, including injection temperature, injection rate, and wellhead pressure. The primary objective was to quantify their influence on the temporal evolution of pressure and temperature profiles along the wellbore and to identify the dominant controls on system performance.

The simulations were based on the well design adopted for the Bern-Forsthaus HTS project (Figure 12). Unless otherwise stated, all simulations were performed using the parameters listed in Table 2, and a single permeable layer located at the bottom of the well was represented as a free-flow boundary in most cases. A simulation period of 30 years was selected to evaluate the long-term response of the system. Constant boundary conditions were imposed at the wellhead throughout the simulation period, thereby excluding the cyclic loading and unloading conditions typically associated with seasonal heat storage. This simplification allows the influence of each operational parameter to be evaluated independently and facilitates interpretation of the results.

For the present sensitivity study, and to isolate the effects of the operational parameters, a simplified modelling approach was employed in which only the wellbore domain was considered. Thus, thermal interaction between the wellbore and the surrounding formation along the cased section was neglected. This assumption is justified by the very short thermal equilibration time observed under typical HTS operating conditions. Figure 13 illustrates the evolution of fluid temperature at the bottom of the wellbore for a range of representative injection rates, considering conductive heat exchange with the surrounding formation according to the analytical solution of Ramey (1962). The results show that fluid injected at a surface temperature of 90°C rapidly reaches near-equilibrium downhole temperatures, initially at 28°C, largely independent of the injection rate. Consequently, conductive heat losses along the cased section have a negligible influence on the long-term thermal behaviour of the system and can be neglected in the synthetic calculations presented herein. The adopted simplifications significantly reduce computational requirements while preserving the physical processes governing the sensitivity of wellbore pressure and temperature to operational boundary conditions. However, under low-flow transient operational environments, as observed in actual Swiss pilot sites, wellbore heat loss is a primary failure mechanism that cannot be ignored in practical engineering designs.

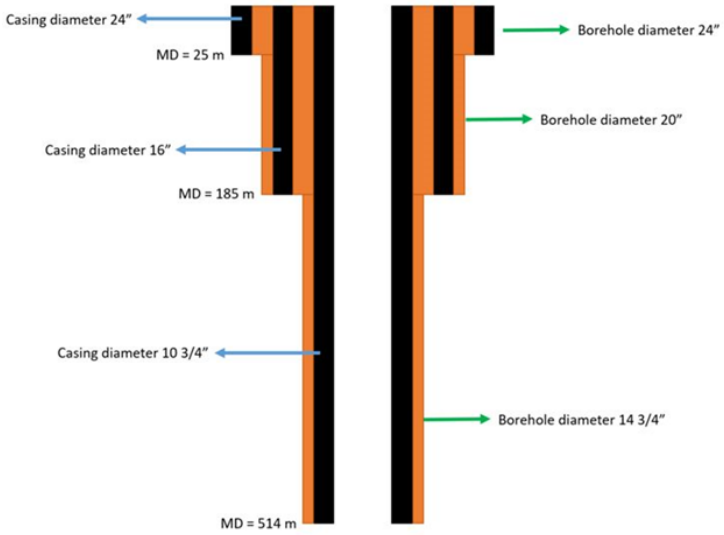


Figure 12. Sketch of the wells at Bern Forsthaus.

Table 2: Input parameters used for the synthetic sensitivity analysis of the response of primary variables to operational boundary conditions. To isolate the influence of the selected operational parameters, conductive heat exchange between the wellbore and the surrounding formation was neglected in these initial simulations.

Fluid properties	**Value**	**Unit**
Density of fluid	985	Kg/m^3
Specific heat capacity of fluid	4180	J/kg/K
Thermal conductivity of fluid	0.6	W/mK
Rock properties		
Permeability of impermeable layer	$2.6 \cdot 10^{-17}$	m^2
Permeability of permeable layer	$3.45 \cdot 10^{-13}$	m^2
Geothermal gradient		
Surface temperature	10	°C
Temperature gradient	30	K/km

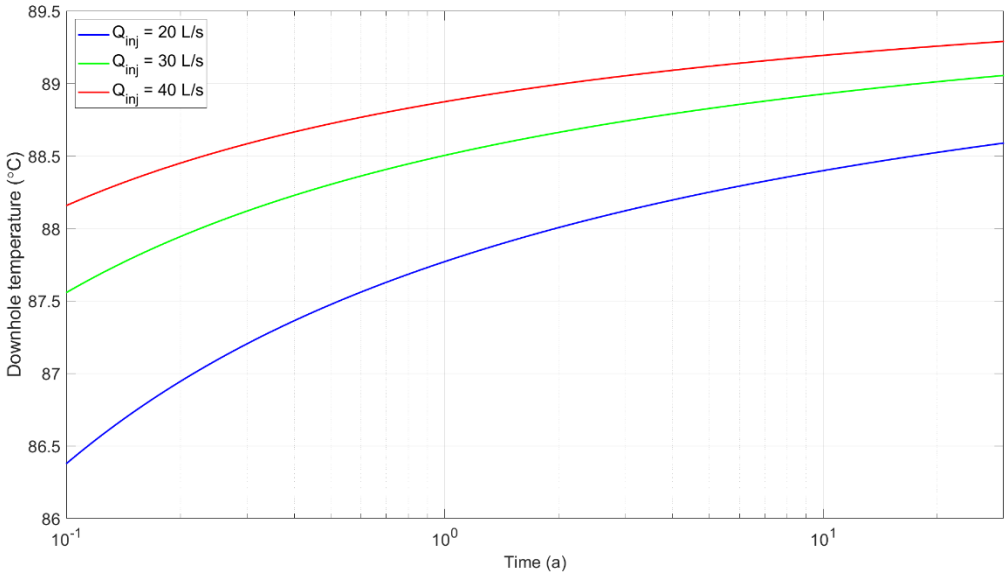


Figure 13. Temporal evolution of fluid temperature at the bottom of the well (measured depth, MD = 600 m) for different injection rates, accounting for conductive heat exchange between the wellbore and the surrounding formation according to the analytical solution of Ramey (1962). The initial formation temperature at MD = 600 m is approximately 28°C. Following the onset of injection at 90°C, downhole temperatures increase rapidly and approach thermal equilibrium, largely irrespective of the injection rate. This demonstrates that, under high flow rate circulation, conductive heat exchange along the cased section of the well has only a minor influence on the long-term thermal behaviour of the system under typical HTS operating conditions.

2.3.1 Impact of injection temperature on fluid temperature

Figure 14 shows the temporal evolution of fluid temperature at the bottom of the wellbore (i.e., the open-hole section) for two different injection temperatures, T_{inj}=50°C (typical reinjection temperature during the unload cycle) and T_{inj}=90°C (load cycle). In both cases, a constant flow rate of 25 L/s was applied at the wellhead. Regardless of injection temperature, a first drop, caused by mixing processes and by the downward propagation of the thermal front through a wellbore that is initially in thermal equilibrium with the geothermal gradient (and therefore colder). This temperature drop largely depends on the initial temperature profile.

Following this initial adjustment period, bottomhole temperatures increase rapidly before gradually approaching the imposed injection temperature. This behaviour is governed by the thermal interaction between the injected fluid and the wellbore components, and between the wellbore and the surrounding formation, the latter neglected in this calculation. At early times, the casing and cement sheath are significantly colder than the injected fluid, resulting in large temperature gradients and therefore high conductive heat fluxes from the fluid to the surrounding well structure. Because the thermal energy transported by the injected fluid exceeds the energy required to heat the casing and cement, the wellbore warms up rapidly and fluid temperatures increase accordingly. As the casing and cement progressively approach the temperature of the injected fluid, the temperature gradients diminish and heat losses decrease. The system therefore evolves asymptotically towards thermal equilibrium, resulting in a progressively slower temperature increase at late times.

The same physical mechanisms would operate if heat exchange with the surrounding formation was explicitly considered. The main effect of the formation would be to increase the thermal mass of the

system, thereby extending the duration of the transient regime and smoothing the temperature evolution. However, the overall behaviour and equilibrium conditions would remain essentially unchanged.

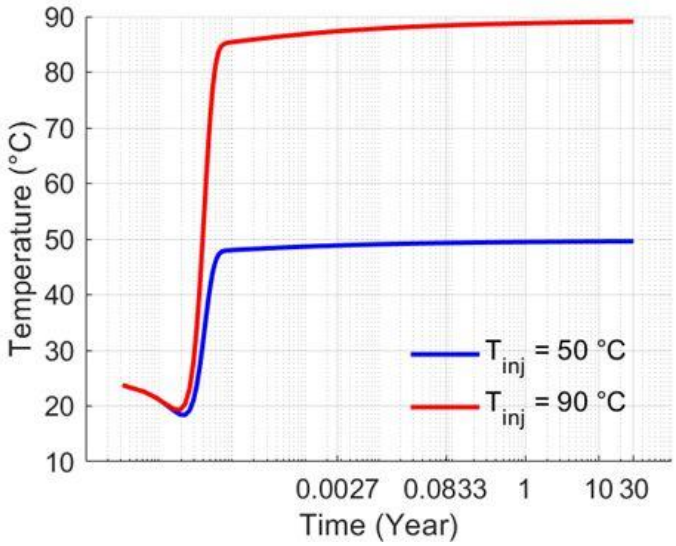


Figure 14: Impact of injection temperature on fluid temperature at the bottom of the wellbore. The injection temperatures of 50°C and 90°C represent typical unload-cycle reinjection and load-cycle injection conditions, respectively. A constant injection rate of 25 L/s was imposed in both simulations.

The corresponding temperature distributions along the wellbore are shown in Figure 15 for four representative times. In both scenarios, temperature decreases with depth. At early times, this behaviour results from the progressive transfer of heat from the fluid to the colder wellbore components, which reduces the thermal energy available to heat deeper sections of the well. At later times, when the wellbore approaches thermal equilibrium, the remaining temperature gradient is primarily controlled by the geothermal gradient, which results in greater heat losses in the shallower and colder sections of the well. The results further show that the fluid column progressively approaches a quasi-steady thermal state with increasing injection time. Although the absolute temperature level is influenced by the imposed injection temperature, the shape of the temperature profile is largely controlled by the geothermal conditions rather than by the injection temperature itself.

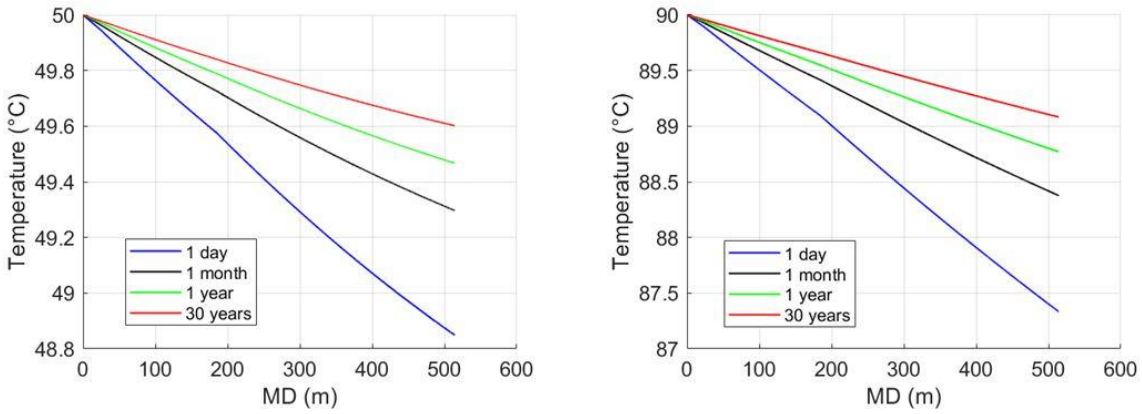


Figure 15: Temperature profiles along the wellbore for injection temperatures of 50°C (left) and 90°C (right).

2.3.2 Impact of injection flow rate on the temperature distribution in the borehole

The influence of injection rate on the thermal response of the well was investigated using the same base model. In all simulations presented in this section, the injection temperature was fixed at 90°C, while injection rates of 15, 25, and 35 L/s were considered. This range of values is typical for HTSs, e.g., 15-20 L/s at Berlin Adlershof (Schwarze et al., 2025), 19.4 L/s at Dingolfing (Dobson et al., 2025), or 27.8-40 L/s as base design at Burgwedel (Zhou et al., 2026). Figure 16 presents the temporal evolution of bottomhole temperature for the three flow rates. As expected, increasing flow rate accelerates the thermal response of the system. Higher injection rates transport larger amounts of thermal energy into the wellbore per unit time, resulting in a more rapid warming of the well and a faster approach towards thermal equilibrium.

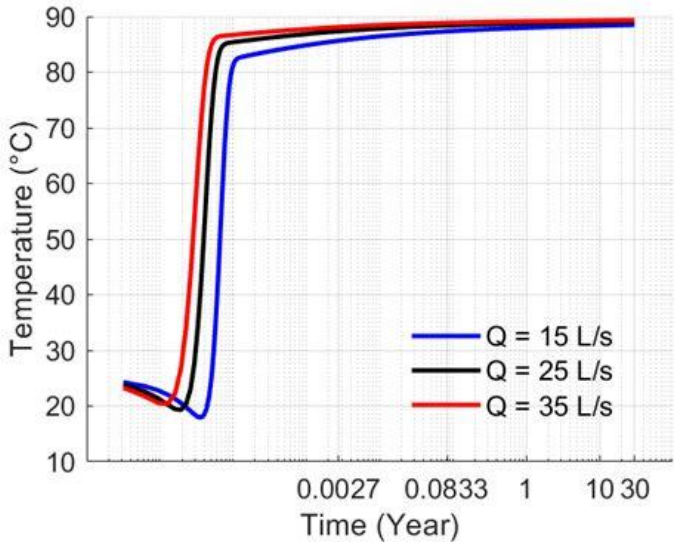


Figure 16. Impact of injection rate on bottomhole temperature.

The effect of injection rate on the temperature distribution along the wellbore is illustrated in Figure 17. For a given injection period, higher flow rates lead to smaller temperature losses along the well because the residence time of the fluid within the well is reduced. Consequently, less heat is transferred from the fluid to the surrounding wellbore components during its downward travel.

As injection continues, the thermal gradient along the well decreases for all flow rates as the casing and cement progressively warm up. The results demonstrate that injection rate exerts a strong control on the transient thermal behaviour of the wellbore, particularly during the early stages of operation, whereas its influence diminishes as the system approaches thermal equilibrium.

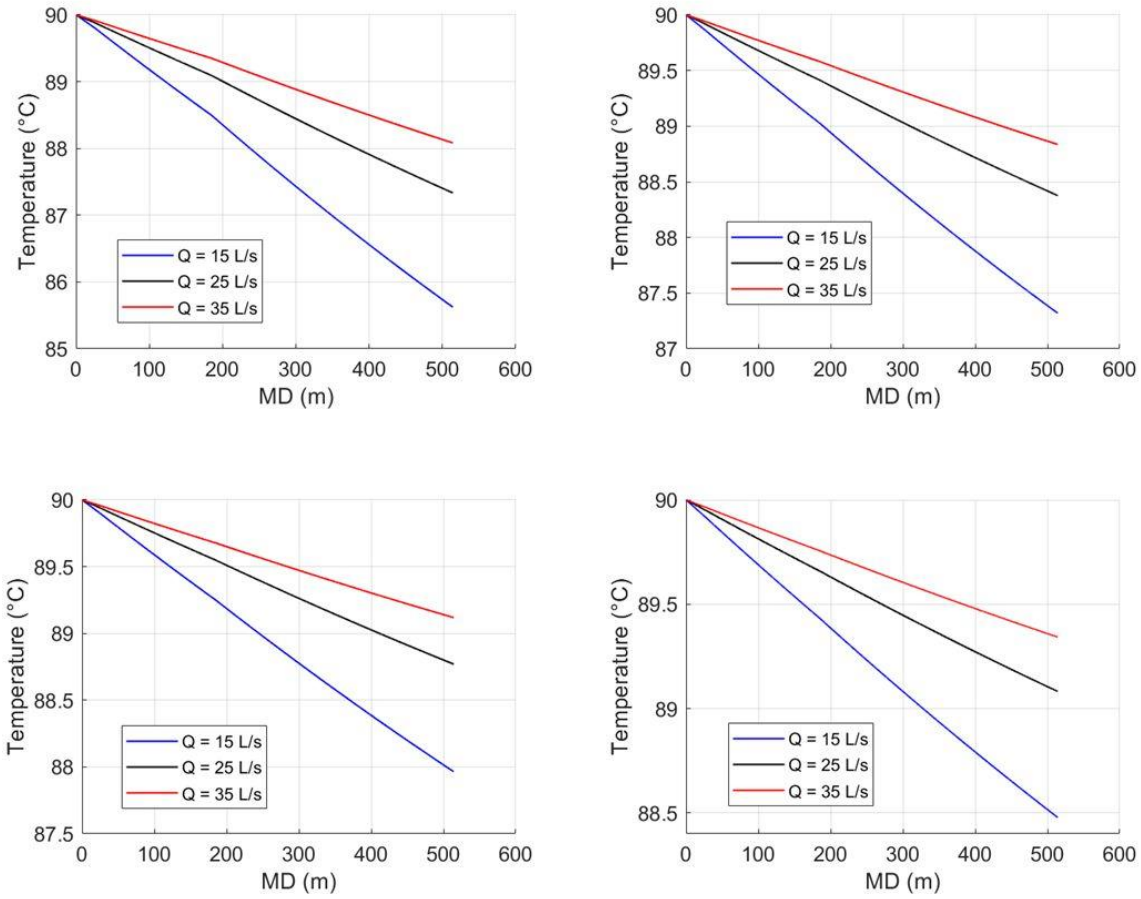


Figure 17. Temperature profiles along the wellbore for different injection rates after one year (left) and thirty years (right) of continuous injection.

However, lower injection flow rates can be expected, e.g., at Bern Forsthaus, in view of the low transmissivity of the conductive layers. In such cases, the hypothesis of small heat losses must be carefully reviewed and a potential insulation of the borehole considered (see section 2.4).

2.3.3 Impact of injection pressure and injection temperature on temperature and pressure distributions

MOSKITO can be operated under either flow-rate-controlled or pressure-controlled boundary conditions. The simulations presented in this section investigate the influence of injection pressure and injection temperature on the pressure and temperature distributions within the well. Unless otherwise stated, simulations were performed using a wellhead injection pressure of 2 MPa, an injection temperature of 90°C, and an injection rate of 25 L/s.

Because the formation is not explicitly represented in the present synthetic calculations, both injection pressure and flow rate have to be specified at the wellhead. This requirement originates from the numerical solution of the Navier-Stokes equations, which requires at least one prescribed-pressure boundary condition. If pressure is specified at the wellhead (i.e., injection pressure, or overpressure above static), the influence of this numerical artifact is meaningless, as shown in Figure 18. In fact, the

simulation using Q=25 L/s leads to the same results as in Figure 14, regardless of injection pressure. Although these calculations have limited physical significance, they provide an important verification of the pressure-controlled implementation within MOSKITO. Such functionality is particularly relevant for future simulations involving prescribed reservoir pressures at inflow boundaries, where pressure-controlled conditions may be required.

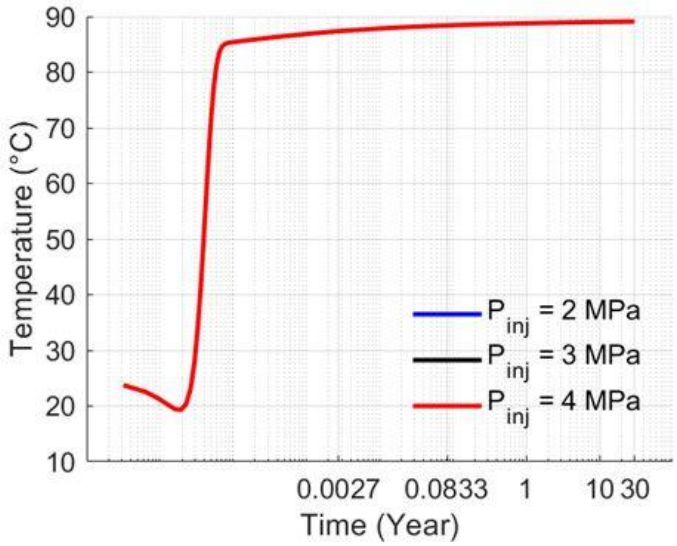


Figure 18 . Influence of injection pressure on bottomhole temperature.

Figure 19 illustrates the influence of injection temperature on pressure evolution within the well. Pressure changes are expressed relative to the initial hydrostatic state. In all cases, pressure increases with depth as a consequence of hydrostatic loading and frictional losses along the well. The simulations further demonstrate a progressive reduction of pressure over time. As the wellbore warms up, fluid density decreases (see section 2.2.5), reducing the hydrostatic contribution to pressure. Simultaneously, temperature-dependent changes in fluid properties influence flow resistance. The resulting pressure evolution is therefore fully consistent with the expected thermodynamic response of the system.

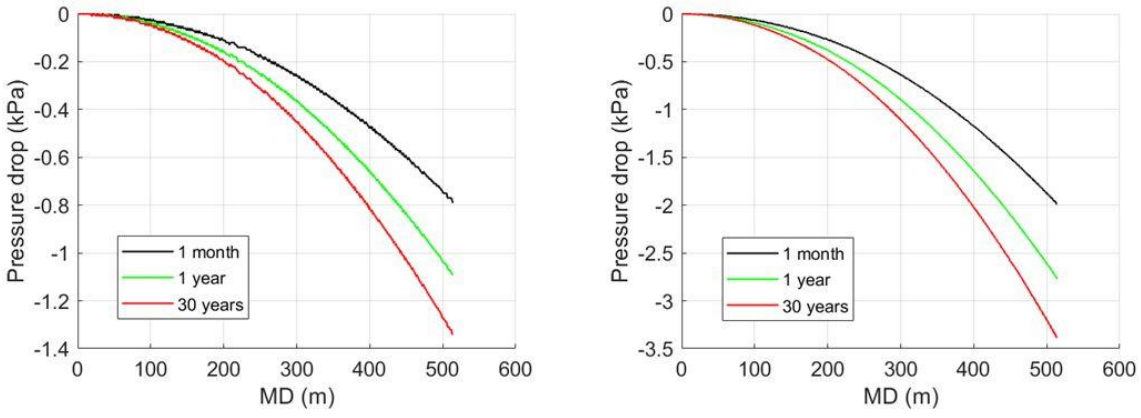


Figure 19. Pressure change relative to initial hydrostatic conditions for injection temperatures of 50°C (left) and 90°C (right).

2.3.4 Impact of additional conductive layers in fluid temperature

The previous simulations assumed that all injected fluid enters the reservoir through a single conductive interval located at the bottom of the well. In reality, however, heterogeneous reservoirs such as the Lower Freshwater Molasse (USM) at Bern-Forsthaus commonly contain multiple permeable layers that may contribute to fluid exchange with the wellbore. To investigate the influence of such conditions, an additional conductive layer was introduced at a depth of 403 m below ground level. In this scenario, 10 L/s of the total injection rate of 25 L/s enters the formation through the upper conductive interval, while the remaining 15 L/s continues towards the deeper target zone. In nature, the distribution of flow between conductive layers is governed by the pressure differential between the wellbore and the surrounding formation and therefore depends on the hydraulic properties of the individual layers. However, because the reservoir is not explicitly represented in the present simulations, the flow partitioning between both intervals was prescribed as a boundary condition. A complete load cycle of eight months was simulated using an injection temperature of 90°C. The resulting temperature profile at the end of the loading period is shown in Figure 20.

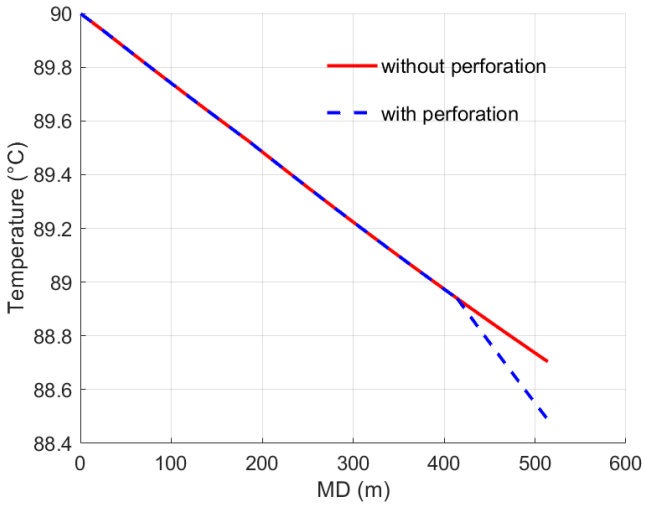


Figure 20. Impact of an additional conductive layer located at 403 m depth on the temperature profile after an eight-month load cycle with an injection temperature of 90°C.

The presence of the additional conductive layer modifies the thermal behaviour of the system by reducing the amount of hot fluid reaching the deepest section of the well. Because a portion of the injected fluid leaves the wellbore at shallower depth, the downward heat transport below the upper conductive interval decreases accordingly. The reduced flow rate in the lower section of the well results in a smaller advective heat flux and a correspondingly lower temperature at depth. As illustrated in Figure 20, the effect on the overall temperature distribution remains moderate. Nevertheless, the results demonstrate that the location and hydraulic contribution of individual conductive layers may influence the thermal efficiency of the storage system by controlling the spatial distribution of injected thermal energy. This effect becomes increasingly important in heterogeneous reservoirs where fluid circulation may be distributed across multiple permeable horizons.

2.3.5 Impact of reservoir temperature in fluid and aquifer properties

Temperature variations induced by HTS operation affect not only the thermal state of the reservoir but also the thermophysical properties of the circulating fluid. These property changes directly influence fluid mobility and, consequently, the hydraulic response of the storage system.

The hydraulic conductivity K [m/s] of a porous medium is controlled by permeability κ [m^2], fluid density ρ [kg/m^3] and viscosity μ [kg/m/s]:

$$K(T) = \frac{\rho(p,T)g\kappa}{\mu(T)} \quad [1]$$

Density is mainly controlled by temperature T [°C] and, to a lesser extent, by pressure of the fluid p [kg/m/s2]. A common definition of fluid density is:

$$\rho(T) = \rho_0 - \beta\,(T - T_0) \quad [2]$$

where β is a commonly applied constant (0.375 $kg/m^3/K$). Instead, viscosity is mainly controlled by temperature:

$$\mu(T) = 239.4{\cdot}10^{7}\cdot 10^{(248.37/(T-273.15+133.15))} \quad [3]$$

The temperature dependence of density and viscosity over the range relevant for the Bern-Forsthaus HTS concept is illustrated in Figure 21. Although the reduction in density tends to decrease hydraulic conductivity, the viscosity reduction is substantially larger and therefore dominates the overall response. As a result, hydraulic conductivity increases significantly with temperature. The resulting hydraulic conductivity enhancement is shown in Figure 22. Relative to the initial reservoir conditions, hydraulic conductivity may increase by a factor of approximately 3-3.5 within the hottest regions of the reservoir during the load cycle, where temperatures approach 90-100°C. Even under unload-cycle conditions, corresponding to temperatures of approximately 50-60°C, conductivity increases by a factor of roughly 1.5-2.5.

These changes have important implications for reservoir injectivity and pressure evolution. Because hydraulic conductivity increases as the reservoir heats up, a given injection rate can be sustained with lower pressure buildup. Conversely, production-induced pressure drawdown is also reduced. The hydraulic behaviour of the system therefore evolves continuously throughout operation as the thermal plume propagates through the reservoir.

This effect is illustrated in Figure 23, which presents the evolution of temperature and pressure at a monitoring location situated 5 m from the injection well during a load cycle. Two simulations are compared: one assuming constant fluid properties and another accounting for the temperature dependence of density and viscosity.

At early times, before the thermal front reaches the monitoring point, both simulations produce nearly identical results because fluid properties remain unchanged. Once the temperature begins to rise, however, the temperature-dependent simulation exhibits a pronounced reduction in pressure buildup. As the reservoir warms and viscosity decreases, fluid mobility increases and pressure dissipates more efficiently. The pressure difference between both simulations progressively increases until thermal equilibrium is reached at the monitoring location.

At late times, the ratio between the pressures predicted using constant and temperature-dependent fluid properties closely matches the corresponding increase in hydraulic conductivity, approximately a factor of three. These results highlight the importance of accounting for temperature-dependent fluid properties when evaluating the hydraulic performance of HTS systems. Neglecting such effects may lead to substantial overestimation of reservoir pressures and, consequently, to overly conservative assessments of injectivity and storage capacity.

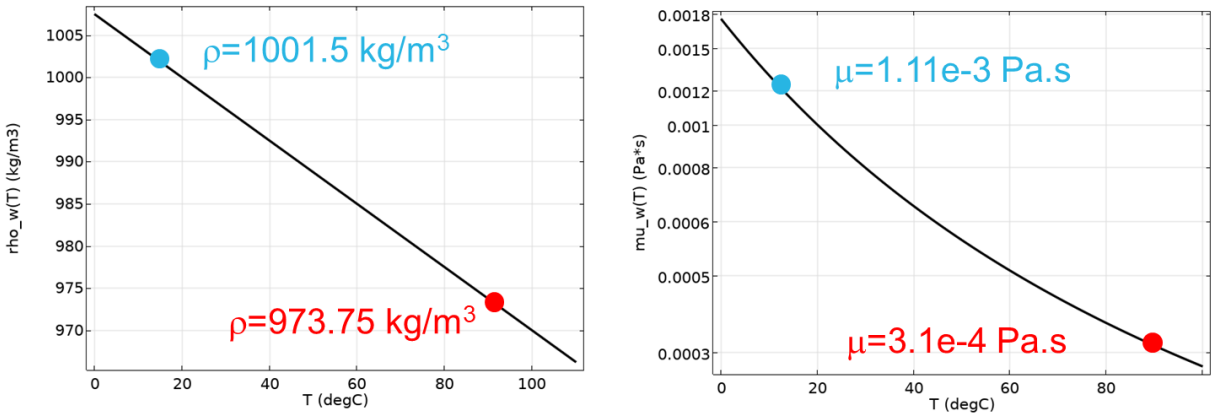


Figure 21 Temperature dependence of fluid density and dynamic viscosity over the expected operating range of the HTS system.

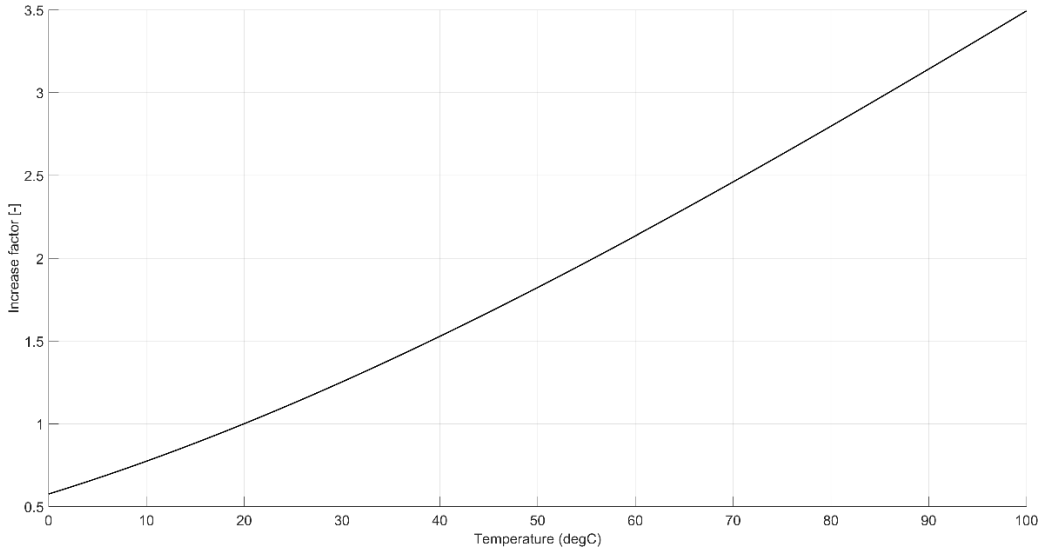


Figure 22. Hydraulic conductivity enhancement factor relative to initial reservoir conditions as a function of fluid temperature.

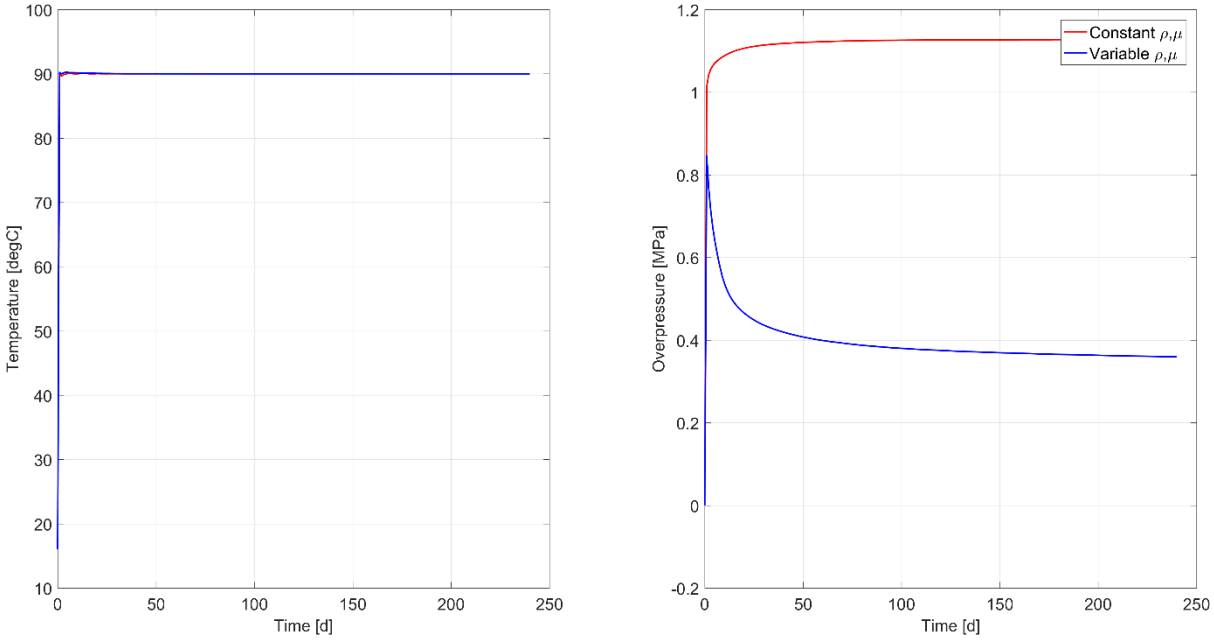


Figure 23 . Evolution of temperature and pressure at a monitoring point located 5 m from the injection well during a load cycle. Comparison between simulations assuming constant fluid properties and temperature-dependent density and viscosity.

2.3.6 Impact of reservoir heterogeneity

The objective of this synthetic exercise is to evaluate the impact of the lateral reservoir heterogeneity on HTS performance. Hydrogeological parameters (Table 3) have been chosen as representative of a generic HTS project, and not out of the hydraulic tests carried out in Bern.

A two-dimensional model representing a heterogeneous sandstone layer with siltstone intercalations was developed. The model domain covers 500 × 500 m and consists of a 5 m thick confined layer located at a depth of 470 m. The layer is bounded above and below by impermeable units, such that vertical pressure diffusion and heat conduction are neglected. The no-flow assumption is justified by the strong horizontal flow induced by the injection-production scheme. However, there is significant vertical heat exchange from the sandstone layer to the surrounding siltstone layers. Two boreholes, represented by injection and production points, are spaced 50 m apart. A surface temperature of 10°C and a geothermal gradient of 0.04°C/m yield an initial reservoir temperature of 29°C. Hydrostatic and geothermal boundary conditions are imposed on all model boundaries and used as initial conditions. One annual operating cycle is simulated, consisting of an 8-month loading period and a 4-month unloading period with a circulation rate of 5 kg/s. The mesh is locally refined around the boreholes (Figure 24).

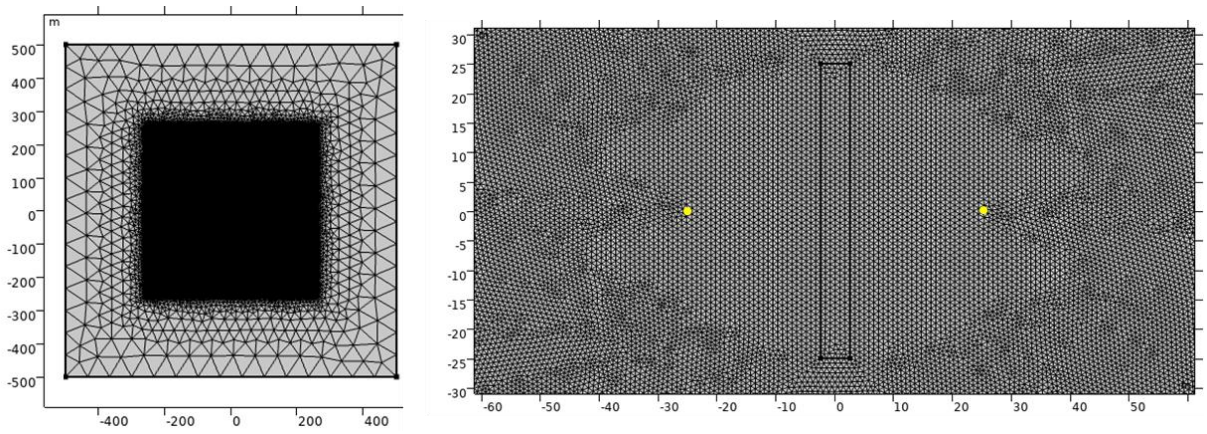


Figure 24. 2D mesh for the modelling of the impact of heterogeneity: (left) global mesh; (right) finely discretized mesh near the boreholes.

Table 3. Solid and fluid parameters for the modelling of the impact of heterogeneity. Note that the mechanical effect is not considered. A= $2.1 \cdot 10^{-12}$ MPa·s and B=1808.5 K for the calculation of water viscosity.

			Sandstone	**Siltstone**	**Fluid**
Thermal conductivity	λ	W/mK	2.67	2.68	0.6
Specific heat	C	J/kgK	1037	881	4180
Density	ρ	kg/m^3	2535	2435	$\rho(p,T) = \rho_0 exp[\alpha T]$
Viscosity	μ	Pa·s	N.A.	N.A.	$\mu(T) = Aexp\left[\frac{B}{273.15+T}\right]$
Transmissivity	T	m^2/s	$2 \cdot 10^{-5}$	$2 \cdot 10^{-7}$	N.A.
Porosity	ϕ	-	0.176	0.1	N.A.
Storage coefficient	S	-	10^{-5}	$1 \cdot 10^{-7}$	N.A.
Volumetric thermal expansion	α	K^{-1}	Not consid-ered	Not considered	$-3.4 \cdot 10^{-4}$

Two homogeneous end-member cases, consisting entirely of sandstone or siltstone, are used as references. Heterogeneity is represented by siltstone lenses (70%) embedded within discontinuous sandstone channels (30%). Ten conditional realizations were generated assuming Gaussian facies distributions, sandstone connectivity around both boreholes, and anisotropic spherical variograms with ranges of 50 m/10 m or 10 m/50 m along the x- and y-directions, respectively, a sill of 0.9 and a nugget of 1.

Figure 25 and Figure 26 present the pressure and temperature distributions for the homogeneous cases after the load (t=240 days) and unload (t=365 days) cycles. As expected, pressure diffusion is pseudo-radial and overpressures are significantly higher in the low-transmissivity siltstone case. Temperature distributions are also pseudo-radial because thermal plumes associated with injection and production overlap.

Figure 27 and Figure 28 show representative heterogeneous realizations corresponding to (i) a conductive sandstone channel directly connecting the boreholes ("parallel flow") and (ii) boreholes intersecting

separate channels ("orthogonal flow"). The remaining realizations exhibit similar qualitative behaviour. Comparison of the heterogeneous simulations reveals two key findings:

- The thermal plume remains largely confined within the sandstone channels, where heat transport is dominated by advection. As a result, the heated area is only slightly larger in the orthogonal-flow case.
- Reservoir overpressures are highly sensitive to channel geometry. Maximum overpressures reach approximately 12 MPa when the boreholes are connected by a conductive channel, but can exceed 90 MPa when they are not, owing to the proximity of low-permeability siltstone boundaries that restrict pressure dissipation.

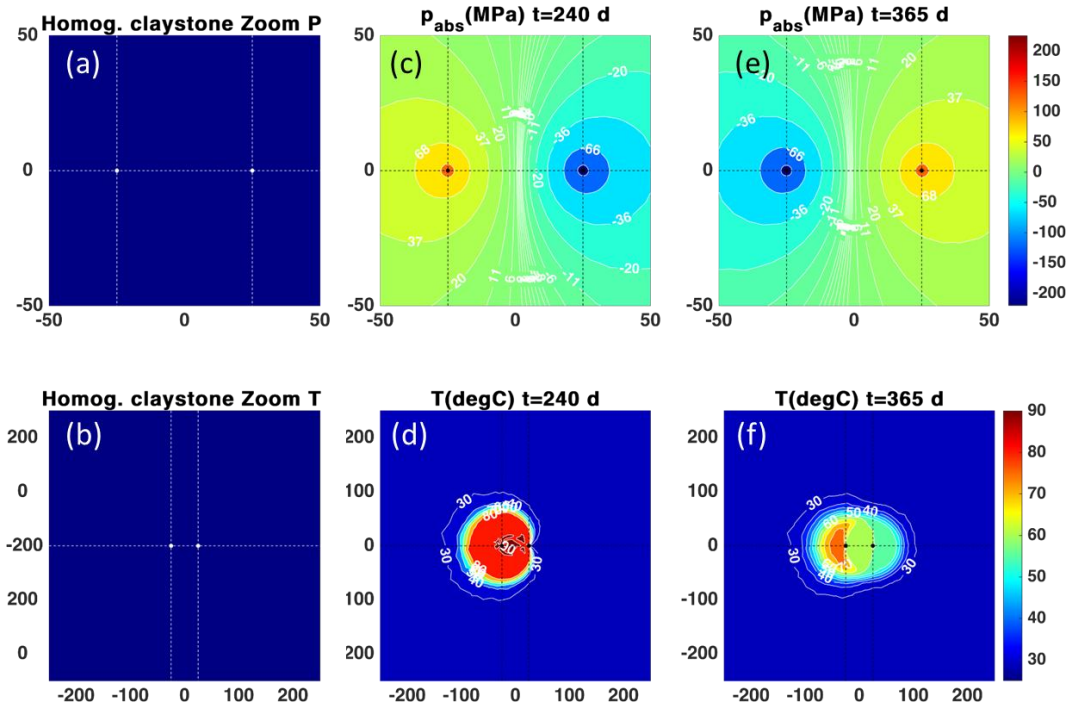


Figure 25. Results for a homogeneous siltstone: (a and b) Location of boreholes; (c and d) pressure and temperature distributions after a load cycle; (e and f) pressure and temperature distributions after the unload cycle.

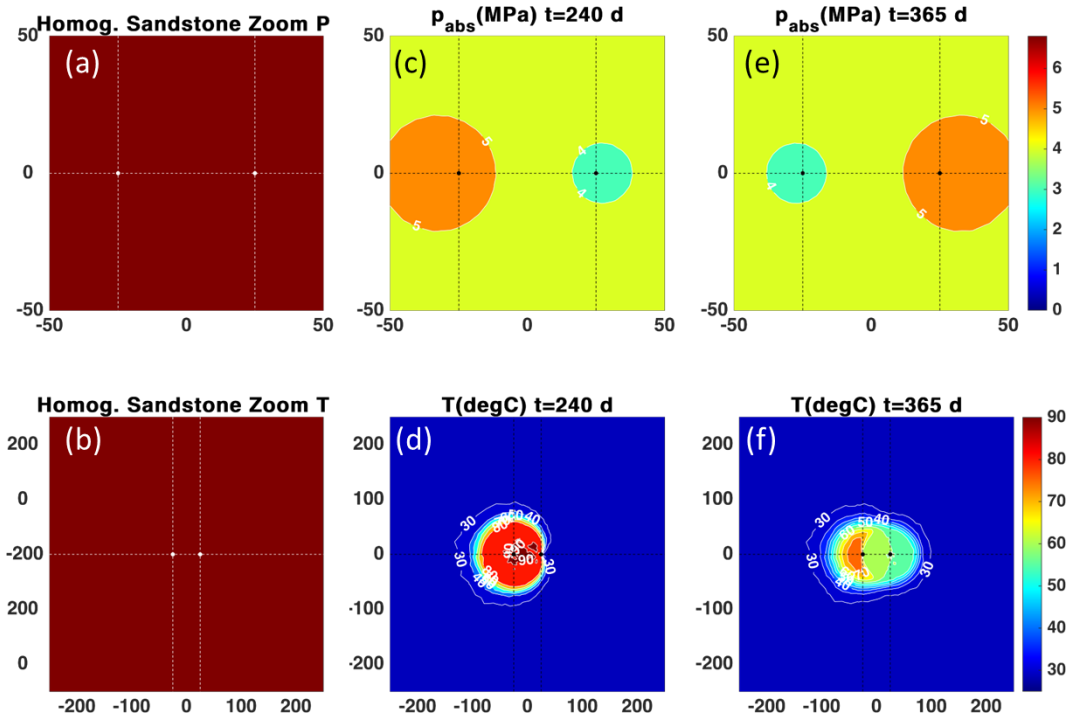


Figure 26. Results for a homogeneous sandstone. See caption of Figure 25.

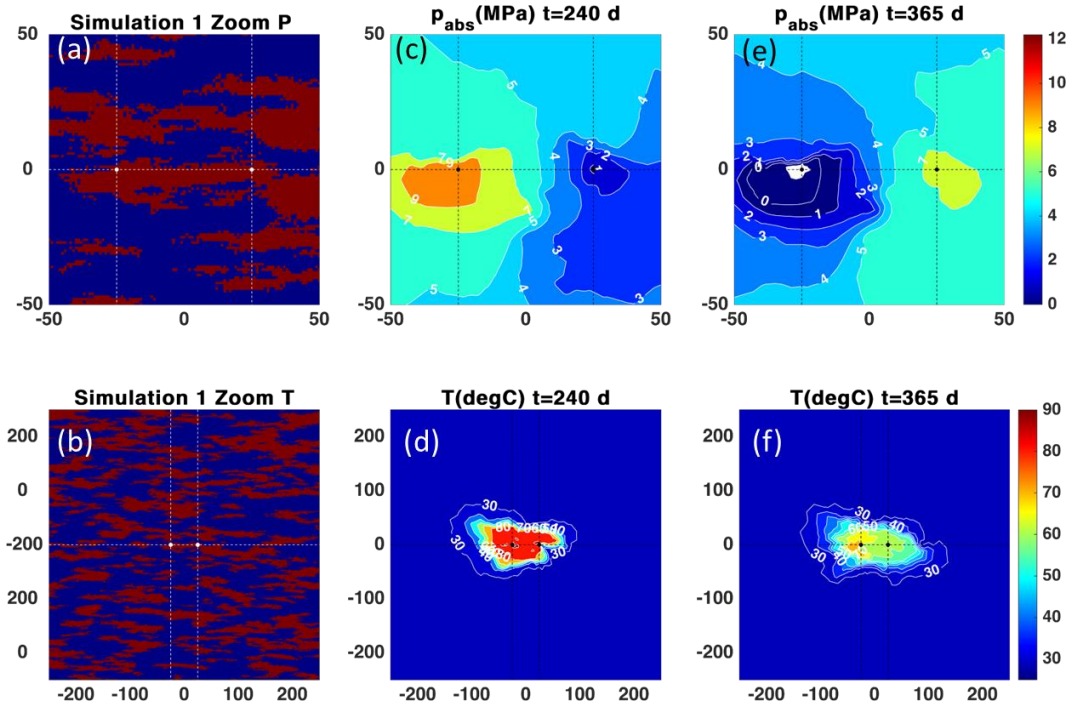


Figure 27. Results for one heterogeneous facies field (sandstone in red; siltstone in blue) assuming parallel flow (i.e., fast flow between boreholes along the channel connecting them). See caption of Figure 25.

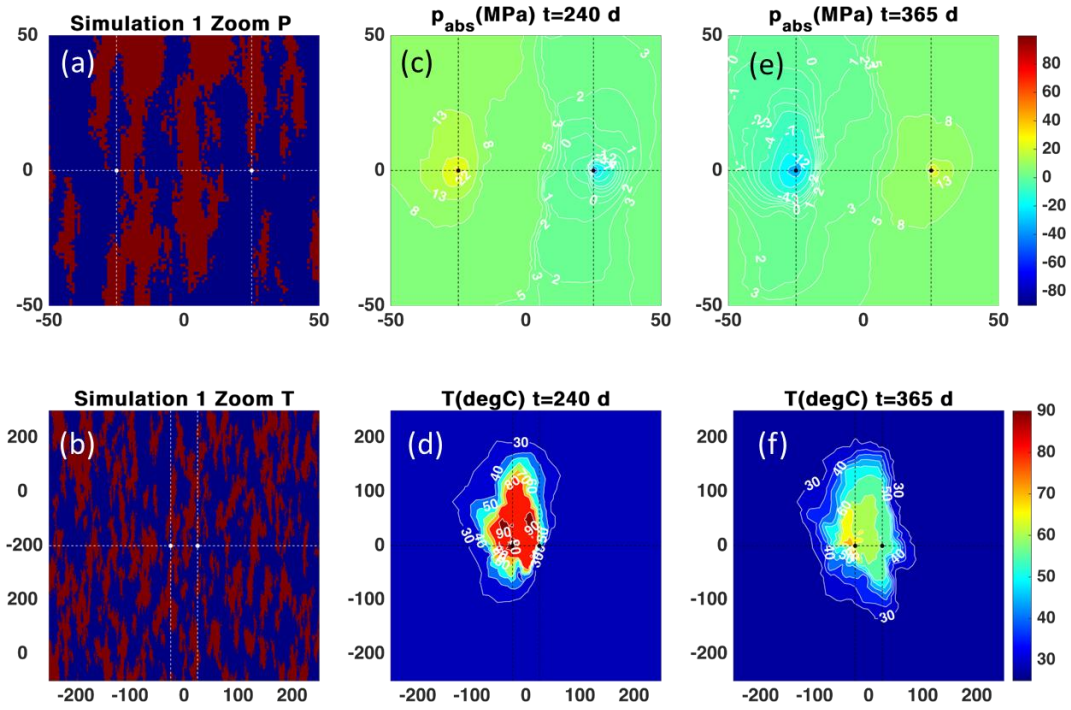


Figure 28. Results for one heterogeneous case (sandstone in red; siltstone in blue) assuming orthogonal flow (i.e., perpendicular flow along various channels. See caption of Figure 25.

Figure 29 illustrates the evolution of hydraulic head at the injection borehole. Significant variability is observed among realizations, primarily controlled by the distance between the borehole and the edge of the transmissive sandstone channel. This distance is typically smaller under orthogonal-flow conditions, resulting in substantially larger pressure buildup. Similar trends are observed at the production borehole.

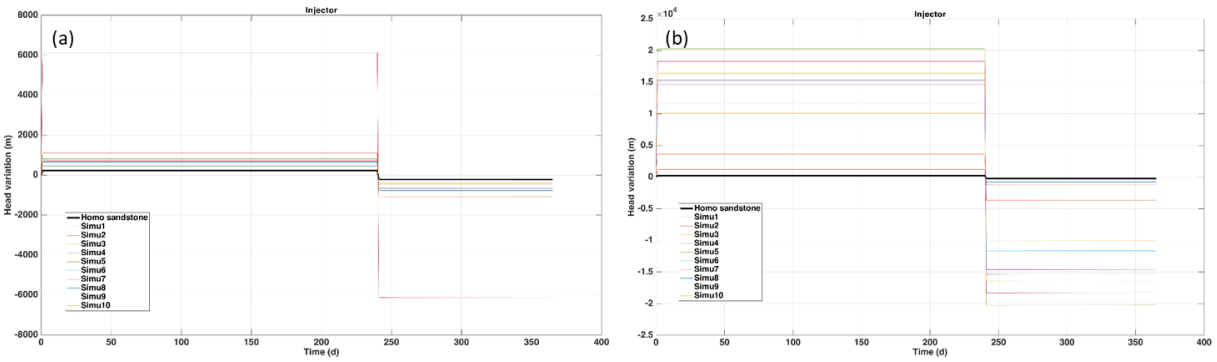


Figure 29. Temporal evolution of hydraulic head at the injection borehole under (a) parallel flow conditions (fast flow between boreholes along the channel connecting them), and (b) perpendicular flow (perpendicular flow along various channels).

Figure 30 compares the temperature evolution at the injection and production wells. Because sandstone and siltstone exhibit similar thermal conductivities, both homogeneous reference cases produce nearly identical thermal responses. In contrast, heterogeneous cases are strongly influenced by channel connectivity. Under parallel-flow conditions, conductive channels connecting the wells promote rapid advective heat transport and premature thermal breakthrough, reducing thermal recovery. Under

orthogonal-flow conditions, direct hydraulic connectivity is limited and heat transport becomes predominantly conductive, resulting in thermal performance comparable to the homogeneous cases. This is best observed in Figure 31, which shows the evolution of the heated area (T > 85°C). The heated volume is considerably larger under orthogonal-flow conditions regardless of the degree of heterogeneity. However, this improved thermal performance comes at the cost of unrealistically high reservoir overpressures when hydraulic connectivity between the wells is poor.

Overall, the simulations demonstrate that reservoir heterogeneity, and specifically the geometry, orientation, and connectivity of permeable sandstone channels, has a first-order impact on HTS performance. While disconnected flow paths may improve thermal storage efficiency, they can also generate pressure increases that are operationally unacceptable. Similar conclusions apply in three-dimensional systems.

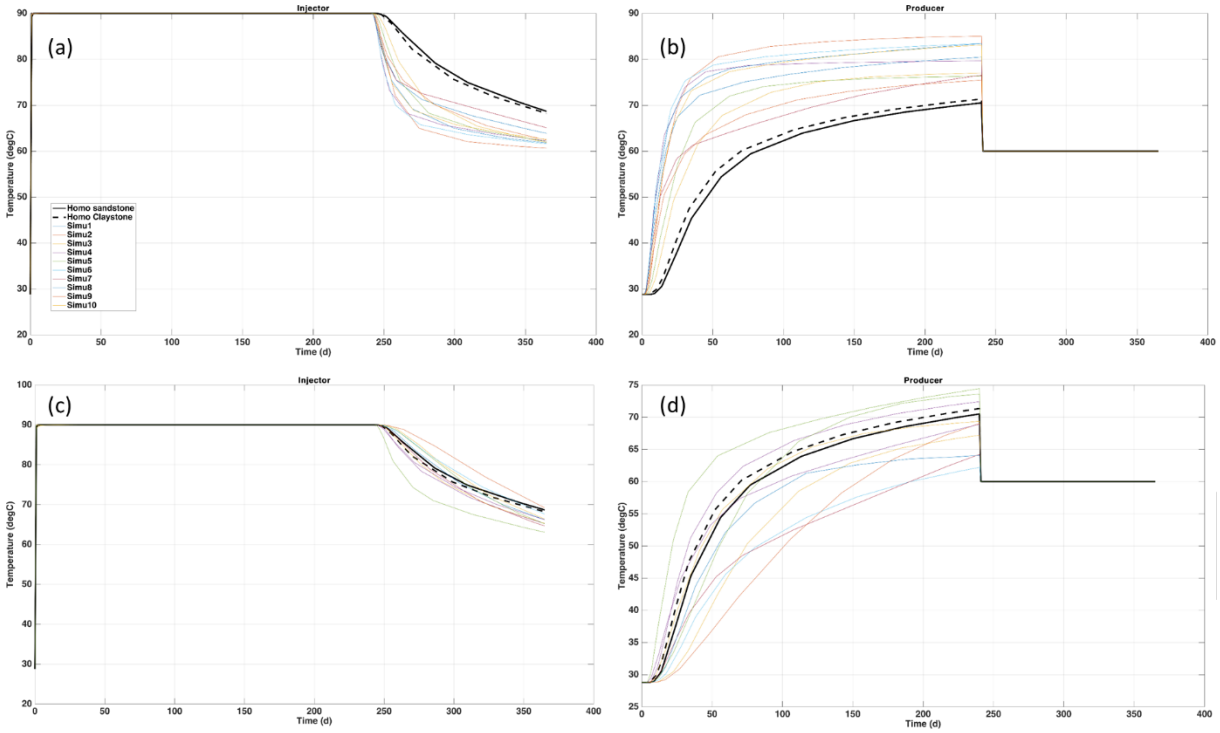


Figure 30. Temporal evolution of temperature at the injection and production boreholes assuming both homogeneous and heterogeneous conditions. Panels a and b: parallel flow case. Panels c and d: perpendicular flow case.

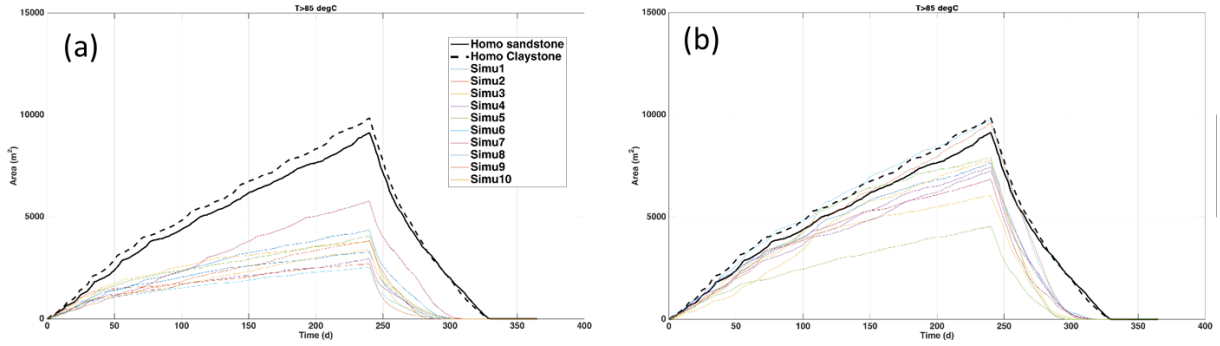


Figure 31. Temporal evolution of heated area (above 85ºC) under parallel (panel a) and perpendicular flow conditions (panel b).

2.3.7 Design of the HTS

A synthetic 3D model inspired by the geological setting and well completion design of the Bern-Forsthaus pilot site, was developed to evaluate (1) the impact of Radial Jet Drilling (RJD), and (2) the effect of the number of auxiliary boreholes on HTS performance. The model comprises a 5 m-thick sandstone layer confined between two 10 m-thick claystone layers (Figure 32). Two HTS configurations were considered, comprising a two-well and a four-well system (Figure 33). The most detailed mesh contains 390'816 tetrahedral elements, with boreholes and radial jets explicitly represented as cylindrical features (Figure 34).

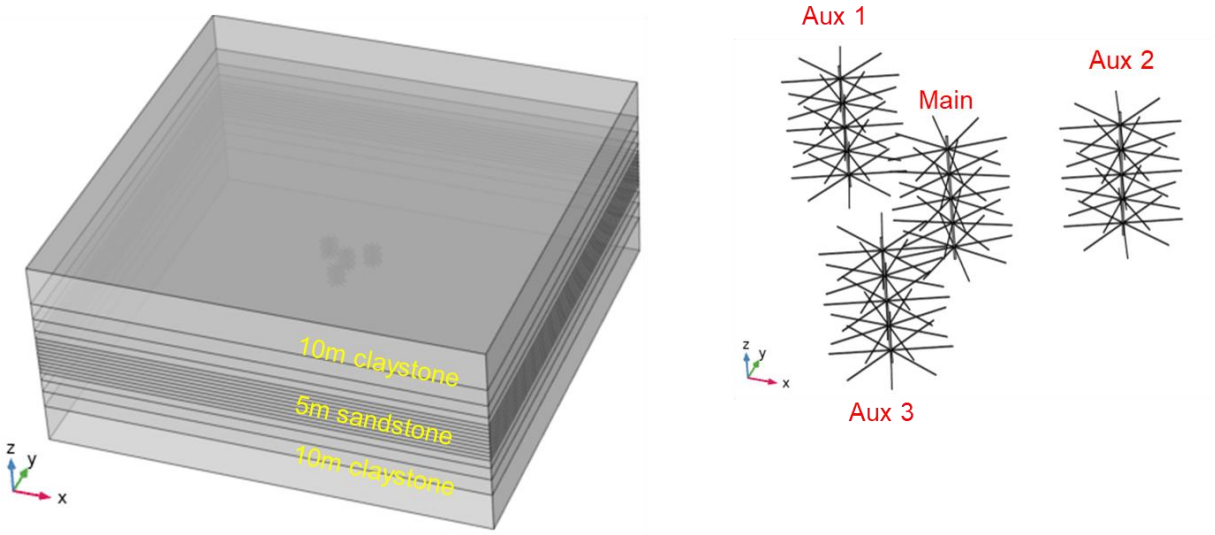


Figure 32. Three-dimensional model setup used to evaluate the influence of the number of auxiliary boreholes and Radial Jet Drilling (RJD) on HTS performance.

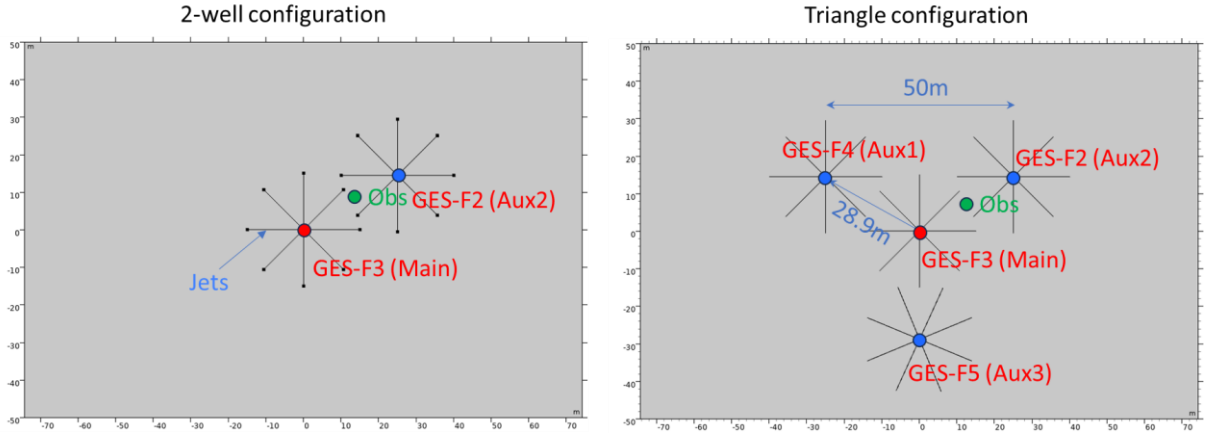


Figure 33. Two-well and four-well configurations representing, respectively, the current layout and the initial target design of the Bern-Forsthaus pilot project.

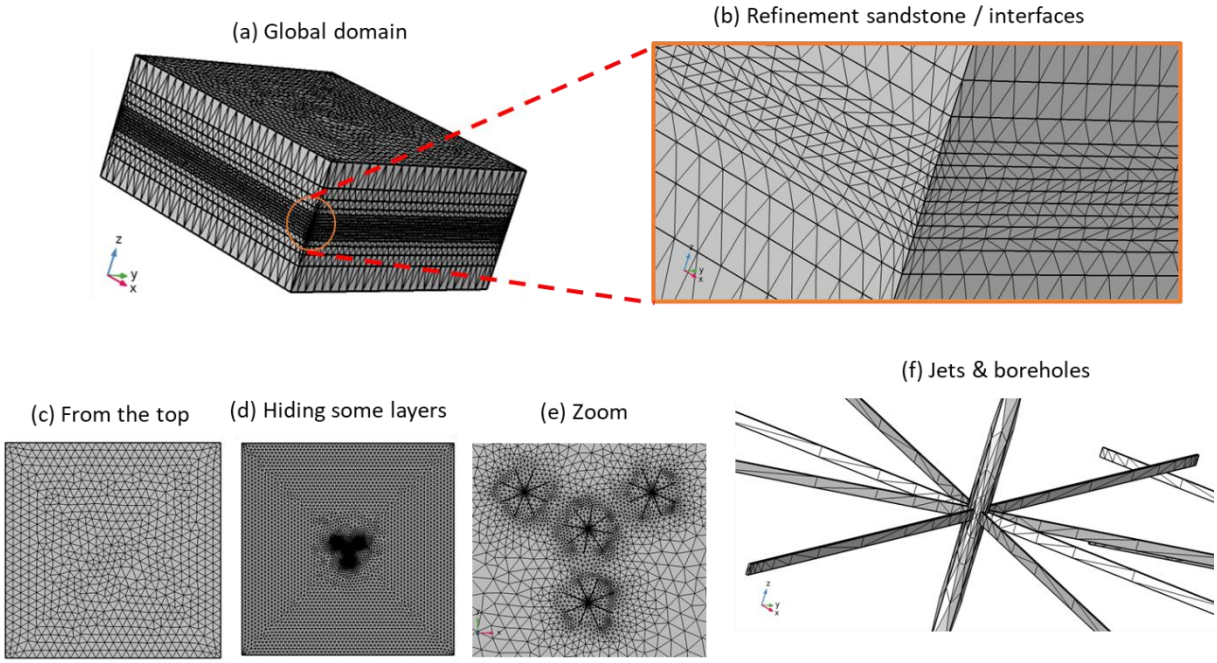


Figure 34. 3D finite-element mesh used to assess the influence of RJD and the number of auxiliary wells on HTS performance: (a) global 3D view; (b) zoom into the sandstone layer and surrounding claystone formations; (c) plan view; (d) horizontal section through the centre of the sandstone layer; (e) detailed view of the central portion of panel (d); and (f) detailed representation of a radial-jet “crown”. Although the rapid rendering mode displays boreholes and jets as planar features, both are explicitly discretized as cylindrical elements in the numerical mesh.

The sandstone layer is perforated by five radial-jet crowns, each comprising eight radial jets and spaced 1 m apart in the vertical direction. The jets have a penetration length of 15 m and a radius of 2 cm, whereas the boreholes have a radius of 20 cm. Both jets and boreholes are modelled explicitly as cylindrical features. The parameterization of the 3D model incorporates site-specific measurements from Bern-Forsthaus (e.g., transmissivity of sandstone $T_s=2\cdot10^{-7}$ m^2/s). Hydrostatic and thermostatic boundary conditions are prescribed at the top, bottom, and lateral model boundaries, with corresponding pressure and temperature initial conditions. Ten annual load-unload cycles are simulated (8 months of loading followed by 4 months of unloading) using a circulation rate of 5 kg/s and injection temperatures of 90°C and 60°C during the loading and unload-ing phases, respectively. Two operating regimes were investigated (Table 4):

- “Forced” regime: injected water is simultaneously pumped from the auxiliary wells during the loading phase (default case unless otherwise stated).
- “Unforced” regime: no pumping occurs during loading.

The simulation results are evaluated either at the main and auxiliary boreholes or at an observation point termed ’Obs’ (Figure 33), located midway between the main well and auxiliary well Aux2. Although inspired by the Bern-Forsthaus site, the simulations are intended to be generic and transferable to other HTS projects through appropriate adaptation of geological, thermal, and hydraulic parameters.

Table 4. Summary of internal boundary conditions applied in the 3D model used to evaluate the impact of RJD and the number of auxiliary wells. Positive flow rates (Q) denote injection, whereas negative values denote pumping. The parameter n_{aux} represents the number of auxiliary wells (1 or 3 in the present study).

	Cycle	Duration (months)	Boundary conditions at main well	Boundary conditions at any auxiliary well
"Unforced" regime	Load cycle	8	Q_{main} = 5 kg/s, T_{main}=90°C	None
	Unload cycle	4	Q_{main} = -5 kg/s	Q_{aux} = +5 / n_{aux} kg/s T_{aux}=60°C
"Forced" regime	Load cycle	8	Q_{main} = +5 kg/s T_{main}=90°C	Q_{aux} = -5 / n_{aux} kg/s
	Unload cycle	4	Q_{main} = -5 kg/s	Q_{aux} = +5 / n_{aux} kg/s T_{aux}=60°C

Impact of Radial Jet Drilling (RJD)

The influence of RJD was evaluated using the four-well configuration, considering cases with and without radial jets. Figure 35 shows temperature and pressure profiles along a vertical section intersecting both the main well and the observation point. The presence of radial jets increases the effective transmissivity of the reservoir and enhances advective heat transport within the sandstone layer. Consequently, a smaller fraction of the injected heat is transferred into the surrounding claystone formations, resulting in a more confined thermal plume. Close to the injection well, heat propagation is initially faster when jets are present; however, these differences become less pronounced with increasing time and distance from the injection point.

As shown in Figure 35, the vertical extent of the thermal plume at the observation point remains essentially identical in the presence and absence of jets, irrespective of simulation time. In contrast, the horizontal extent of the thermal plume within the sandstone layer is greater when RJD is included, as evidenced by the differences between the solid and dashed curves within the sandstone interval. During the early stages of the load cycle (red and green curves), the temperature at the observation point (and therefore the lateral extent of the thermal plume) is significantly higher in the presence of jets because advective transport dominates heat propagation. At later times, the thermal plume extent becomes similar in both cases.

The most pronounced effect of RJD is observed in the pressure response (Figure 35, right panels). In the absence of radial jets, absolute pressures exceed 20 MPa in the vicinity of the injection well, substantially higher than the estimated minimum principal stress (~6 MPa at 470 m depth). Such pressure levels could induce hydraulic fracturing, fault reactivation, or surface uplift. The introduction of radial jets markedly reduces pressure buildup and significantly improves hydraulic feasibility.

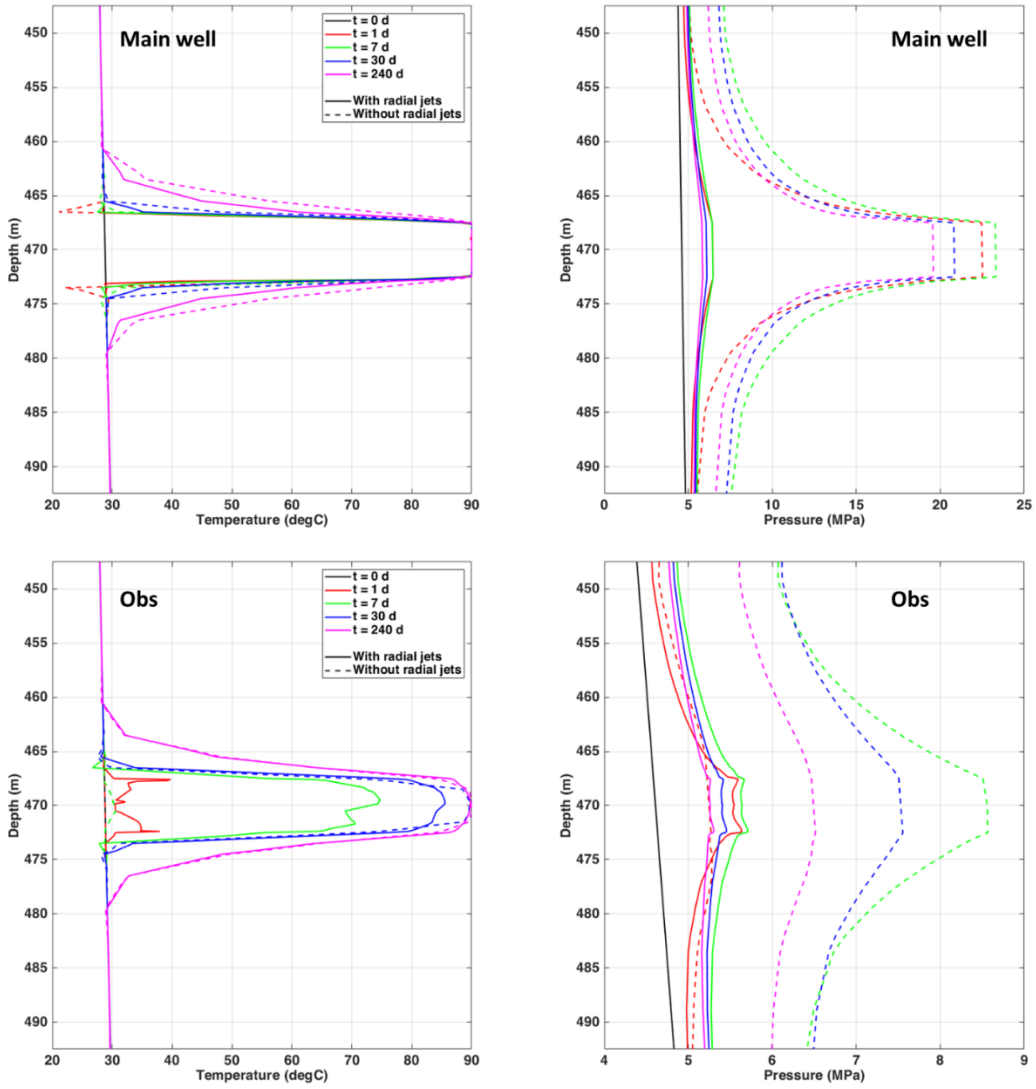


Figure 35. Distribution of temperature (left panels) and absolute pressure (right panels) along a vertical profile intersecting the main well (upper panels) and the observation point (lower panels). Results are shown for the four-well configuration with radial jets (solid lines) and without radial jets (dashed lines). Colours indicate different times during the loading phase.

Figure 36 shows the horizontal extent of the thermal plume within the sandstone layer at the end of the first loading and unloading cycles, both in the presence and absence of radial jets. As observed, the thermal plume extends farther in the absence of RJD because advective transport is less pronounced. While this behaviour results in a slight increase in thermal storage efficiency, Figure 37 demonstrates that the associated pressure levels become operationally unacceptable.

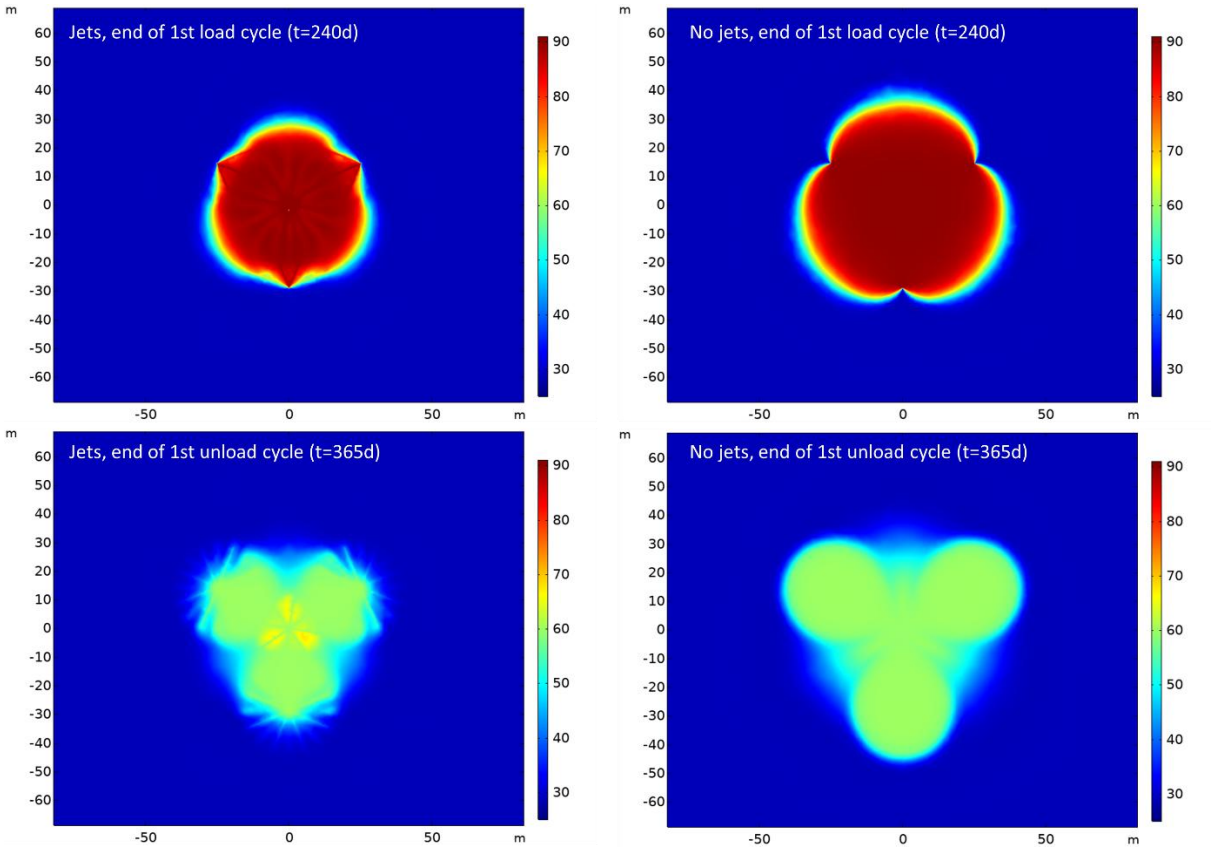


Figure 36. Spatial distribution of temperature (°C) at the end of the first loading cycle (top row) and first unloading cycle (bottom row) for simulations with and without radial jets (left and right columns, respectively) using the four-well configuration. Results are shown on a horizontal plane through the centre of the sandstone layer.

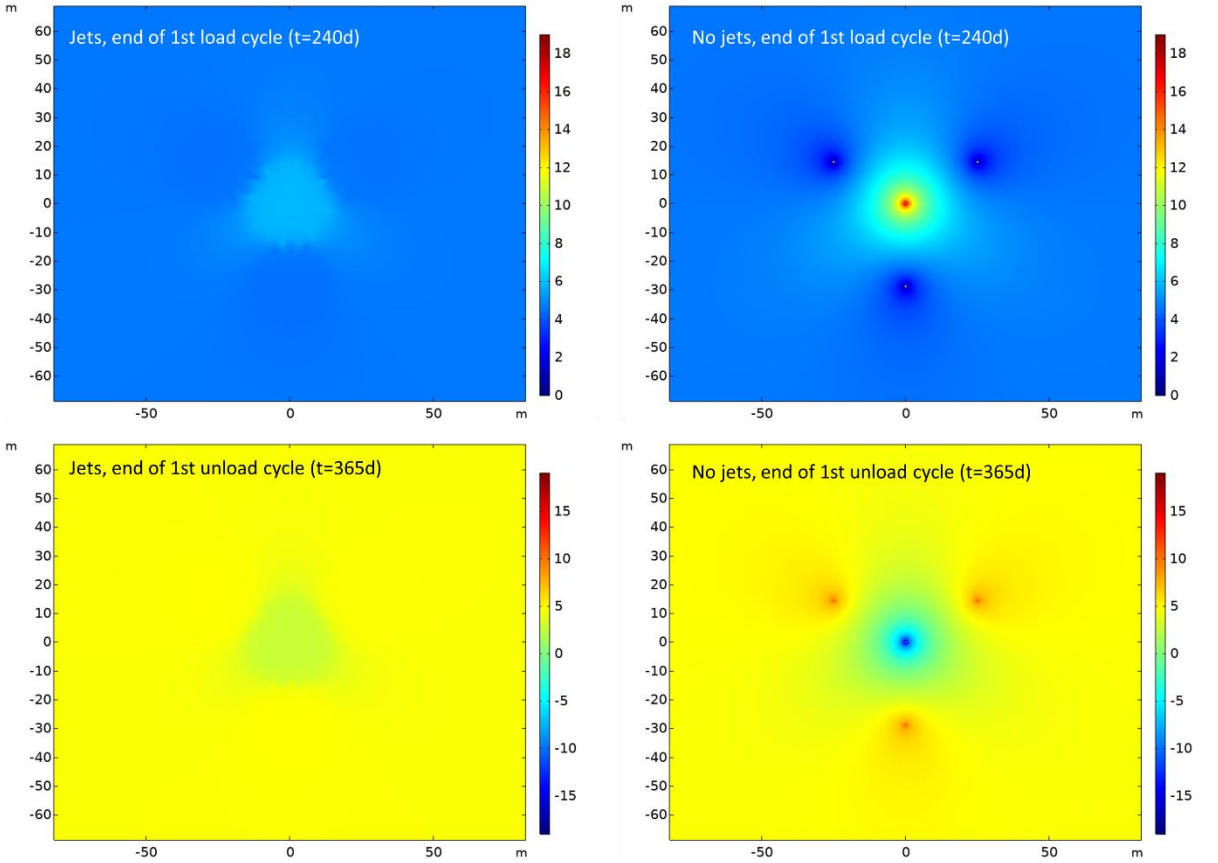


Figure 37. Spatial distribution of absolute pressure (MPa) at the end of the first loading cycle (top row) and first unloading cycle (bottom row) for simulations with and without radial jets (left and right columns, respectively) using the four-well configuration. Results are shown on a horizontal plane through the centre of the sandstone layer.

The sensitivity of system performance to jet length was also evaluated (Figure 38). Longer radial jets increase reservoir transmissivity, thereby reducing pressure buildup but also decreasing recovery temperatures during the unloading phase. This result confirms that jet length constitutes a key design parameter that must be optimized to achieve an appropriate balance between injectivity and thermal performance.

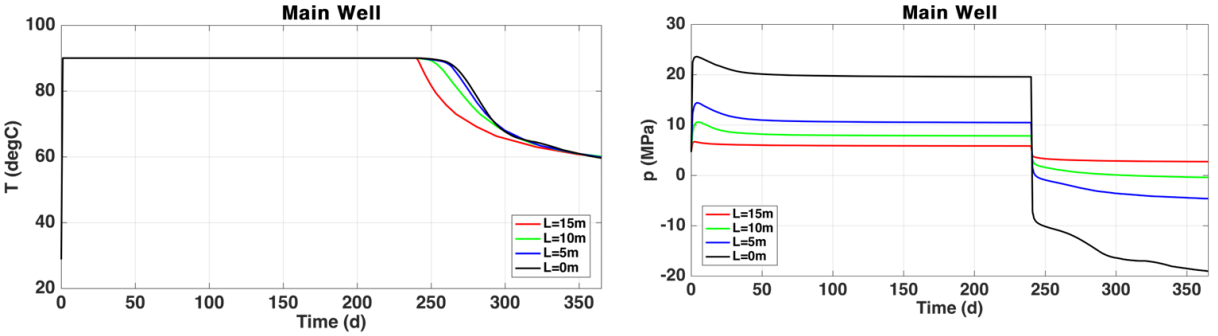


Figure 38. Temporal evolution of temperature (left) and pressure (right) at the main well for the four-well configuration and different radial-jet lengths. The case L = 0 m corresponds to the configuration without radial jets.

3D modelling of the impact of the number of boreholes and injection scheme

The performance of the current two-well configuration at Bern-Forsthaus was compared with that of a four-well configuration representing the initially planned HTS layout (Figure 33). All simulations in this section include radial jets, which enhance the effective reservoir transmissivity and aim at maintaining injection pressures within operationally acceptable limits. The two operating regimes described in Table 4 were also evaluated.

Figure 39 and Figure 40 present the temporal evolution of temperature and absolute pressure, respectively, at the main and auxiliary wells for both configurations under the unforced operating regime. Under this loading/unloading strategy, the four-well configuration exhibits superior thermal performance (Figure 39). Recovery temperatures remain elevated for longer periods, indicating improved heat storage and extraction efficiency. At the same time, pressure buildup is moderately reduced because pumping during the unloading phase is distributed among several auxiliary wells (Figure 40). Nevertheless, absolute pressures still reach values of approximately 18 MPa, significantly exceeding the estimated minimum principal stress and therefore remaining operationally problematic.

The same overall conclusions are obtained under the forced operating regime (Figure 41 and Figure 42). Distributed pumping during the loading phase increases the lateral extent of the thermal plume while simultaneously reducing pressure buildup. However, recovery temperatures during the unloading phase are slightly lower than those obtained under the unforced regime (Figure 43).

The differences between both operating strategies become more apparent when examining the evolution of the thermal plume (Figure 44). Under forced conditions, pumping at the auxiliary wells rapidly captures part of the injected, thereby confining the thermal plume within the well pattern. In contrast, under unforced conditions, the plume expands more freely through the reservoir, increasing the volume of heated rock and enhancing thermal storage efficiency. The improved thermal performance of the unforced regime, however, comes at the cost of substantially higher reservoir pressures, as shown in Figure 40.

Overall, the simulations indicate that the number of auxiliary wells primarily influences the hydraulic performance of the system by reducing pressure buildup, whereas the operating strategy governs the balance between thermal recovery and hydraulic safety. The four-well configuration consistently provides lower injection pressures than the two-well layout, while the unforced operating regime yields the highest thermal recovery at the cost of increased pressure levels. Consequently, the selection of the well layout and injection strategy should be based on a compromise between thermal efficiency and operational feasibility.

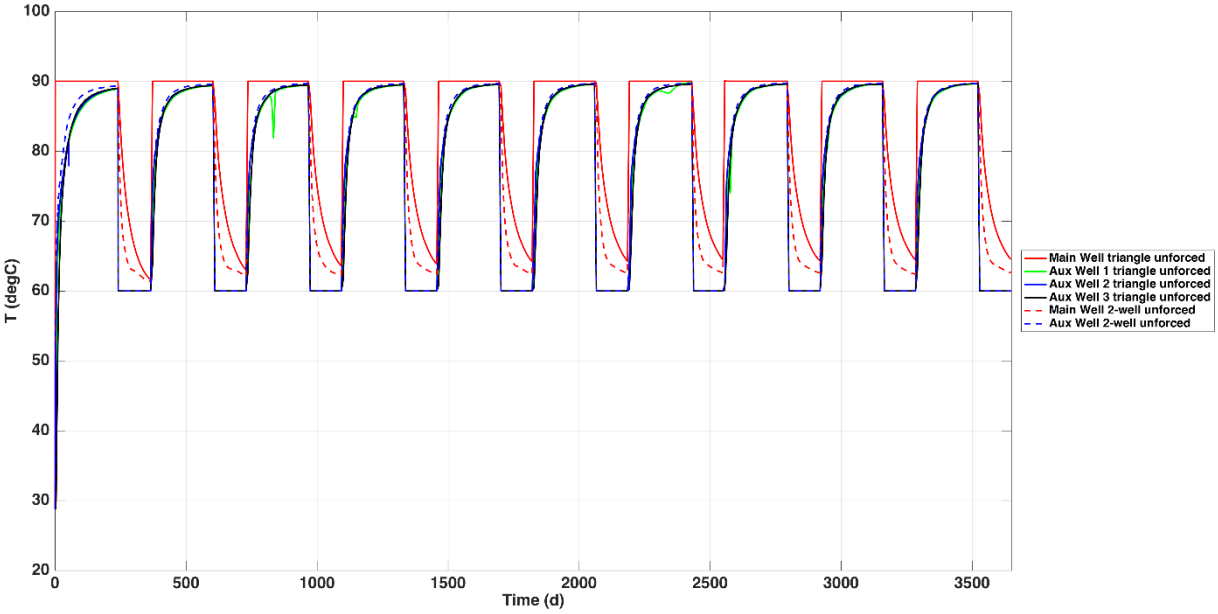


Figure 39. Influence of the number of boreholes on HTS thermal performance. Temporal evolution of temperature at the main and auxiliary wells for the two-well and four-well configurations under the unforced operating regime.

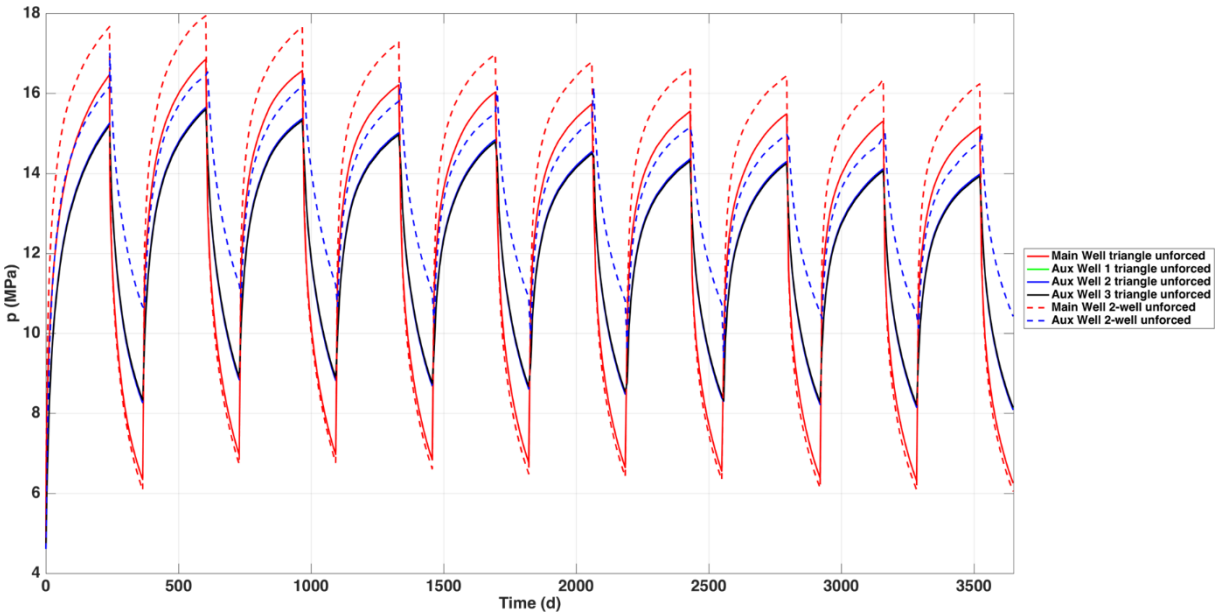


Figure 40. Influence of the number of boreholes on HTS hydraulic performance. Temporal evolution of absolute pressure at the main and auxiliary wells for the two-well and four-well configurations under the unforced operating regime.

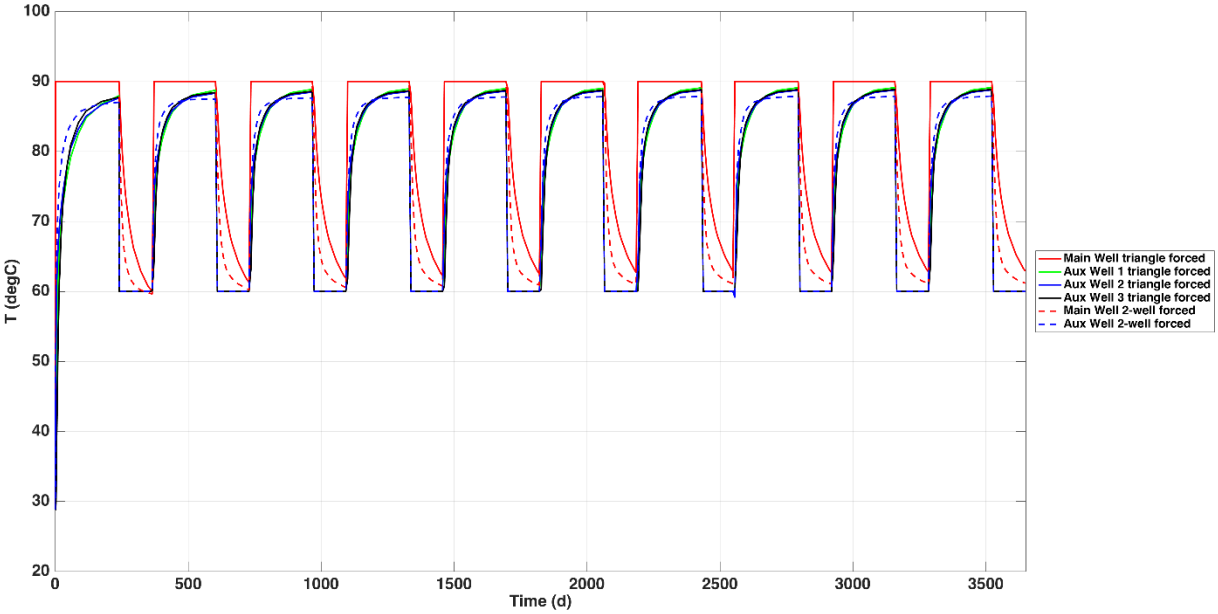


Figure 41. Influence of the number of boreholes on HTS thermal performance. Temporal evolution of temperature at the main and auxiliary wells for the two-well and four-well configurations under the forced operating regime.

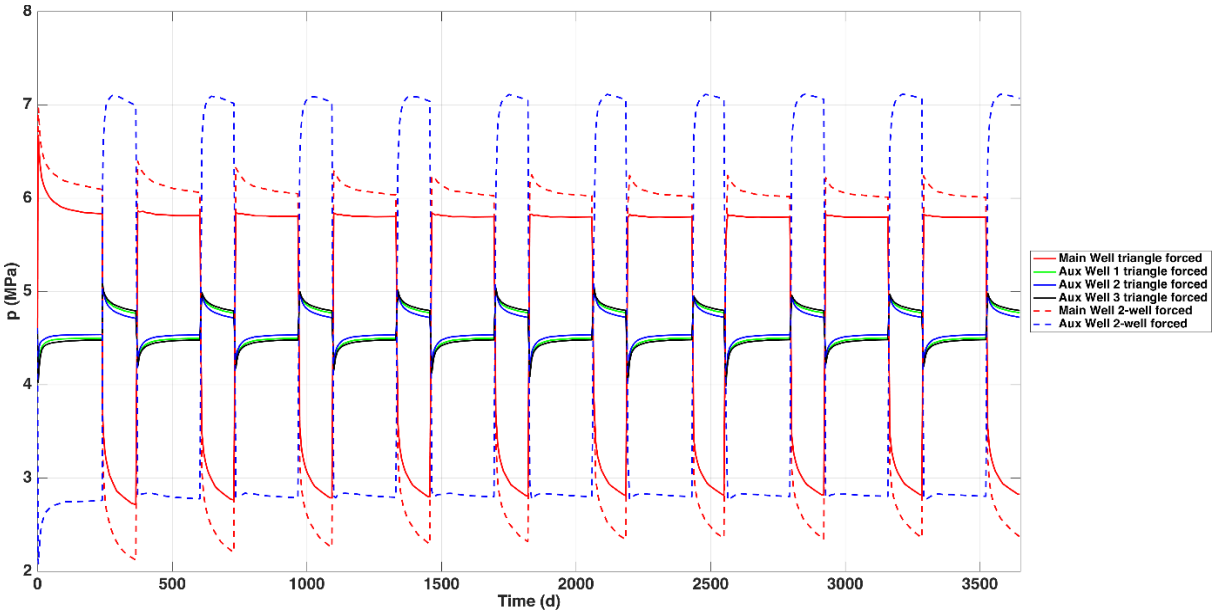


Figure 42. Influence of the number of boreholes on HTS hydraulic performance. Temporal evolution of absolute pressure at the main and auxiliary wells for the two-well and four-well configurations under the forced operating regime.

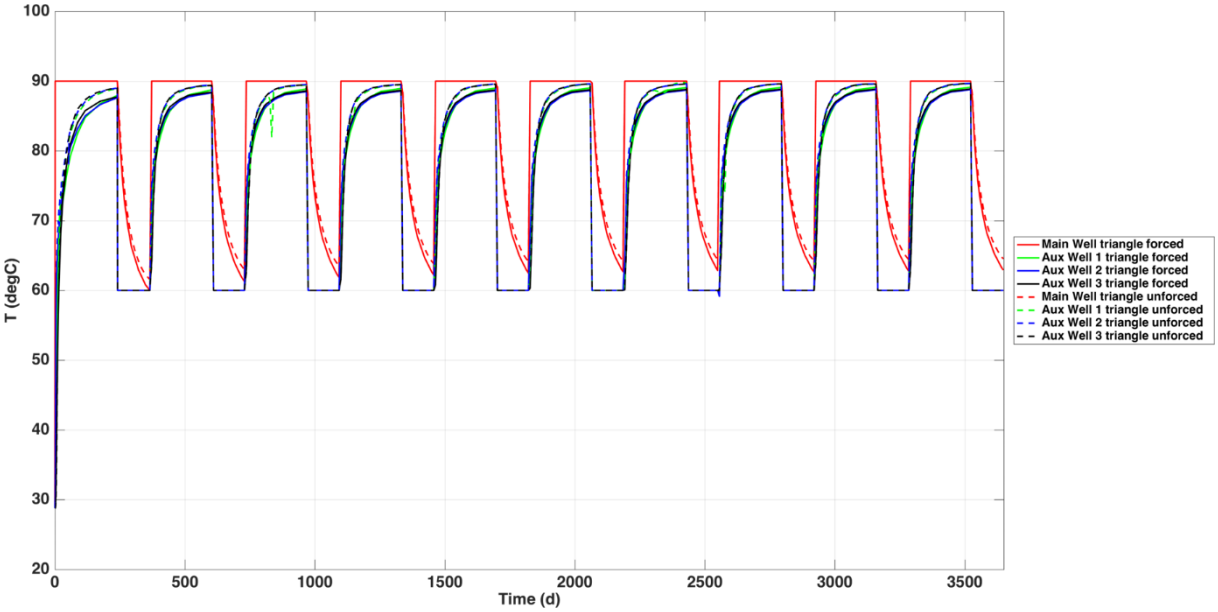


Figure 43. Comparison of temperature evolution at the main well for the four-well configuration under the forced and unforced operating regimes.

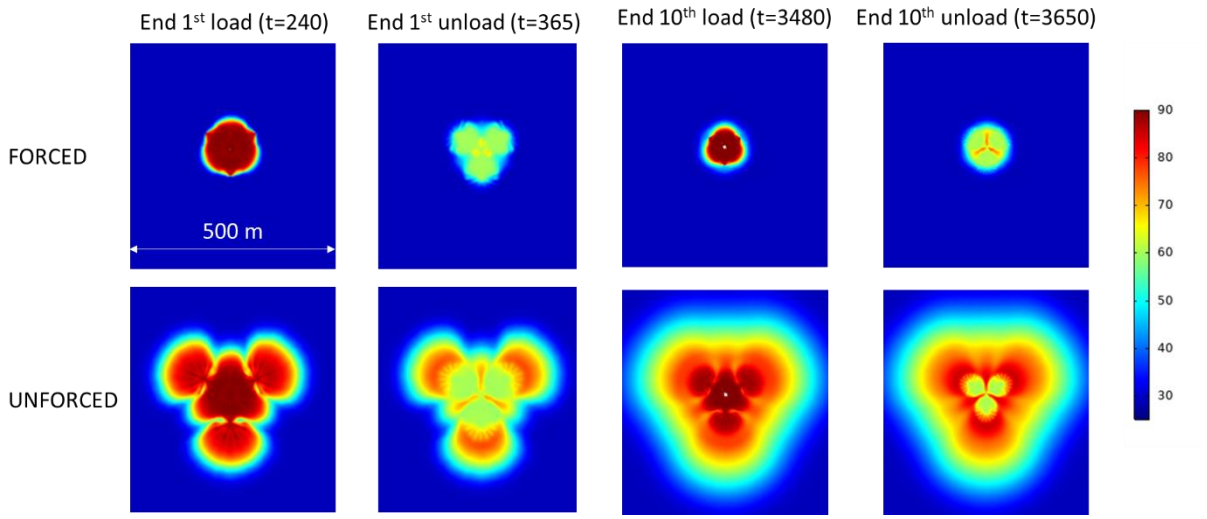


Figure 44. Spatial distribution of temperature (°C) at the end of the first and tenth loading and unloading cycles for the forced and unforced operating regimes (top and bottom rows, respectively). Simulations correspond to the four-well configuration with radial jets. Results are shown on a horizontal plane through the centre of the sandstone layer.

2.3.8 Evaluation of Horizontal Multilateral Wells for HTS

Horizontal laterals are a well-established technology in groundwater engineering, petroleum engineering and geothermal energy to improve well productivity by increasing the contact area between the well and the reservoir. In hydrogeology, similar concepts are widely employed in horizontal collector wells

(Ranney wells) and wells with radial drains (Joshi, 1991; Zhan and Zlotnik, 2002; Collins and Houben, 2020), whereas in the petroleum industry they are commonly referred to as multilateral wells. Compared with conventional single-trajectory wells, horizontal laterals increase the effective drainage radius and reduce hydraulic gradients around the well, thereby improving injectivity and productivity. Within the coupled MOSKITO-PorousFlow-Geochemical framework, multilateral wells can be represented naturally by prescribing complex well trajectories consisting of a vertical section connected to one or more horizontal branches. Consequently, the modelling workflow is applicable to both Radial Jet Drilling (RJD) and conventional horizontal multilateral wells.

To investigate the influence of increased well reach on HTS performance, KIT carried out a synthetic numerical study using a synthetic reservoir representative of the geological conditions envisaged for a typical HTS (Yan et al., 2025). The objective was to quantify the influence of the number of horizontal laterals on heat recovery efficiency and reservoir hydraulics as a first step towards site-specific simulations.

Four well configurations were analysed, comprising vertical wells only and wells equipped with one, two or three horizontal laterals at both the injection and production wells (Figure 45). In the numerical model, each lateral extends 100 m from the main wellbore. Although this length exceeds the reach typically achievable, it was intentionally selected to magnify the hydraulic and thermal responses, thereby providing a demanding benchmark for assessing the numerical robustness and stability of the coupled modelling workflow.

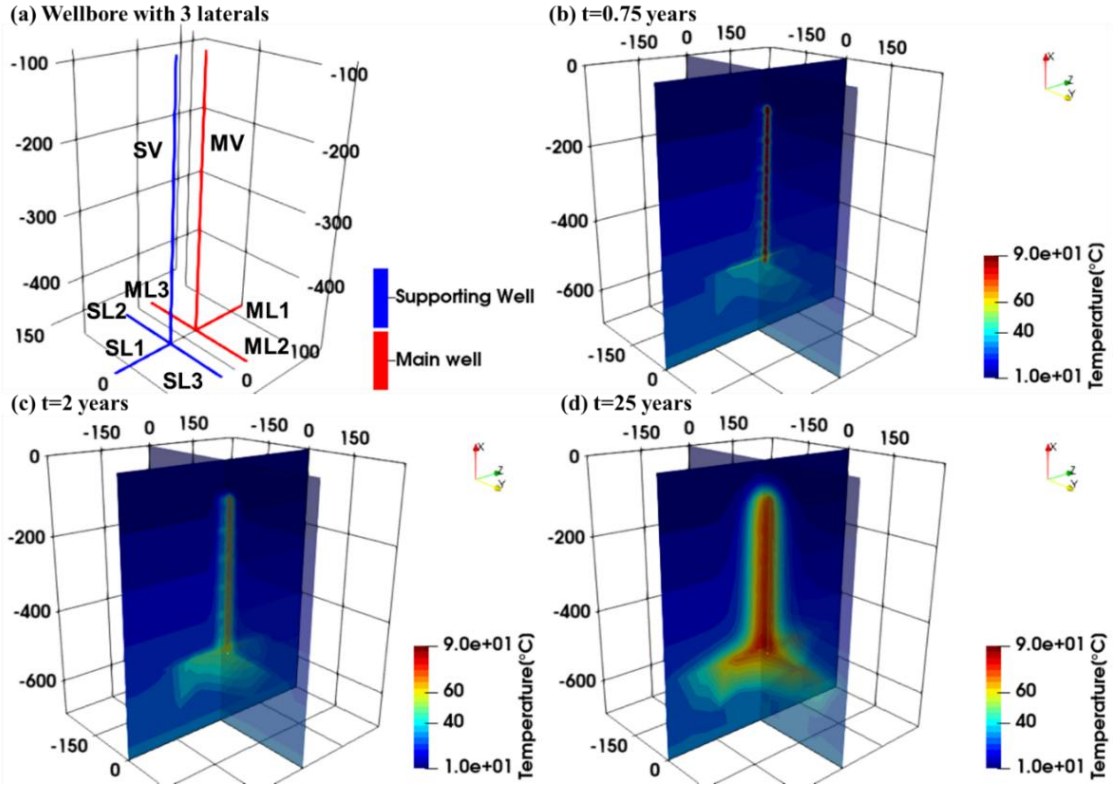


Figure 45. Configurations of the multilateral wells considered in the synthetic numerical study. (a) Well layouts comprising (1) vertical wells SV and MV only (i.e., without laterals), (2) one horizontal lateral per well (the vertical wells SV, MV, and lateral wells SL1, ML1), (3) two horizontal laterals per well (the vertical wells SV, MV and lateral wells SL1, SL2, ML1, ML2) and (4) three horizontal laterals per well (all). Panels (b-d) illustrate the temperature distribution for the configuration with three horizontal laterals after (b) the first loading period (t = 0.75 years), (c) the second unloading period (t = 2 years), and (d) the twenty-fifth unloading period (t = 25 years).

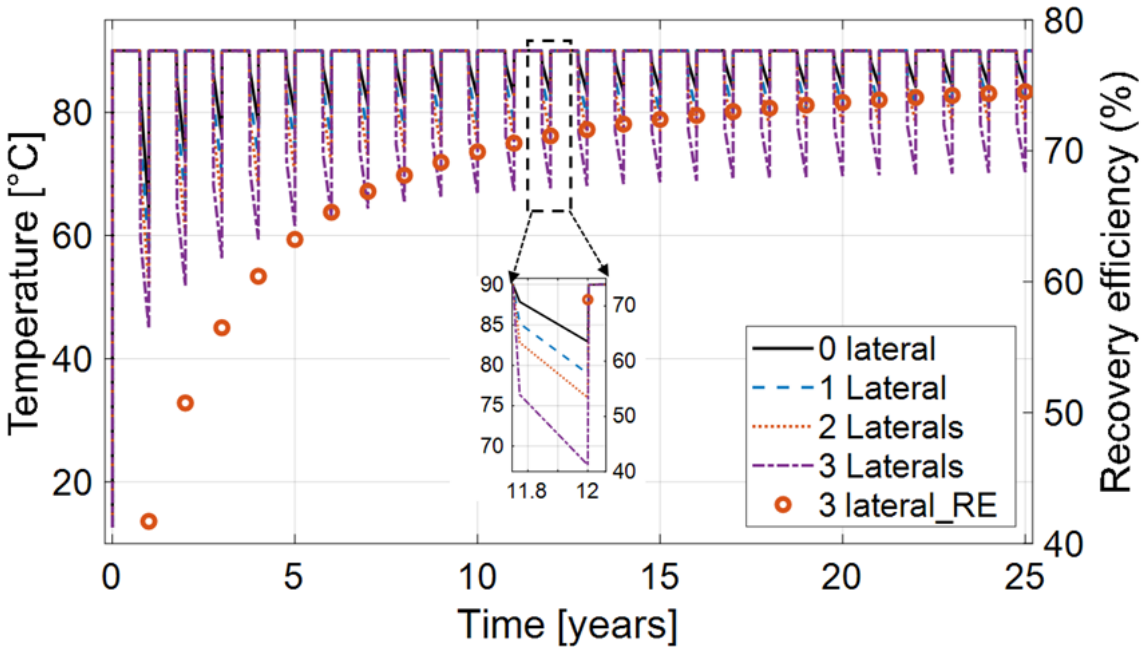


Figure 46. Temporal evolution of production temperature at borehole SV for a circulation rate of 25 L/s. Orange symbols indicate the annual thermal recovery efficiency (RE) for the configuration with three horizontal laterals. 'RE' means recovery efficiency (%).

Because the injected water enters borehole MV at 90°C, well above the ambient reservoir temperature (10-30°C), heat is continuously transferred from the injection well into the surrounding formation. Consequently, the rock volume around the injection well progressively warms during successive loading cycles (Figure 45b-d). This gradual thermal charging results in a steady increase in production temperatures over time. The minimum production temperature at the production borehole increases from approximately 42°C after the first operational year to about 68°C after 25 years of cyclic operation (Figure 46). The corresponding recovery efficiency also increases progressively, from 41.7% during the first cycle to 74.9% after 25 years, reflecting the progressive thermal conditioning of the storage reservoir. However, increasing the number of horizontal laterals systematically reduces the recovered temperature for a given operating cycle. The larger contact area between the well and the reservoir enhances advective heat transport and enlarges the heated volume, but simultaneously promotes greater conductive heat losses into the surrounding formations. Consequently, the thermal recovery efficiency decreases as the number of laterals increases. The same behaviour was independently observed in the modelling study performed by GES (section 2.3.7).

The influence of flow rate was also investigated for the configuration comprising three horizontal laterals (Figure 47). Owing to the substantially larger contact area between the reservoir and the well, multilateral wells experience significantly lower pressure gradients than conventional vertical wells. This hydraulic advantage enables larger injection and production rates while maintaining reservoir pressures within acceptable operational limits. At relatively low flow rates (≤15 L/s), however, the enlarged heat exchange surface increases conductive heat losses to the surrounding formations, leading to lower thermal recovery efficiencies. As flow rate increases, the residence time of the circulating fluid decreases and advective heat transport becomes increasingly dominant, partly compensating for these additional conductive losses. Consequently, numerical models suggest that the principal benefit of horizontal multilateral wells is not an intrinsic increase in thermal efficiency, but rather the theoretical possibility of operating at substantially higher circulation rates without exceeding hydraulic constraints, provided the formation matrix possesses sufficient baseline permeability to support enhanced connectivity

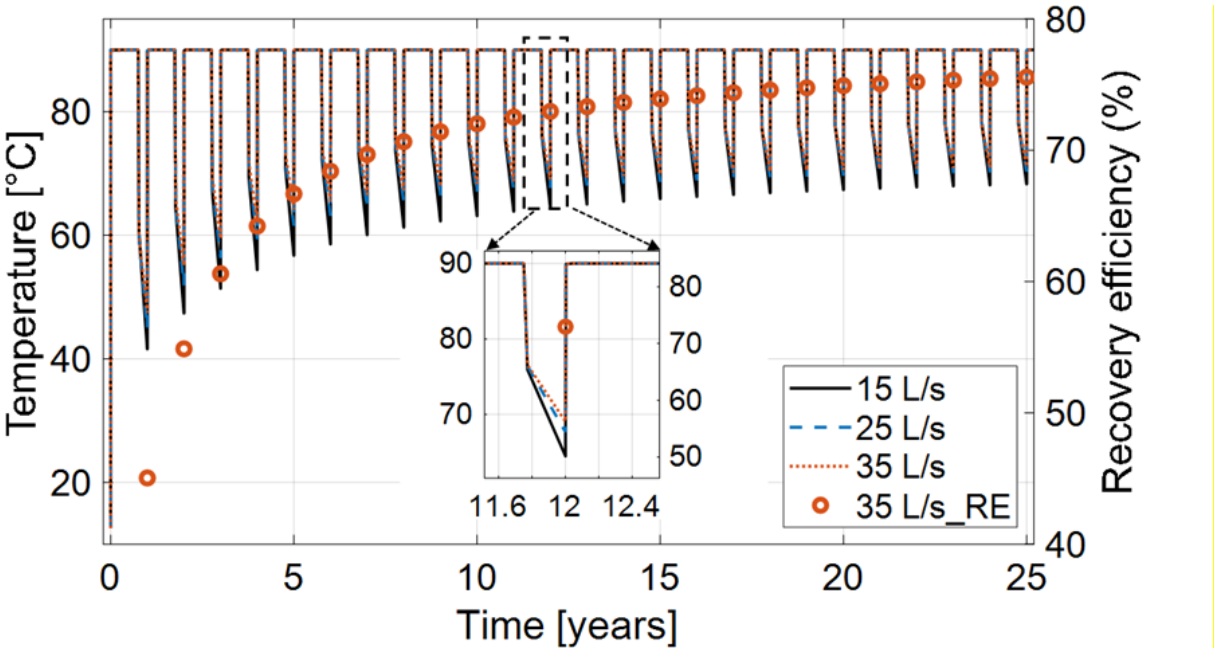


Figure 47. Influence of circulation rate on production temperature for the configuration with three horizontal laterals. Results are shown for flow rates of 15, 25 and 35 L/s. Orange symbols indicate the annual thermal recovery efficiency (RE) for the case with Q = 35 L/s.

2.3.9 Summary of findings

Table 5 summarizes the main findings from the synthetic wellbore and reservoir simulations performed for HTS design optimization. The table summarizes the investigated parameters, the numerical approach adopted, the resulting impact on key performance indicators, and the practical implications for HTS design.

Table 5. Main findings from the synthetic wellbore and reservoir simulations performed for HTS design optimization.

Investigated parameter / optimization strategy	**Numerical approach**	**Impact on key performance indicators**	**Main findings and practical implications for HTS design**
Injection temperature	Wellbore simulations with constant injection rate (25 L/s) and injection temperatures representative of unload (50°C) and load (90°C) cycles	Controls absolute fluid temperature and recovered heat quality; limited influence on the shape of temperature profiles along the well	Higher injection temperatures increase the thermal energy stored in the system. However, transient temperature evolution is mainly controlled by the initial thermal state of the well and geothermal gradient. Injection temperature should therefore be optimized together with operational strategy and storage objectives.
Injection flow rate	Wellbore simulations with Q = 15, 25 and 35 L/s and T_{inj} = 90°C	Higher flow rates reduce residence time and wellbore heat losses; accelerate thermal stabilization; increase transported thermal power	Flow rate is a key parameter controlling early-time thermal performance. High circulation rates improve thermal delivery efficiency but require sufficient reservoir injectivity. Low-flow systems may experience significant thermal losses and require additional insulation or improved well completion strategies.

Injection pressure boundary condition	Comparison between pressure-controlled and flow-controlled MOSKITO simulations	Limited effect on wellbore temperature when flow rate is imposed; influences hydraulic response through hydrostatic and frictional components.	Pressure-controlled operation is numerically validated and required for future coupled reservoir simulations. Operational pressure remains controlled primarily by reservoir properties rather than wellhead pressure alone.
Additional conductive layers / multi-layer in-flow	Wellbore model including an additional conductive interval at 403 m depth with 10 L/s entering the upper layer and 15 L/s reaching the deeper target	Modifies vertical distribution of injected thermal energy; reduces heat delivery to deeper zones	Reservoir heterogeneity and inflow distribution between permeable layers influence thermal efficiency. Accurate characterization of productive intervals is re-quired for reliable HTS design.
Temperature-dependent fluid properties	Reservoir simulations comparing constant and temperature-dependent density and viscosity.	Hydraulic conductivity increases by approximately a factor of 3–3.5 at 90–100°C; reduced pressure buildup during operation.	Temperature effects on fluid properties are critical for predicting injectivity and storage capacity. Neglecting viscosity reduction leads to overestimation of pressure requirements and underestimation of reservoir performance.
Reservoir heterogeneity/channel connectivity	2D stochastic reservoir models comparing homogeneous sandstone, siltstone and heterogeneous sandstone-channel configurations.	Strong influence on pressure response and thermal recovery. Over-pressures vary from ~12 MPa (connected channels) to >90 MPa (poor connectivity).	Geological architecture is a first-order control on HTS feasibility. Highly conductive pathways improve circulation but may cause premature thermal breakthrough, whereas poorly connected systems can generate unacceptable pressure buildup.
Radial Jet Drilling (RJD)	3D simulations comparing four-well configurations with and without radial jets.	Increased effective transmissivity; reduced pressure buildup; slightly increased advective heat transport.	RJD improves hydraulic feasibility by lowering injection pressures and increasing reservoir contact. However, excessive enhancement of connectivity may reduce thermal recovery by accelerating heat transport.
Radial jet length	Sensitivity analysis using different jet lengths.	Longer jets reduce pressure buildup but may decrease recovered temperature during unloading.	Jet length requires optimization between hydraulic performance and thermal recovery. Maximum reservoir stimulation is not necessarily optimal for HTS operation.
Horizontal multilateral wells	Synthetic reservoir simulations with vertical wells and 1–3 horizontal laterals per well.	Increasing laterals lowers hydraulic gradients and allows higher circulation rates; recovery efficiency decreases for identical flow conditions.	The main advantage of multilateral wells is improved injectivity rather than inherently higher thermal efficiency. Their application is most beneficial in low-permeability systems where higher flow rates are required.
Circulation rate in multilateral wells	Simulations with 15, 25 and 35 L/s.	Higher rates increase advective heat transport and reduce the relative impact of conductive losses.	Multilateral wells enable operation at higher flow rates while maintaining acceptable pressures, provided sufficient reservoir permeability exists.

Number of auxiliary wells	Comparison between two-well and four-well HTS configurations.	Additional wells reduce pressure buildup and improve thermal recovery stability.	Increasing the number of wells improves hydraulic control and operational flexibility. However, increased infrastructure complexity must be balanced against the achievable thermal benefit.
Injection strategy (forced vs unforced circulation)	3D cyclic simulations comparing pumping during loading versus passive storage.	Forced operation reduces pressure buildup but limits thermal plume expansion; unforced operation maximizes stored heat but increases pressure.	Operating strategy determines the compromise between thermal efficiency and hydraulic safety. Forced circulation is preferable where pressure constraints dominate, whereas unforced operation maximizes heat recovery where reservoir conditions allow.
Overall HTS design optimization strategy	Integrated evaluation of wellbore, reservoir and completion concepts.	Thermal recovery, hydraulic feasibility and pressure management are strongly coupled.	Optimal HTS design requires balancing reservoir contact enhancement (RJD, laterals, additional wells) with pressure constraints. and thermal breakthrough risk. Maximizing connectivity alone does not guarantee improved system performance.

2.4 Objective 2. Development of monitoring concepts and operational surveillance strategies

Although the low permeability of the sandstone layers at Bern-Forsthaus currently precludes the development of a HTS, a number of lessons regarding monitoring and surveillance have been learned from the hydraulic tests and CO_2 injection campaigns conducted to date, particularly concerning the deployment of control sensors and the surveillance of the HTS during its development and operational lifetime. These lessons, transferrable to other HTS projects, are described below.

2.4.1 Monitoring concept

The proposed monitoring system is based on industry-standard instrumentation installed in both the main (central) well and the peripheral wells. It comprises downhole pressure and temperature sensors installed within the interval(s) of interest (i.e., the permeable layers of the USM), together with corresponding surface sensors and flowmeters. These devices provide continuous measurements that are integrated into a centralized data acquisition system, enabling real-time monitoring and analysis throughout the project lifetime. This robust monitoring concept has been successfully implemented at Bern-Forsthaus. By relying on proven instrumentation, the system minimizes operational complexity while delivering the high-quality datasets required for day-to-day reservoir management and long-term performance assessment.

2.4.2 Completion concept

At Bern-Forsthaus, it has been observed that thermal losses along the boreholes are significant because (1) wellbore diameters are large; (2) no thermal insulation is provided along the borehole. Similar conclusions were reached during Phase 2 of the BEACH (Bedretto Energy Storage and Circulation of Geothermal Energy; https://www.aramis.admin.ch/Texte/?ProjectID=55870) project at Bedretto. To mitigate thermal losses, it is planned in Phase 3 of the BEACH project to inject the hot fluid through a smaller-diameter tubing after removing the fluid from the wellbore annulus, thereby replacing the highly

conductive water column in the annulus with air, which substantially reduces conductive heat losses. The zonal-isolation approach implemented in borehole ST1 at Bedretto, based on a multi-packer system, is recommended for improved control of the HTS and to enable interval-specific testing and monitoring. Selected intervals can be accessed through, e.g., plug-and-perf completions and, where required, micro-sidetrack drilling to enhance wellbore-to-formation connectivity, as successfully demonstrated at Bern-Forsthaus.

2.4.3 System surveillance

The monitoring concept proposed above provides point measurements at selected intervals or at the surface. In addition, we propose the deployment of permanent fibre-optic cables in the well(s) to provide Distributed Temperature Sensing (DTS) and Distributed Strain Sensing (DSS) behind casing and along the entire wellbore profile. Fibre-optic monitoring has proven to be a valuable tool at Bern-Forsthaus, providing continuous temperature measurements throughout the wellbore.

The usefulness of DTS technology was demonstrated during a cold-water injection test conducted in borehole F1 at Bern-Forsthaus (Figure 48), where the DTS system successfully tracked the injected thermal perturbation within the monitored interval. The resulting temperature profiles provided valuable insight into the temperature distribution within the reservoir that could not have been obtained from conventional point measurements alone. In addition, the DTS data enabled the identification and subsequent removal of a wellbore blockage in well F1, thus demonstrating the usefulness of DTS (and DSS) during the long-term operational life of a HTS. The resulting temperature anomaly clearly highlighted the affected interval, allowing rapid diagnosis of the issue and demonstrating the value of fibre-optic monitoring for both reservoir characterization and operational diagnostics.

DSS is a proven technology that can provide early indications of reservoir deformation associated with HTS operations, offering an additional means for monitoring reservoir integrity before any effects become observable at the surface. Nevertheless, and despite the operational injection pressures are expected to remain relatively low and are therefore unlikely to induce measurable surface deformation, a systematic and periodic topographic survey within a safety perimeter surrounding the HTS is also recommended.

2.5 Objective 3. Definition of safe operating envelopes for HTS systems.

Rather than relying on conservative empirical limits, which depends on local hydrogeological properties, VESTA-CH established a quantitative framework that combines coupled TH modelling, geomechanical analyses and operational constraints to identify combinations of operating parameters that maximize thermal performance while maintaining reservoir integrity.

A safe operating envelope is defined here as the range of operating conditions for which heat storage and recovery can be performed without inducing unacceptable hydraulic, mechanical or thermal impacts on the storage reservoir and its surrounding formations. Potential chemical issues, e.g., corrosion or scaling, can be tackled by means of chemical inhibitors (section 2.6). The principal operational variables include injection and production flow rates, injection temperature, reservoir pressure, cycle duration, well configuration and stimulation strategy.

The work carried out in Objectives 1 and 2 provides the scientific basis for constructing these envelopes. The coupled numerical simulations quantify the evolution of pressure, temperature and flow during repeated loading and unloading cycles, while the geomechanical analyses (see section 2.5.1) evaluate the corresponding stress changes and their implications for fault stability, hydraulic fracturing and long-term reservoir integrity. Together, these results allow the identification of operational thresholds beyond which the system may become hydraulically or mechanically unstable.

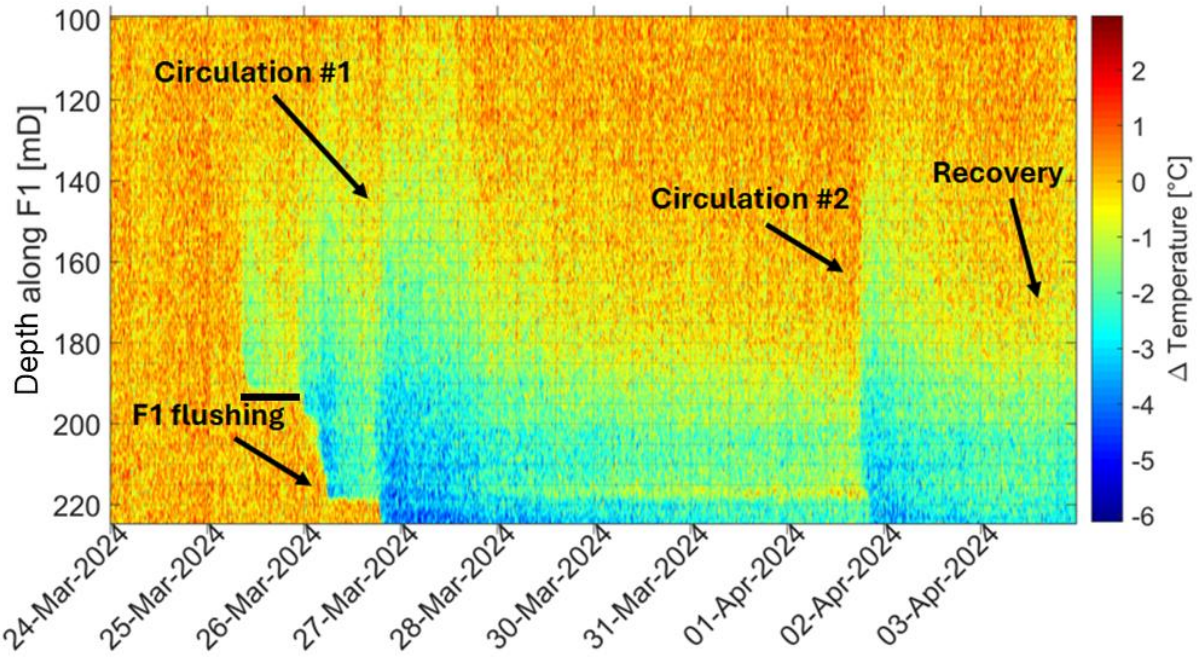


Figure 48. Temporal evolution of DTS profiles along well F1, showing the thermal perturbation relative to the thermostatic temperature profile before, during, and after the flushing operation. The black arrows indicate significant events, particularly the two 24-hour cold water circulation periods. During the recovery phase, the sections above 220 meters (corresponding to the cased Quaternary clay section) return rapidly to formation temperature, whereas the screened open-hole section below 220 meters exhibits a more prolonged recovery. The thick black line indicates the top of the originally clogged section of F1. Results are expressed as differential temperature, defined as the difference between the temperature at any given time and the thermostatic temperature (mean temperature profile from 10/03/2024 to 20/03/2024).

2.5.1 Geomechanical analyses

In the context of VESTA, Lawrence Berkeley National Laboratory (LBNL) applied the three-dimensional reservoir model developed by GES to investigate the coupled thermo-hydro-mechanical (THM) processes governing the operation of high-temperature aquifer thermal energy storage (HTS) systems. The complete modelling methodology and results are presented in Rutqvist et al. (2026). The main findings relevant to the VESTA-CH project are summarized below.

The primary objective of the study was to evaluate the long-term thermo-hydraulic and geomechanical response of cyclic HTS operation and to identify operating conditions that maximize thermal performance while maintaining reservoir pressures and stresses within safe limits (objective 3 of VESTA-CH). In addition, the work aimed to assess suitable monitoring strategies capable of detecting undesirable geomechanical responses during operation and providing early warning of potential reservoir damage (objective 2 of VESTA-CH). These objectives are particularly relevant for the Bern-Forsthaus pilot site, where the storage reservoir consists of thin, laterally heterogeneous sandstone bodies embedded within a low-permeability clay matrix, making the hydraulic performance highly sensitive to reservoir connectivity.

The simulations were performed using the coupled TOUGH3-FLAC3D framework (Itasca, 2018; Jung et al., 2022), which simultaneously solves fluid flow, heat transport and geomechanical deformation. The model was built directly from the three-dimensional geological model previously developed by GES and explicitly represents the complex stratigraphy of the Lower Freshwater Molasse, including the main sandstone storage horizons, surrounding clay layers, and the existing well geometry. Temperature-dependent fluid properties, buoyancy effects, conductive and advective heat transport, thermal expansion of the rock mass, and stress changes resulting from pressure variations were all considered within the fully coupled THM formulation. The reference operational scenario consisted of ten annual loading-

unloading cycles, with hot water injected into the main well during the loading phase and cooler water injected through the auxiliary wells during unloading. Pressure-controlled boundary conditions were applied throughout the simulations to reproduce the proposed operational strategy and to minimize reservoir overpressure.

One of the most important outcomes of the study is that reservoir transmissivity constitutes one of the dominant controlling parameters governing HTS feasibility and performance. The permeability distribution obtained from site investigations produced insufficient transmissivity to sustain the target circulation rates of approximately 20–25 L/s without generating excessive pressure buildup. Consequently, the transmissivity of the hydraulically connected sandstone layers had to be increased by approximately one order of magnitude, representing the expected effect of successful reservoir stimulation. This result demonstrates that achieving sufficient hydraulic connectivity between the storage wells is a prerequisite for practical HTS implementation. Once adequate transmissivity was assumed, the model predicted stable circulation rates exceeding the project targets while maintaining bottom-hole pressures substantially below the estimated lithostatic stress (Figure 49), thereby avoiding hydraulic fracturing and excessive mechanical deformation.

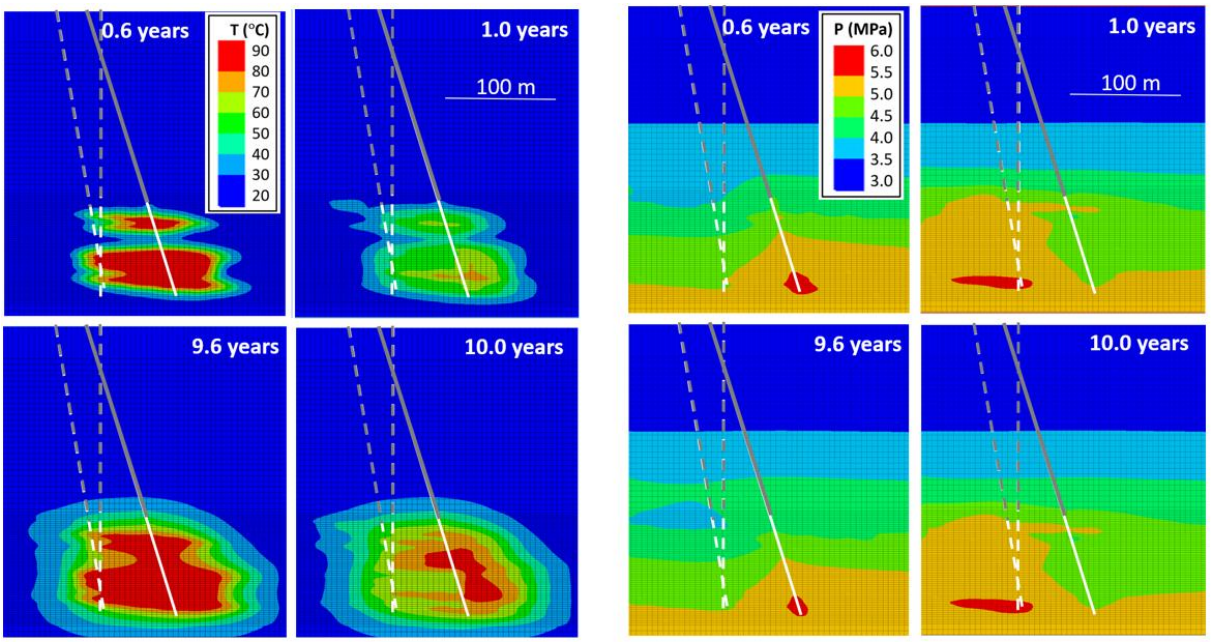


Figure 49. Vertical cross-section showing simulated (a) temperature and (b) pressure distributions at the end of the 1st and 10th load and unload cycles.

The thermal simulations further showed that the heated reservoir volume progressively expands over successive operational cycles until approaching a quasi-steady state. Consequently, thermal recovery efficiency improves continuously as residual heat accumulates within the storage formation. The predicted round-trip efficiency increases rapidly during the first years of operation before gradually stabilizing, reaching approximately 55% when considering only the main production well and more than 90% when the thermal energy recovered from all wells is included. Simultaneously, the system is capable of delivering thermal power exceeding 6 MW during the unloading periods, indicating that the proposed operational concept can provide substantial seasonal heat storage capacity once the reservoir has been thermally conditioned (Figure 49).

From a geomechanical perspective, the simulations demonstrate that pressure-controlled operation fundamentally changes the mechanical behaviour of the reservoir. Reservoir pressure variations remain limited to approximately ±2 MPa around the initial hydrostatic state, while the maximum reservoir pressure stays well below the lithostatic stress. As a result, thermally induced deformation dominates the mechanical response, producing gradual volumetric expansion that closely follows the spatial evolution of the thermal plume. Maximum vertical displacement reaches approximately 30 mm near the storage horizon but attenuates to only a few millimetres at the ground surface. Furthermore, both maximum and minimum effective principal stresses remain within safe limits throughout the simulated operating period, indicating negligible risk of tensile failure, hydraulic fracturing or shear reactivation under the proposed operating conditions (Figure 50).

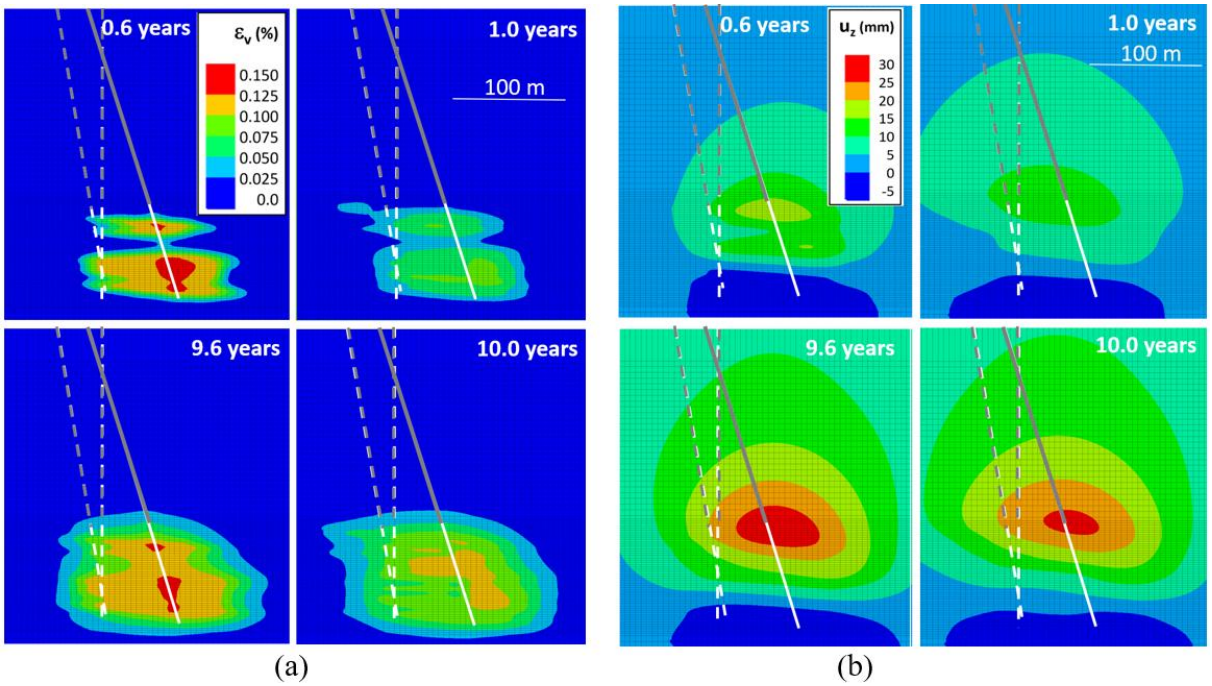


Figure 50. Vertical cross-section showing simulated (a) volumetric strain and (b) vertical displacement at the end of the 1st and 10th load and unload cycles.

An additional objective of the study was to evaluate monitoring concepts capable of verifying safe HTS operation. The coupled THM simulations revealed a very strong spatial correlation between temperature and thermally induced strain under normal operating conditions. This finding demonstrates that distributed fibre-optic temperature and strain measurements (DTS/DSS) can be used not only to monitor the evolution of the thermal plume but also to verify the mechanical integrity of the storage reservoir. Dedicated high-pressure sensitivity analyses further showed that pressure-induced opening of weak bedding planes produces localized strain anomalies that are clearly distinguishable from the smooth thermal expansion observed during normal operation (Figure 50). Consequently, deviations from the expected temperature-strain relationship provide an effective early-warning indicator of abnormal reservoir behaviour and could trigger operational adjustments, such as reducing injection pressure before significant mechanical damage develops.

Overall, the LBNL study demonstrates the importance of fully coupled THM modelling for the design and optimization of HTS systems. Beyond confirming the feasibility of the Bern-Forsthaus concept, the work identifies reservoir transmissivity, pressure management and real-time monitoring as the three principal controls governing HTS performance. Adequate transmissivity is required to sustain economically attractive circulation rates without excessive pressure buildup, pressure-controlled operation effectively minimizes geomechanical risks while maintaining good thermal performance, and distributed fibre-optic

monitoring provides a practical tool for validating model predictions and ensuring safe long-term operation. These conclusions directly support the design philosophy adopted within VESTA-CH and provide a robust basis for optimizing future HTS installations in heterogeneous sedimentary aquifers.

2.5.2 Safe operating envelopes

The modelling results demonstrate that reservoir transmissivity is the dominant parameter controlling the safe operating window. Low-transmissivity reservoirs provide favourable thermal confinement but are susceptible to excessive pressure buildup during injection. Conversely, increasing the effective transmissivity through reservoir stimulation, RJD or horizontal multilateral wells substantially reduces overpressure and improves injectivity, although it also promotes advective heat transport and slightly decreases thermal storage efficiency. Consequently, the design of HTS systems requires balancing thermal performance against hydraulic feasibility, which is indeed site-dependent.

The simulations performed within VESTA-CH show that several engineering measures can effectively enlarge the safe operating envelope. Increasing the number of auxiliary wells distributes hydraulic loads more uniformly throughout the reservoir, reducing local pressure peaks while improving heat recovery. Similarly, operating under a forced circulation scheme further limits pressure buildup by actively extracting fluid during the loading phase, albeit with a modest reduction in thermal recovery efficiency. The implementation of RJD (or, where technically feasible, horizontal multilateral wells) provides an additional means of increasing the effective well radius and improving injectivity without requiring large-scale reservoir stimulation.

The safe operating envelope therefore cannot be represented by a single limiting pressure or flow rate. Instead, it constitutes a multidimensional design space in which thermal efficiency, injectivity, reservoir pressure and geomechanical stability are simultaneously satisfied. The optimum operating strategy depends on site-specific geological conditions, reservoir properties and operational objectives.

One of the principal outcomes of VESTA-CH is the development of an integrated numerical workflow capable of constructing these operating envelopes for arbitrary HTS sites. The workflow combines geological characterization, coupled THC simulations, geomechanical stability assessment and sensitivity analyses to evaluate alternative well configurations, operating schedules and reservoir enhancement techniques. The methodology is transferable to future HTS projects through appropriate parameterization of site-specific geological, hydraulic and thermal properties.

Table 6 summarizes the principal controls defining the safe operating envelope identified in VESTA-CH. Rather than prescribing universal operating limits, the table identifies the governing parameters, their influence on hydraulic and thermal performance, and the corresponding engineering implications. The quantitative limits remain site-specific and should be established through coupled THMC simulations.

Table 6. Summary of the principal parameters controlling the safe operating envelope of HTS systems identified in VESTA-CH.

Parameter	Benefit	Limitation	Design recommendation
Reservoir transmissivity	High transmissivity → Lower pressure buildup, higher injectivity	Earlier thermal breakthrough	Primary design parameter; maximize within acceptable thermal recovery
Injection flow rate	High flow rate → Higher thermal power, reduced residence time	Higher pumping requirements and reservoir pressure	Limited by injectivity and pressure constraints
Injection temperature	High injection temperature → Greater stored thermal energy	Larger thermal stresses	Optimize according to storage objective
Number of auxiliary wells	Larger → Lower pressure peaks, improved hydraulic control	Higher drilling cost	Recommended where pressure is limiting
Forced circulation	Lower overpressure	Slightly lower thermal recovery	Suitable where hydraulic safety dominates
RJD / multilateral wells	Improved injectivity, lower pressure	Slight reduction in recovery efficiency	Attractive in low-transmissivity reservoirs
Reservoir heterogeneity. High connectivity	Low pressure	Faster thermal breakthrough	Characterize channel geometry before design
Reservoir heterogeneity. Low connectivity	Better thermal storage	Excessive pressure buildup	May require stimulation

Overall, VESTA-CH outlines a theoretical and modelling framework illustrating how the evaluation of HTS operating parameters can be evaluated through the coupling of reservoir engineering, THMC modelling, and targeted optimization techniques. The proposed workflow provides a systematic methodology to investigate operating conditions that could optimize heat recovery in future HTS projects. Although the methodology has been demonstrated using representative and site-inspired case studies, its application to future HTS projects will require calibration and validation against field data as operational experience becomes available.

2.6 Objective 4. Assessment of geochemical risks and mitigation strategies.

Corrosion and scaling models are most often developed in academic and research institutions, where they are typically calibrated under well-controlled laboratory conditions. However, transferring these

models to complex geothermal field environments remains a significant challenge (Singer, 2017). A large number of predictive analytical models exist for specific geochemical systems and operating conditions. Such models are mainly based on conventional polynomial fitting and non-linear regression techniques (Bai, 2020) and usually fail to accurately reproduce a broader range of thermodynamic and hydrodynamic conditions, including the high temperatures, elevated pressures, multiphase flow conditions, and variable fluid compositions encountered in deep geothermal reservoirs. On the other hand, numerical models based on, for example, the finite element method are computationally expensive (Liu and Kelly, 2019), especially when they are fully coupled with thermal-hydraulic-mechanical-chemical (THMC) models. Recently, machine learning methods have been applied to the modelling of corrosion (Coelho et al., 2022), offering the possibility of identifying complex, non-linear relationships from large experimental and field datasets while significantly reducing computational costs. In this context, advanced neural network approaches have recently been explored by KIT (personal communication).

Within VESTA-CH, geochemical risk assessment focused on predicting the long-term evolution of fluid chemistry and its interaction with reservoir rocks, well completions, and surface facilities. Corrosion and mineral scaling are among the principal geochemical risks affecting the technical and economic performance of High-Temperature Storage (HTS) systems, as they may reduce injectivity and productivity, impair heat exchanger efficiency, damage well casings and tubing, and ultimately increase maintenance requirements and operational downtime.

The geochemical risks associated with scaling and corrosion can be analysed using the chemical module implemented in MOOSE (see Section 2.1) by comparing the initial fluid chemistry and mineralogy with those at any given time. The coupled reactive transport simulations allow the prediction of mineral dissolution and precipitation, changes in fluid composition, gas exsolution, pH evolution, and corrosion potential throughout both the storage reservoir and the wellbore. This provides a quantitative basis for identifying operating conditions that minimise geochemical degradation while maximising thermal recovery.

Figure 51 displays a representative synthetic calculation, developed by KIT, of corrosion rate for a wide range of operating pressures and temperatures. As expected, corrosion rates increase with decreasing pH, consistent with experimentally observed trends for CO_2-induced corrosion in low-pressure systems (<2 MPa). It is also clear that distinct combinations of pressure and temperature produce significantly elevated corrosion rates, represented by the yellow and red semi-oval regions. Such operating windows can be identified automatically within the modelling framework and subsequently incorporated into the safe operating envelopes developed under Objective 3.

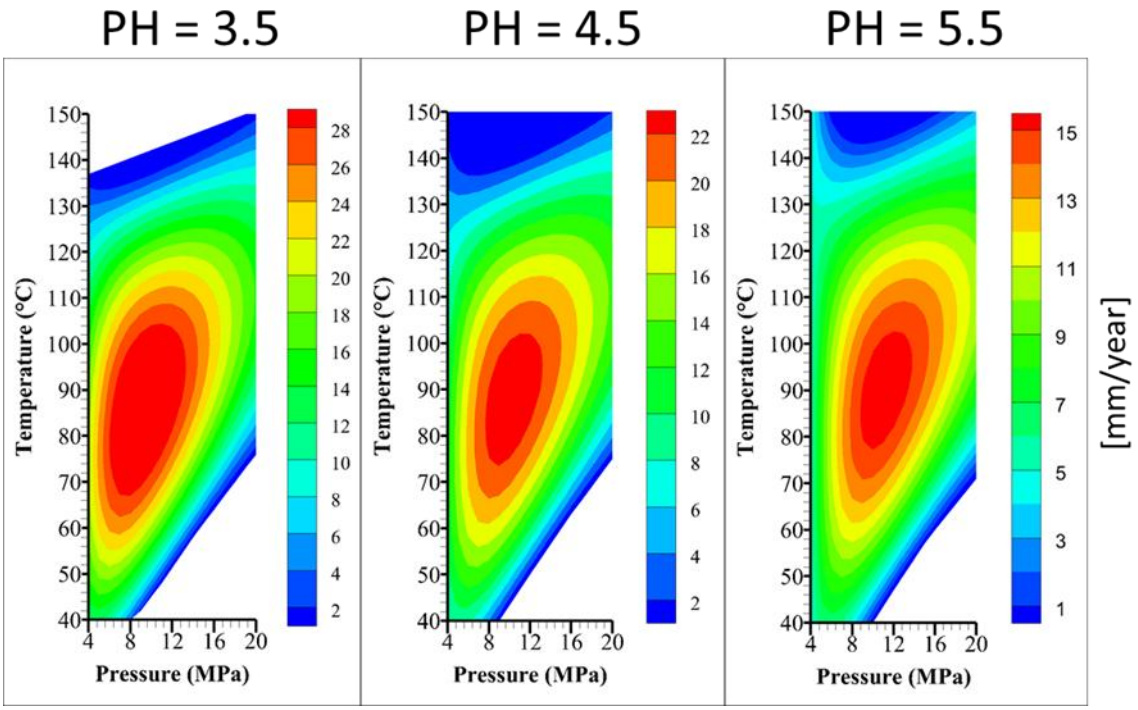


Figure 51. Calculated corrosion rates for a) pH=4.5 b) pH=5.5 c) pH=6.5.

Beyond corrosion, the same modelling framework can be employed to predict the precipitation of mineral scales such as carbonates (e.g., calcite), silica, sulphates (e.g., anhydrite or barite), and iron-bearing minerals. Scaling potential depends strongly on temperature evolution, pressure decline, fluid mixing, CO_2 degassing, and changes in water-rock equilibrium. Coupling reactive transport simulations with reservoir-scale flow models, as in VESTA-CH, enables the quantification of where and when mineral precipitation is likely to occur and evaluate its impact on reservoir permeability, well injectivity, production performance, and surface installations.

The predictive capability developed in this objective supports the design and optimisation of mitigation strategies in future HTS projects. Corrosion is commonly mitigated through the injection of chemical corrosion inhibitors, pH adjustment, oxygen scavengers, and the selection of corrosion-resistant materials or protective coatings for wells and surface equipment. Scaling can be controlled through the use of scale inhibitors, pH management, controlled pressure and temperature operation, filtration of suspended solids, and periodic mechanical or chemical cleaning of wells, pipelines, and heat exchangers. In some geothermal systems, operational measures such as controlling production rates or avoiding rapid pressure changes can substantially reduce scaling tendencies without additional infrastructure.

The economic impact of these mitigation measures is generally modest compared with the capital expenditure associated with drilling and completing deep geothermal wells. Chemical inhibitor programmes typically represent a relatively small fraction of annual operating costs, while periodic maintenance operations are considerably less expensive than productivity losses, workovers, or premature replacement of wells and surface equipment. Consequently, reliable prediction of scaling and corrosion risks enables cost-effective preventive maintenance strategies that improve system availability, reduce operational risk, and maximise the long-term economic performance of HTS installations.

2.7 Objective 5 Design implications

RJD represents a trade-off between thermal efficiency and hydraulic feasibility. Although radial jets slightly reduce HTS thermal efficiency by promoting advective heat transport, they are essential in low-transmissivity formations to maintain injection pressures within operationally acceptable limits. Therefore, pressure management rather than thermal performance is likely to be the primary driver for implementing RJD in HTS projects. Jet penetration length should be selected as the minimum value required to achieve acceptable injectivity while avoiding excessive hydraulic short-circuiting and thermal losses.

In the same line of arguments, Horizontal multilateral wells increase the effective drainage radius of the boreholes and substantially enhance the hydraulic connectivity between the wells and the reservoir. The resulting increase in effective transmissivity significantly reduces pressure buildup around the injection and production wells, thereby improving the hydraulic feasibility and operational safety of HTS systems. The improved injectivity enables the use of larger circulation rates while maintaining acceptable reservoir pressures, which can ultimately increase the recoverable thermal power of the storage system. For a fixed circulation rate, however, increasing the lateral extent of the wells generally reduces thermal recovery efficiency because the larger contact area promotes greater heat dissipation into the surrounding formations.

Increasing the number of wells improves both thermal recovery and pressure management. Multi-well configurations should therefore be preferred whenever reservoir geometry and project economics allow.

The choice of operating regime is governed by the trade-off between thermal efficiency and hydraulic constraints. Unforced operation maximizes thermal storage but generates excessive overpressures. Forced circulation provides lower thermal efficiency but maintains pressure levels closer to operational limits. In low-permeability reservoirs, forced operation is therefore likely to represent the most practical and robust long-term strategy.

3 Conclusions and outlook

The VESTA-CH project aimed to develop scientifically based protocols and modelling methodologies that enhance the design, operation, and long-term performance of current High-Temperature Storage (HTS) systems. By improving the efficiency and reliability of underground thermal energy storage, HTS technology can reduce the mismatch between renewable energy production and energy demand, thereby facilitating the integration of intermittent renewable energy sources and contributing to the reduction of greenhouse gas emissions. As such, the outcomes of VESTA-CH have direct relevance for the implementation of the Swiss Energy Strategy and the transition towards a low-carbon and ultimately CO_2-neutral heating supply.

The work carried out within VESTA-CH establishes the scientific and methodological foundations for the assessment of the coupled thermo-hydro-mechanical-chemical (THMC) processes governing the long-term behaviour of HTS systems. By integrating advanced multiphysics capabilities within the MOOSE framework, the project demonstrates how coupled numerical simulations can be employed to evaluate reservoir performance, mechanical stability, thermal efficiency, and geochemical evolution in a consistent modelling environment.

A major achievement of the project is the development of an integrated TH(M)C modelling workflow capable of supporting all phases of HTS system development, from site assessment and system design to operational planning and long-term risk management. This integrated approach enables the simultaneous evaluation of thermal recovery, pressure evolution, rock deformation, and geochemical risks, providing a substantially more realistic representation of subsurface processes than conventional uncoupled analyses.

The results demonstrate that numerical simulations can provide valuable guidance for defining safe and efficient operational envelopes. Mechanical analyses allow the identification of injection pressures and temperatures that minimise fault reactivation and reservoir damage, while reactive transport modelling enables the prediction of corrosion and mineral scaling under a broad range of operating conditions. Consequently, the efficiency and lifetime of HTS systems can be substantially improved by properly designing the maximum injection and reinjection temperatures, optimising the duration of loading and unloading cycles, and implementing appropriate mitigation measures to minimise corrosion and mineral scaling within wells and surface installations. Together, these capabilities support simulation-guided operational strategies that increase thermal recovery, reduce maintenance requirements, and improve the long-term reliability of HTS installations.

An important feature of the developed methodology is its broad applicability. Although the modelling framework has been developed using site-specific data from the High-Temperature Storage system at the Bern-Forsthaus pilot site, the proposed workflows, modelling strategies, and risk assessment methodologies are sufficiently generic to be transferred to other HTS projects in Switzerland and abroad. The project therefore provides a valuable scientific basis for future underground thermal energy storage developments and contributes to reducing technical uncertainties associated with the deployment of this emerging technology.

Although the reactive transport capabilities implemented within MOOSE provide a robust basis for evaluating corrosion and mineral scaling, further work is required to validate these models against laboratory experiments and long-term field observations under representative HTS operating conditions. Future developments should also investigate more complex fluid chemistries, multiphase flow, gas exsolution, and the dynamic coupling between geochemical reactions and evolving hydraulic properties.

Overall, the project demonstrates that fully coupled THMC modeling constitutes a supportive design tool for optimizing the development and verifying the feasibility of underground High-Temperature Storage systems. The developed framework integrates thermal performance, geomechanical integrity, and geochemical risk evaluation within a single modelling environment, thereby providing a comprehensive decision-support tool for HTS design and operation, with criteria that are strongly site-dependent. The successful implementation of these methodologies is expected to improve the technical robustness, operational safety, and economic viability of future HTS projects. Continued development and field validation of the proposed methodologies will therefore contribute directly to the wider deployment of HTS technology and support Switzerland's transition towards a sustainable and CO_2-neutral energy system.

4 National and international cooperation

VESTA-CH forms part of the broader international VESTA initiative, which brings together several research institutions, utilities, and industrial partners to advance the development of High-Temperature Storage (HTS) technologies. Within this broader framework, Geo-Energie Suisse AG (GES) contributes to Work Package 1 (WP1), which focuses on numerical modelling and performance assessment of HTS systems through close collaboration with the Karlsruhe Institute of Technology (KIT, Germany). Participation in the VESTA consortium provides VESTA-CH with access to complementary expertise, advanced modelling capabilities, and valuable experience gained from related HTS and geothermal projects across Europe.

The collaboration between GES and KIT is formalized through a cooperation agreement established within the framework of the VESTA-CH project. The purpose of this collaboration is the joint development, application, and validation of advanced numerical tools for the simulation of coupled thermo-hydro-chemical (THC) processes in HTS systems, while fostering knowledge transfer between academic and industrial partners. The respective contributions of the project partners are summarized below.

GES

- Contribution of the experience gained during the planning, drilling, testing, and evaluation of the Bern-Forsthaus pilot project towards the development of a generalized HTS storage concept.
- Provision of the geological, hydrogeological, operational, and monitoring data required for numerical simulations and model calibration.

KIT

- Execution of the wellbore simulations using the MOSKITO simulation framework.
- Delivery of simulation results.
- Facilitation of knowledge transfer and exchange of experience between GES and the German partners participating in the VESTA consortium, particularly within WP4, which is coordinated by KIT.

Joint activities

- Joint development of the conceptual and numerical modelling framework, including the definition of model geometry, material properties, input parameters, initial conditions, boundary conditions, and simulation workflows.
- Joint interpretation and evaluation of modelling results.
- Continuous exchange of knowledge and experience regarding HTS technologies, numerical modelling approaches, and operational concepts.

Beyond the collaboration with KIT, additional scientific in-kind support is provided by the University of Bern, which contributes expertise on geochemical processes and fluid-rock interactions under the pressure and temperature conditions relevant to the Bern-Forsthaus site. These activities support the interpretation of reservoir chemistry, the assessment of scaling and corrosion risks, and the evaluation of geochemical processes that may affect the long-term performance of HTS systems. Furthermore, the Lawrence Berkeley National Laboratory has utilized the three-dimensional reservoir model developed by GES to investigate thermo-hydro-mechanical (THM) processes associated with HTS operation. These in-kind studies include the assessment of thermally induced ground deformation, such as uplift and subsidence, and their implications for long-term system performance and environmental safety. The combination of industrial experience, field observations, advanced numerical modelling, and international scientific collaboration provides a unique framework for advancing the understanding, optimization, and implementation of HTS technologies in Switzerland and beyond.

5 Publications and other communications

Esmaeilpour M., (2023). Numerical Simulation of non-isothermal Complex Fluid Mixtures in Deep Geothermal Systems. Dissertation. DOI: 10.5445/IR/1000159240.

Esmaeilpour M., Nitschke F., Kohl Th (2024). GenEOS: An accurate equation of state for the fast calculation of two-phase geofluids properties based on gene expression programming. Computer Physics Communications 297, 109068.

Kohl T., Schill E., Bremer J., Nitschke F., Blöcher G., et al. (2022). VESTA - Very-High-Temperature Heat Aquifer Storage. Proceedings of the European Geothermal Congress (EGC 2022). DOI: 10.5445/IR/1000152235

Kumar R., Neupane G., Jin W., Atkinson T., McLing T., Dobson P., Schill E., Kohl T., Bauer F., Nitschke F., Bremer J. (2024). Development of Reactive Transport Models for Very High Temperature Heat Aquifer Storage (VESTA) at a Pilot Site in Germany. Proc. 2024 Geothermal Rising Conference.

Rutqvist J., Zhang Y., Alcolea A., Castilla R., Meier P., Dobson P. (2026). Insights from a coupled thermo-hydro-mechanical analysis of a layered high-temperature thermal energy storage reservoir. Journal of Energy Storage 175, 123303, https://doi.org/10.1016/j.est.2026.123303.

Yan G., Kohl T. (2025). Optimization of Wellbore Parameter for high-temperature Aquifer Thermal Storage Systems. Proceedings of the European Geothermal Congress (EGC 2022). DOI: 10.5445/IR/1000152235

Yan G., Andersen P., Qiao Y., Hatzignatiou D. G., Feng B., Kohl Th. (2025). Investigating the impact of wellbore lateral heat transfer on the performance of high-temperature aquifer thermal energy storage system by the coupling of wellbore and reservoir simulators, Geoenergy Science and Engineering, Vol. 251, 2025, 213874, https://doi.org/10.1016/j.geoen.2025.213874.

Ancillary

Website of the international VESTA project: https://geothermics.agw.kit.edu/english/vesta.php

Website of MOSKITO: https://www.m2clab.com/moskito

Data sets for THM modelling (LBNL): https://gdr.openei.org/submissions/1796

6 References

Aunzo, Z.P. (1990): GWELL: A multi-component multi-feed zone geothermal wellbore simulator. University of California, Berkeley.

Aunzo, Z.P., Bjornsson, G., Bodvarsson, G.S. (1991). Wellbore Models GWELL, GWNACL, and HO-LA User's Guide, Physical Review of Particle Physics. University of California, Berkeley.

Bai, H. (2020) Mechanism analysis, anti-corrosion techniques and numerical modeling of corrosion in energy industry. Oil & Gas Science and Technology - Revue d'IFP Energies nouvelles, Institut Français du Pétrole (IFP), 2020, 75, pp.42.

Coelho, L.B., Zhang, D., Van Ingelgem, Y. et al. Reviewing machine learning of corrosion prediction in a data-oriented perspective. Material Degradation 6, 8 (2022). https://doi.org/10.1038/s41529-022-00218-4

Collins L., Houben G. (2020). Horizontal and radial collector wells: simple tools for a complex problem. Hydrogeology Journal, 28(6):1-11

Dobson P., McLing T., Spycher N., Fleuchaus P., Neupane G., Doughty C., Zhang Y., Smith R., Atkinson T., Jin W., Blum P., Dinkelman D., Veldkamp H. (2025). High-Temperature Aquifer Thermal Energy Storage (HT-ATES) Projects in Germany and the Netherlands. Review and Lessons Learned. Energies, 18(23), 6292.

Esmaeilpour M., (2023). Numerical Simulation of non-isothermal Complex Fluid Mixtures in Deep Geothermal Systems. Dissertation. DOI: 10.5445/IR/1000159240.

Esmaeilpour M., Nitschke F., Kohl Th (2024). GenEOS: An accurate equation of state for the fast calculation of two-phase geofluids properties based on gene expression programming. Computer Physics Communications 297, 109068.

Gaston D., Newman C., Hansen G., Lebrun-Grandié D. (2009). MOOSE: A parallel computational framework for coupled systems of nonlinear equations. Nuclear Engineering and Design, 239(10): 1768-1778.

Gudmundsdottir, H., Jonsson, M.T., Palsson, H.: The Wellbore Simulator FloWell. Proceedings: 38th Workshop of Geothermal Reservoir Engineering, Stanford University, Stanford, California, (2013).

Gunn, C., Freestone, D., 1991. An integrated steady-state wellbore simulation and analysis package. Proceedings: 13th New Zealand Geothermal Workshop. Auckland, New Zealand, (1991).

Guo, L., Huang, H., Gaston, D.R., Permann, C.J., Andrs, D., Redden, G.D, Lu, C., Fox, D.T., Fujita, Y. (2013). “A parallel, fully coupled, fully implicit solution to reactive transport in porous media us-ing the preconditioned Jacobian-Free Newton-Krylov Method”. Advances in Water Resources, 53:101-108.

Heldt S., Beyer C., Bauer S. (2024). Uncertainty assessment of thermal recovery and subsurface temperature changes induced by high-temperature aquifer thermal energy storage (HT-ATES): A case study. Geothermics, 122, 103086

Itasca (2018). Flac3d Version 6.0 - Fast Lagrangian Analysis of Continua in 3 Dimensions. ITASCA Consulting Group Inc. https://www.itascacg.com/software/flac3d

Joshi S. D. (1991). Horizontal Well Technology. Tulsa, OK, U.S.A: Pennwell Books

Jung Y., Pau G.S.H., Finsterle S., Pollyea R.M. (2022). TOUGH3: A new efficient version of the TOUGH suite of multiphase flow and transport simulators. Computational Geosciences, 108, 2–7. https://doi.org/10.1016/j.cageo.2016.09.009.

Korzani, M. G., Held, S., Nitschke, F., & Kohl, T. (2019). The Development of a Fully Coupled Well-bore-Reservoir Simulator for Geothermal Application. Transactions - Geothermal Resources Council, 43, 927-936.

Liu, C., Kelly, R.G. (2019). “A Review of the Application of Finite Element Method (FEM) to Localized Corrosion Modeling“. Corrosion 75(11): 1285-1299. https://doi.org/10.5006/3282

Mcguinness, M.J.: SwelFlo User Manual. (2015).

Mégel T., Kohl T., Hopkirk R.J., 2007. The potential of the use of dense fluids for initiating hydrau-lic stimulation. Geothermics, 35, (2007), 589-599.

Nordbeck J., Lüders K., Hornbruch G., Bauer S. (2023). Experimental results of a high-temperature aquifer thermal energy storage test site. Storage efficiency and thermal impact on the environment. GeoBerlin 2023. DOI: 10.48380/s73x-sm13.

Oldenburg C.M., Moridis G.J., Spycher N., Pruess K. (2004) EOS7C version 1.0: TOUGH2 module for carbon dioxide or nitrogen in natural gas (methane) reservoirs. LBNL report 56589.

Pan L., Oldenburg C.M. (2014). T2Well: an integrated wellbore-reservoir simulator. Comput. Geosci. 65, 46-55.

Peaceman, D. W. (1983). Interpretation of well-block pressures in numerical reservoir simulation with non-square grid blocks and anisotropic permeability. Society of Petroleum Engineers Journal 23.03 (1983): 531-543.

Permann, C.J.; Gaston, D.R.; Andrš, D.; Carlsen, R.W.; Kong, F.; Lindsay, A.D.; Miller, J.M.; Peterson, J.W.; Slaughter, A.E.; Stogner, R.H.; et al. MOOSE: Enabling massively parallel multiphysics simulation. SoftwareX 2020, 11, 100430.

Pruess K., Battistelli A. (2002). TMVOC, a numerical simulator for three-phase non-isothermal flows of multicomponent hydrocarbon mixtures in saturated-unsaturated heterogeneous media. LBNL report 49375.

Pruess K. (2004). The TOUGH codes - A family of simulation tools for multiphase flow and transport pro-cesses in permeable media. Vadose Zone Journal, 3: 738-746. https://doi.org/10.2136/vzj2004.0738.

Pruess K. (2005). ECO2N: A TOUGH2 Fluid Property Module For Mixtures of Water, NaCl, and CO2, Lawrence Berkeley National Laboratory Berkeley, CA, 2005.

Ramey H.J. (1962). Wellbore heat transmission. J. Petrol. Technol. 14 (4), 427-435.

Sanchez-Upton, P.: The Wellbore Simulator SIMU2000. Proceedings World Geothermal Congress, Kyushu-Tohoku, Japan, (2000), 2851-2856.

Schwarze C., Pei L., Virchow L., Petrova E., Norden B., Regenspurg S., Kieling K., Blöcher G., Kranz S. (2025). Characterization of the hydraulic properties of a planned High Temperature Aquifer Thermal Energy Storage (HT-ATES) system during well development. Advances in Geosciences, 67, 69-78

Singer M. (2017). Limitations in the use of TLC predictive models. In Trends in Oil and Gas Corrosion Research and Technologies, Ed. A.M. El-Sherik, Elsevier, ISBN: 9780081011058, 926pp.

Vidal R. et al. "Heat storage efficiency, ground surface uplift and thermo-hydro-mechanical phenomena for high-temperature aquifer thermal energy storage." Geothermal Energy 10.1 (2022): 23.

Wang, J., Nitschke, F., Korzani, M. G., & Kohl, T. (2019). Temperature log simulations in high-enthalpy boreholes. Geothermal Energy, 7(1), 32.

Wilkins A., Green C.P., Ennis-King J. (2020). PorousFlow: a multiphysics simulation code for cou-pled problems in porous media. Journal of Open Source Software, 5(55), 2176. https://doi.org/10.21105/joss.02176

Wilkins A., Green C.P., Ennis-King J. (2021a). An open-source multiphysics simulation code for coupled problems in porous media. Computers & Geosciences, Volume 154, September 2021, 104820.

Wilkins A., Green C.P., Harbour L., Podgorney R. (2021b). The MOOSE geochemistry module. Journal of Open Software, 6(68), 3314, https://doi.org/10.21105/joss.03314.

Willhite G.P. (1967). Overall heat transfer coefficients in steam and hot water injection wells. J. Petrol. Technol. 19 (5), 607-615.

Xiong W., Bahonar M., Chen Z. (2016). Development of a thermal wellbore simulator with focus on improving heat-loss calculations for steam-assisted-gravity-drainage steam injection. SPE Reservoir Eval. Eng. 19 (2), 305-315.

Yan G., Andersen P., Qiao Y., Hatzignatiou D. G., Feng B., Kohl Th. (2025). Investigating the impact of wellbore lateral heat transfer on the performance of high-temperature aquifer thermal energy storage system by the coupling of wellbore and reservoir simulators, Geoenergy Science and Engineering, Vol. 251, 2025, 213874, https://doi.org/10.1016/j.geoen.2025.213874.

Zhan H., Zlotnik V. A. (2002). Groundwater flow to a horizontal or slanted well in an unconfined aquifer, Water Resour. Res., 38(7), doi:10.1029/2001WR000401.

Zhou D., Li K., Gao H., Tatomir A., Ganzer L., Brenner G., Jaeger P., Sauter M. (2026). Injection strategy analysis of high-temperature aquifer thermal energy storage system, an insight from the study case in Burgwedel, Germany. Renewable Energy, vol. 256(1), 124722, https://doi.org/10.1016/j.renene.2025.124722.

Ziabakhsh-Ganji Z., Kooi H.(2012). An equation of state for thermodynamic equilibrium of gas mixtures and brines to allow simulation of the effects of impurities in subsurface CO2 storage, Int. J. Greenh. Gas Control 11 (2012) S21-S34, https://doi.org/10.1016/j.ijggc.2012.07.025.